Infragravity wave resonance over coral reef lined coasts

MSc Thesis

R. V. van Noort

Technische Universiteit Delft

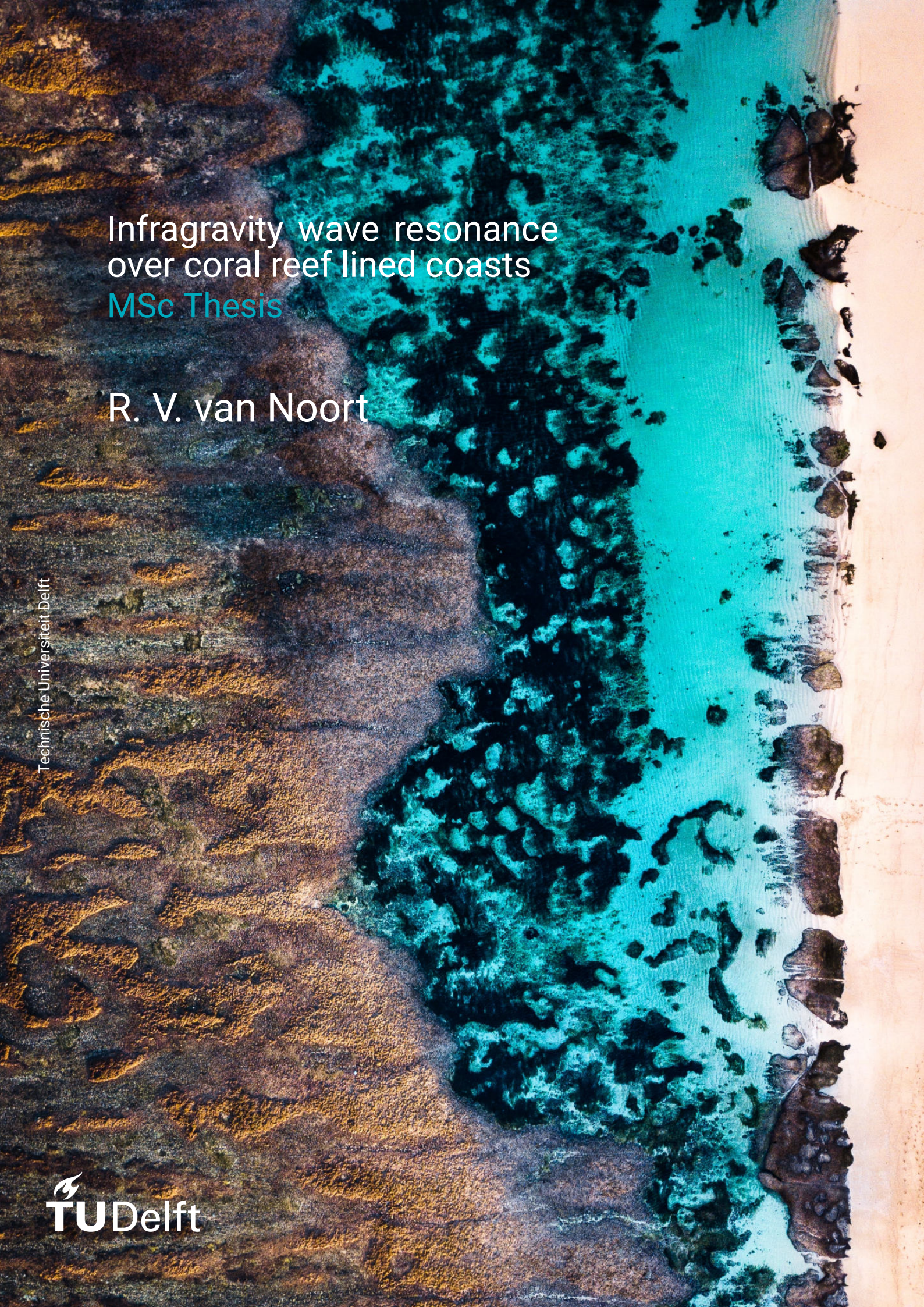

TU Delft

Infragravity wave resonance over coral reef lined coasts

MSc Thesis

by

R. V. van Noort

to obtain the degree of Master of Science
at the Delft University of Technology,

Student number:	4434617	
Project duration:	March, 2021 – December, 2021	
Thesis committee:	Dr. M. F. S. Tissier	TU Delft, supervisor
	Prof. Dr. Ir. A. J. H. M. Reniers	TU Delft
	Dr. Ir. J. A. Alvarez Antolínez	TU Delft

TU Delft

Abstract

Coral reefs are vital to the prosperity of the world and the local communities by providing food and coastal protection. Coral reefs are home to 25% of marine life and have therefore gained the nickname 'rainforest of the sea'. However, the reefs are being damaged by climate change and human intervention, resulting in an alarming rate of degradation. The combination of higher water levels on reef flats and the reduced friction due to reef degradation lead to greater risks of flooding and overwash on low-lying islands.

These aforementioned effects already present a threat to small islands that are naturally fronted by coral reefs. However, there is one more threat of damage to these islands: resonance. The characteristic bathymetry of the coral reefs can induce this type of threat, which is likely to be enhanced through climate change. Fringing reefs can display harbour-like resonance under the right conditions, because of their generally steep fore reefs and shallow horizontal reef flats. This has been shown to occur during various occasions, but the conditions that lead to are still unclear. What drives the occurrence and magnitude of resonance?

Resonance has been observed during high-energy events on various pacific islands, and though it occurs only 3.6% of the time, its damaging potential is larger than any other form of infragravity (IG) wave propagation. Various numerical models have been set up to study the behaviour and drivers of resonance, yet the defining characteristics and drivers of the phenomenon remain enigmatic.

To get a better understanding of the parameters that influence the occurrence and magnitude of resonance in fringing reef environments, a SWASH model is used. At the base of this model lies the schematized bathymetry of Roi-Namur island, RMI. The incoming sea swell (SS) wave field is schematized into a bichromatic wave field with amplitudes ranging from 0.8 m to 1.37 m for wave 1 and 0.57 m to 0.96 m for wave 2. The period of wave 1 is varied from 11 s to 19 s, while the period of wave 2 is varied depending on the desired group period. The fore reef slope varies from 1/5 to 1/10. The amplification of the incoming IG wave is determined by comparing the incoming IG wave energy at the beach toe for a beach boundary to an absorbing sponge layer boundary. If the ratio of incoming IG energy is greater than unity, resonance is expected to occur.

In general, the amplification ratio (AR) of incoming IG wave energies roughly remains below a factor of 4, indicating that the the incoming IG wave height is not more than doubled due to resonant amplification. The magnitude of the AR is largely dependent on the characteristics of the incoming SS wave field and coral reef bathymetry: a great modulation and a gentle fore reef slope lead to a large amplification. Additionally, a lot of incoming SS wave energy corresponds to a limited amplification of the incoming IG wave, likely due to the interaction of the released bound long wave and the IG wave generated through break point forcing, which are 180°out of phase. Therefore, the largest amplification occurs for a strongly modulated wave field without being too energetic. There is no clear relationship between the incoming SS wave periods and the amplification, the height of the incoming IG wave is similar for various situations. The amplification appears to depend on the combination of the fore reef slope and incoming SS wave periods. Different SS wave periods lead to different amplifications depending on the slope of the fore reef they pass over.

The height of the incoming IG wave is largest for the steepest slopes under consideration. Thus, for these conditions, the risk of flooding is largest. However, the greatest amplification occurs for the gentler slopes under the considered conditions. It should be noted that this relationship is heavily dependent on the combination of incoming SS periods and the steepness of the fore reef slopes.

The period for which resonance occurs is always higher than the theoretical fundamental eigenperiod, which is found through water depth integration from the location of minimum IG wave height to the beach toe. Integrating the water depth from the most offshore point of break point forcing leads to a smaller deviation of the theoretical fundamental eigenperiod from the observed period, yet this method needs further exploration. The insights acquired by this research can be used as a base for site-specific modelling, which can provide circumstances under which certain areas are at risk of flooding due to IG wave resonance.

Preface

This thesis touches upon a few aspects of the transformation of waves approaching coral reefs, but it mostly touches upon the knowledge that there is still a vast ocean of processes and concepts that are yet to be understood, though the importance of understanding these processes is only increasing.

I would like to thank my supervisors Marion, Ad and José for helping me shape and execute this project. José, for all the work he put in to making my method and future work infinitely more efficient. Ad, for all the ideas and interesting perspectives on the results that have never not led to new conclusions (and more questions than we started with). In particular, thanks to Marion, for always listening to my ideas, thoughts and struggles, and for helping me make pick the directions to work towards. Thank you for pushing me, your supervision has taught me at least as much about myself as it has about infragravity waves.

A special thanks to friends and family for supporting me, providing me with enough coffee and putting up with my endless stories about waves. It was much appreciated.

R. V. van Noort
Delft, December 2021

List of symbols and abbreviations

Symbol	Unit	Description
$a1$	m	Offshore amplitude of the first component of the bichromatic SS wave field
$a2$	m	Offshore amplitude of the second component of the bichromatic SS wave field
cg	m/s	Wave group celerity
c_{in}	m/s	Celerity of the incoming component (of the IG wave)
c_{out}	m/s	Celerity of the outgoing component (of the IG wave)
AR		Amplification Ratio
E	J/m^2	Energy density per unit area of the SS wave field
$f0$	$1/s$	Mean frequency of the bichromatic wave field
$f1$	$1/s$	Frequency of the first component of the bichromatic wave field
$f2$	$1/s$	Frequency of the second component of the bichromatic wave field
fg	$1/s$	Frequency of the bichromatic wave group
g	m^2/s	Gravitational acceleration
h	m	Water depth
H_{max}	m	Maximum wave height
H_{mean}	m	Mean wave height
H_s	m	Significant wave height
IG		Infragravity
L	m	Width or length of the basin or reef flat
MWL	m	Mean water level
RC		Reflection Coefficient
SS		Sea swell
SWL	m	Still water level
$T0$	s	Wave period corresponding to the mean frequency of the bichromatic SS wave field
$T1$	s	Wave period of the first component of the bichromatic SS wave field
$T2$	s	Wave period of the second component of the bichromatic SS wave field
Tg	s	Period of the bichromatic SS wave group
T_p	s	Peak period of the bichromatic SS wave field
u_{IG}	m/s	Flow velocity of the IG component of the wave field
var	m^2	Variance of the incoming SS wave field
η	m	Water elevation

Contents

1 Introduction

Coral reefs are important for the world's health and the communities finding protection and food from the reefs. Almost 40 % of the world's population lives within 100 km from the coast, this number is expected to increase over the coming decades (Hassan, 2005). Additionally, more than 500 million people worldwide depend on coral reefs for food, income, coastal protection, and more (NOAA, 2021). Moreover, coral reefs are vital for biodiversity in the oceans, as 25% of marine species can be found in coral reef environments (NOAA, 2021).

However, over the past decades the health and abundance of coral reefs has decreased due to direct interventions by humans or by the implications of climate change (Birkeland, 2018). Since coral reefs play a key role in reducing wave energy impacting the shore (Ferrario et al., 2014), coral reef degradation leads to increased risks for many communities and ecosystems world wide. The risks lie not only at direct damage to infrastructure on the low-lying land, but also at the contamination of fresh water lenses present at these locations (Storlazzi et al. (2018), Oberle et al. (2017)). Since local communities depend on these fresh water lenses for survival, low-lying lands may become uninhabitable long before the land itself has disappeared due to sea level rise (Storlazzi et al., 2015).

A better understanding of coral reefs and the principles that govern the hazards in these locations is of key importance to ensure habitable environments over the coming decades.

1.1. Overwash over low-lying islands

Climate change is damaging to all ecosystems on earth, but in particular small island states fronted by a coral reef must deal with various climate-change induced problems. Most famous is the degradation of the coral reefs, which causes a reduction in bottom friction as coral reefs induce a greater resistance than sandy sloping bottoms or bare limestone. Since dissipation due to friction is a large factor that contributes to the efficiency of coral reefs as coastal protection, degradation implies that more wave energy can propagate onto the reef and reach the shoreline (Storlazzi et al., 2019).

Climate change induces another effect that increases the risks of flooding on coral reef hinterland: sea level rise. Sea level rise in itself is a hazard to many communities around the world when it comes to the disappearance of land, but an increased water depth also decreases the influence of bottom friction on incident waves in fringing reef environments (Nwogu and Demirbilek, 2010). The increased risk of large run up and overwash on coral reefs have thus far been observed under storm conditions, when water levels are generally elevated (Cheriton et al. (2016), Péquignet et al. (2009), Roeber and Bricker (2015), Becker et al. (2016) Merrifield et al. (2014)).

Another cause for a water level elevation on the coral reef flat, and thus increased risk of damage due to overwash and run up, is resonance. The fundamental resonant mode occurs when incoming long waves are of the same period as it takes half a wave to travel from the start of the reef to the beach toe and back. These long, infragravity, waves (which are generally in the order of a few minutes), temporarily increase the water level much more than under non-resonant conditions, allowing for higher waves to penetrate the reef flat. This means that damage due to overwash is more likely to occur. Moreover, mean water level increase over the reef flat reduces the eigen period as the wave celerity is higher for a larger water depth. Since reef flats are usually in the order of hundreds of metres (Quataert et al., 2015), this means that the decrease in fundamental eigen period due to sea level rise becomes more in line with the period of long waves that naturally occur in these areas (Cheriton et al. (2016), Pomeroy et al. (2012b)).

1.2. Understanding systems fronted by coral reefs

In order to protect communities and ecosystems that depend on coral reefs, an understanding of governing processes of resonance is required. It has been observed that resonance occurs on coral reefs (during super typhoon Haiyan in the Philippines (Shimozono et al. (2015)), during storm Man-Yi on Guam (Péquignet et al., 2009), and during a 5-month field research on Kwajalein atoll, RMI (Cheriton et al. (2016), Gawehn et al. (2016)). To simulate resonant behaviour, numerical models XBeach and SWASH have been used (Pomeroy et al. (2012b), Pearson et al. (2017), Gaido (2019)), as well as physical models (Buckley et al. (2018)). In these models, it has been shown that resonance indeed increases the risk of damage due to run up and overwash, however knowledge is still limited on the conditions that can enhance or limit resonance.

This study is aimed at increasing the understanding of the processes governing resonance on coral reef lined coasts. With this understanding, areas at risk can be identified and measures can be taken to decrease the risks of resonant behaviour on coral reefs. Moreover, coral reef restoration as coastal protection (Roelvink, 2019) may have an extra benefit if resonance is reduced.

1.3. Research questions

The main research question is:
What processes and conditions influence the characteristics of infragravity wave resonance on coral reef lined coasts?

The sub questions that require answering include:

- What is the influence of the incoming sea swell (SS) wave heights on infragravity (IG) wave resonance?
- What is the influence of the incoming SS wave periods on IG wave resonance?
- What is the influence of the fore reef slope on IG wave resonance?
- How is the period for which maximum amplification occurs shaped by the characteristics of the incoming SS wave field and the bathymetry of the coral reef?

1.4. Outline of this thesis

In this chapter, the relevance of the research is given along with its position in recent literature. In Chapter 2, background information is given on coral reefs and theoretical resonance, as well as how resonance has been observed in coral reef environments. In Chapter 3 the methodology is presented that includes the schematizations of the bathymetry and the incoming wave field, along with the conditions that are evaluated. In Chapter 4 the results from the numerical simulations are summarized. In Chapter 5, the results and their implications are discussed. Chapter 6 provides answers to the research questions. In Chapter 7 some recommendations and suggestions for further research are given.

2
Background

In this chapter, background information is given on coral reef characteristics, long wave generation and transformation on coral reef lined coasts, and resonance of long waves in theory and practice.

2.1. General information on coral reef development and characteristics

Coral reefs consist of clustered groups of polyps that are held together by calcium carbonate at coastlines where a tropical climate is dominant. Most coral reefs that can currently be found on the planet are less than 10 000 years old, as they were formed after the melting of glaciers in the last ice age that caused widespread flooding of continental shelves (Kleypas and Gattuso, 2006). Due to the requirements of coral reef growth (among other things: high mean sea temperatures of 20 °C; enough light available for photosynthesis; nutrients for carbonate growth; water flow to allow for nutrient redistribution (Osinga et al., 2011)), coral reef growth is restricted to tropical coastlines. Once the coral polyps attach themselves to suitable submerged foundation, the coral reef grows in vertical direction. Reefs that grow too slow to keep up with the rising water level die off due to the lack of available light at the reef's location (Kleypas and Gattuso (2006), Osinga et al. (2011)).

2.1.1. Development and types of coral reefs

Coral reef growth can be categorized in three stages, a theory first hypothesised during Charles Darwin's voyage of the Beagle (Figure 2.1). In this theory, corals are formed around the waterline nearby extinct volcanoes. As the volcano subsides (panel (i)), the corals continue to grow toward the light to form a coral reef. Depending on the stage of the development of the reef, three types can be distinguished: (ii) a fringing coral reef, where the reef is directly attached to the land, (iii) a barrier reef, where the subsided land has made space for a lagoon between the reef and the land and (iv) an atoll, in which case the land has become completely submerged and a ring shaped coral reef surrounds a lagoon.

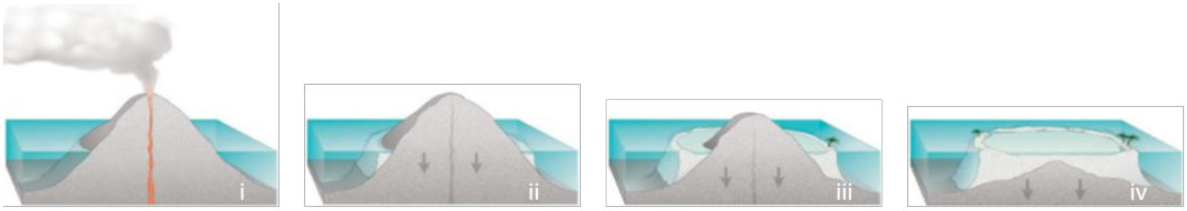

Figure 2.1: The stages of atoll formation according to Darwin's theory. (i) a volcano becomes extinct, starting subsidence of the land (ii) a coral reef starts forming just below sea level, also known as a fringing reef (iii) the volcano subsides even further, creating a lagoon between the reef and the land, this is also know as a barrier reef (iv) the land has subsided completely, leaving a ring shaped coral reef centered by a lagoon: an atoll has formed. Fringing reefs take around 10 000 years to form, whereas barrier reefs and atolls can take up to 30 million years to form (NOAA, 2021). Image from Field et al. (2002).

2.1.2. Bathymetry of fringing coral reefs

The bathymetry of fringing reefs, which are the most common coral reef type (NOAA, 2021), can be schematized to consist of two general areas (Figure 2.2).

The onshore part of the fringing coral reef can be identified as the reef flat, a shallow area with a width between 100 and 500 m, with outliers of up to 1000 m. The water depth of this region is mostly constant and in the order of 1 m and can be exposed during low tide events (Quataert et al., 2015).

Offshore of the reef flat the fore reef can be found, where waves can be transformed through shoaling, refracting or breaking. This part of the reef is characterized by a relatively steep slope in the order of 1/6 to 1/20 and descends into deep water (Quataert et al., 2015). Though at larger water depths less light is present which is generally not beneficial for coral reefs, the reduced wave energy allows for different types of coral to grow at this location (NOAA, 2021).

At the interface between these two areas the reef crest is located, which can have an elevation that is larger than the elevation of the reef flat.

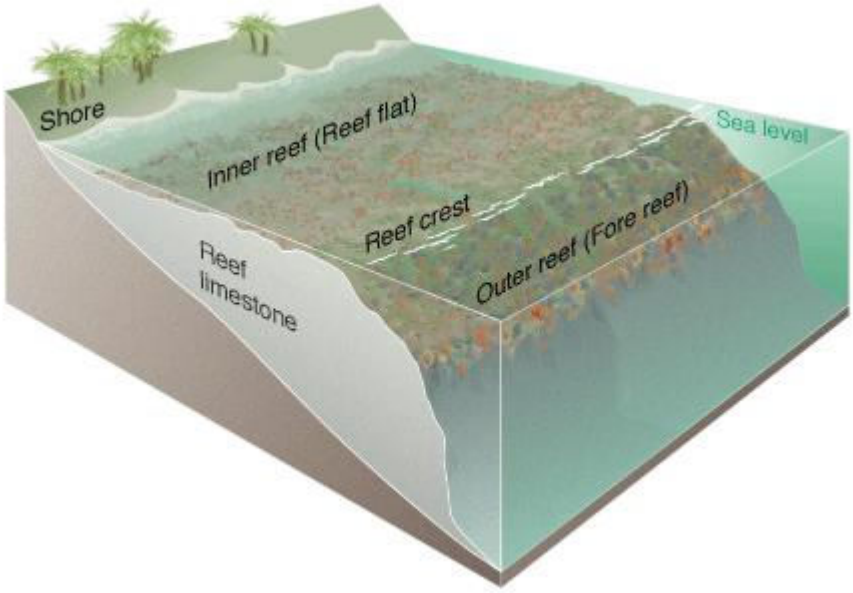

Figure 2.2: Schematization of the bathymetry of a fringing coral reef. Three distinct features can be distinguished from onshore to offshore: the inner reef, which is a nearly horizontal shallow flat; the reef crest, the edge of the reef flat which can be slightly higher than the inner reef; the outer reef, a slope steeper than 1:20 (Quataert et al., 2015) that descends into the ocean. From Field et al. (2002).

2.2. Sea swell waves on coral reefs

The bathymetry of a coral reef as described in Section 2.1.2 varies from regular sandy coasts, which causes the area to therefore be subject to specific nearshore processes in both the low and high frequency bands of the spectrum (Van Dongeren et al. (2013), Lee and Black (1978)). In this section, some aspects of sea swell (SS) wave behaviour on coral reefs are discussed.

2.2.1. Dissipation of SS waves

The combination of a long, shallow reef flat with a higher roughness due to the nature of corals, has been linked to shore protection due to wave dissipation. In approach to the reef crest, the SS waves steepen and break. At the reef flat, where breaking is minimal due to limited decrease in water depth, wave energy is mostly dissipated due to bottom friction (Lowe, 2005). Coral reefs therefore play an important role in the protection of tropical shorelines of wind and swell waves (Ferrario et al. (2014), Lowe (2005), Shimozono et al. (2015)).

2.2.2. Wave induced set-up

The change in momentum flux induced by the breaking of SS waves over the reef flat is balanced by a pressure gradient resulting in a higher water level near the beach toe. In coral reef environments, this set up due has been observed to be as high as 1.3 m (Vetter et al., 2010), which is higher than typical set up on sandy beaches. This increased water level near the shoreline contributes to an increased risk of overwash and flooding (Quataert et al. (2015), Cheriton et al. (2016)).

Contrary to a situation with a gently sloping beach, wave set up over coral reef lined coasts cannot be estimated using the analytical solution $\eta = \frac{5}{16}\gamma_b H_b$ (from Battjes (1974)). Research by Vetter et al. (2010) does use

this approach, however a prediction of H_b must be made based on field data. Therefore, a different approach is required considering the bathymetry of fringing reefs. This can be done numerically, or for instance by the method by Gourlay (1996). Here the maximum value for set-up ($\overline{\eta}_r$) is a relation between the factors $\frac{\overline{\eta}_r}{T\sqrt{gH_o}}$ and $\frac{\overline{\eta}_r+h_r}{H_o}$, in which T is the wave period, g is the gravitational acceleration H_o is the offshore wave height (H_{rms} in the case of an irregular wave field) and h_r is the submersion of the reef without set up. Iteration is required to find the value for $\overline{\eta}_r$ under certain conditions.

2.3. Infragravity wave generation

Infragravity waves (IG) are long waves with frequencies of up to 0.04 Hz. Contrary to the much shorter gravity (SS) waves (with frequencies >0.04 Hz), generation of IG waves is caused by the interaction of wind waves (Longuet-Higgins and Stewart, 1962). This generation can be accounted to three processes: bound IG wave release, moving break point and bore merging. For coral reefs with a relatively steep fore reef, the moving break point mechanism is found to be dominant (Pomeroy et al., 2012b).

2.3.1. Release of the bound IG wave

One of the three mechanisms responsible for IG wave generation is the release of an IG wave that is bound to a wave group. Through wind generation, waves are often generated at a wide range of frequencies. In deep water, wave signals with similar frequencies create a wave group due to their differences in celerity (Figure 2.3, top panel). For a bichromatic wave field with the same amplitude for each of the individual SS waves, the local wave amplitude could be a maximum of twice the SS wave amplitude or minimum of zero. Due to the non-linear interactions between these waves, slight variations in the mean water level occur (Figure 2.3, bottom pane). This can be attributed to the difference in momentum that is being transported by high and low amplitude waves (Longuet-Higgins and Stewart (1962), Bertin et al. (2018)). As a result, the wave group that consists of two SS waves with similar periods and amplitudes is accompanied by an IG wave with a period equal to the group period, and a rather small amplitude. The celerity of the IG wave is equal to the group velocity, which means that it is not in line with the free wave celerity of such an IG wave. When this wave group reaches a sloping bottom, the phase of the IG wave lags further behind the wave group, allowing for energy transfer from the wave group to the IG wave, which then grows in size and is released from the wave group, resulting in a free IG wave(Janssen et al., 2003). This phenomenon is especially dominant for mildly sloping bottoms (Battjes et al., 2004).

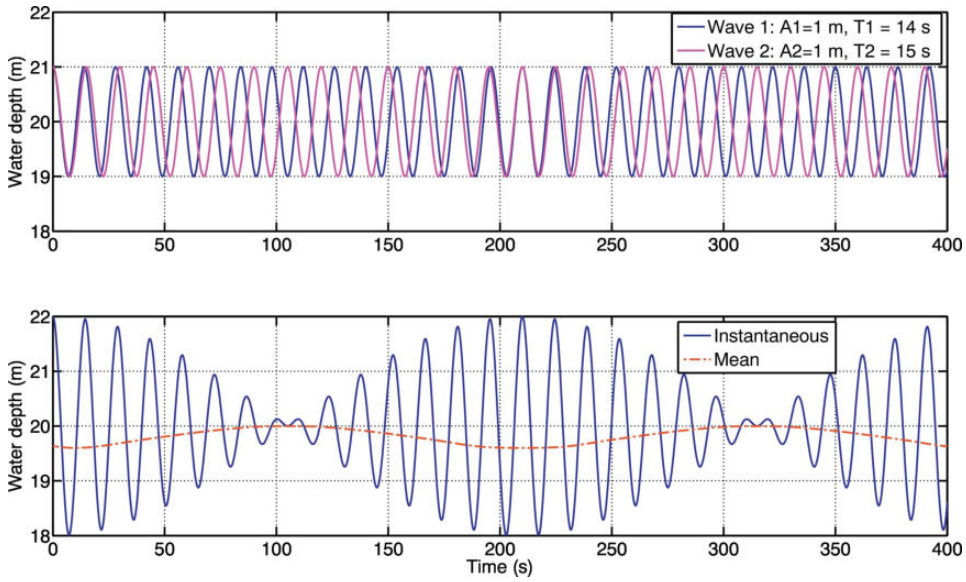

Figure 2.3: The interaction of two SS waves (top) and the resulting bound IG wave (bottom). Due to the differences in transfer of momentum between the highest and lowest peaks in the wave groups, locally water level depressions are found that take the form of an IG wave. This IG wave travels with the celerity of the wave group and is therefore bound until the highest waves of the group start to break. (from Bertin et al. (2018))

2.3.2. Break point forcing

The second mechanism driving IG wave generation is the movement of the break point due to the varying wave height of the incoming SS waves, this is the dominant mechanism for coral reef lined coasts (Pomeroy et al., 2012b). Due to shoaling and the subsequent breaking of waves, the lowest mean water level for a given wave signal is located at its break point. The location of the break point depends on the ratio of wave height and water depth. For a constantly sloping bottom, a larger wave breaks further offshore than a smaller wave. For wave groups (see Figure 2.3 bottom panel) the break point would therefore shift along with the onshore progression of the wave group (Figure 2.4) (Symonds et al., 1982). This moving of the break point acts as an IG wave generator. Since the location of the break point oscillates in the frequency of the wave group, the period of the IG wave generated through break point forcing is the same as the period of the wave group and therefore the same as the period of the released bound IG wave.

It has been assumed by many (Baldock et al., 2000; Contardo and Symonds, 2013; Masselink, 1995; Pomeroy et al., 2012a) that the bound long wave is 180 °out of phase with the incoming wave group and that the incoming and outgoing IG wave generated by break point forcing are in phase and 180 °out of phase with the wave group, respectively. However, Contardo et al. (2018) discuss that the phase lag of the incoming and outgoing break point generated wave is dependent on the beach slope, group frequency and the wave heights of the incoming wave field. If the slope is gentle and the group period of the SS waves is short, the phase of the break point generated IG wave may shift with respect to the SS wave group. It is expected that in coral reef environments the aforementioned assumptions hold, given the steep slopes on which the IG waves are being generated, especially for large incoming group periods.

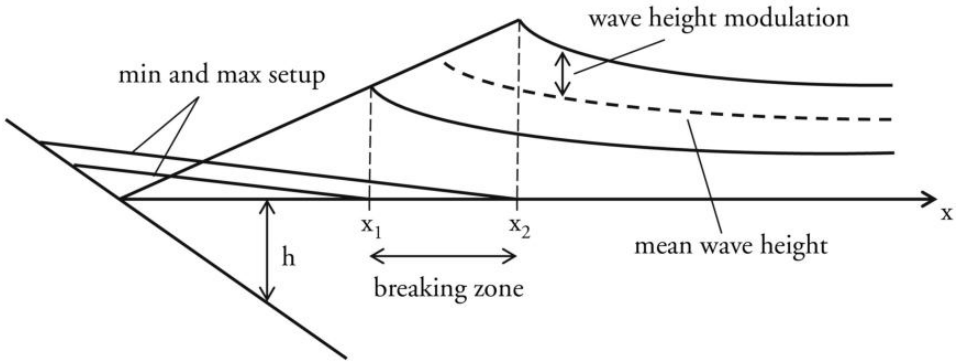

Figure 2.4: Visualisation of the shifting break point as an IG wave generating mechanism. Due to the differences in wave height within a wave group, the break point shifts with increasing and decreasing wave height. The movement of the location of minimum water level in x direction acts as an IG wave generator of onshore and offshore propagating IG waves (from Bertin et al. (2018)).

2.3.3. Bore merging

The third mechanism governing the generation of IG waves is the merging of bores (hydraulic jumps). When waves break, the wave front propagates further as a bore. The celerity of the bore depends on the water depth and the height of the bore, with deeper water and larger bores leading to higher celerities. Therefore, a bore travelling on the crest of an IG wave has a higher celerity than a bore travelling in a trough, allowing one bore to overtake another. The waves merge and the wave energy is transferred from the higher frequencies to lower frequencies. The contribution in spectral energy of bore merging to the lower frequencies is significantly less than from the release of bound IG waves and the moving of the break point (Bertin et al., 2018), however the combination of bore merging with other generated IG waves could have a significant effect on wave run-up and overwash (Cheriton et al., 2020).

The presence of IG or very low frequency (VLF) waves may enhance the merging of bores and as such the movement of energy from the high frequencies to the lower frequencies of the spectrum. Furthermore, bore merging creates onshore pitched IG waves (Cheriton et al. (2020), Ning et al. (2019)).

2.4. IG wave hydrodynamics over fringing coral reefs

There are various aspects that influence the behaviour of IG waves on a coral reef. It is known that due to the steep fore reef slope, the dominant wave generation mechanism is break point generation (see Section 2.3). In approach to and on the reef flat, the IG wave is subject to variations and transformations.

2.4.1. Physical properties that influence IG wave behaviour

The first parameter that influences the way IG waves behave over the reef flat is the local water depth. Since the water depth at reef flats is generally limited (Quataert et al., 2015), the system is highly subject to change by time-varying factors such as tidal surge, storm surge, and set up due to wave breaking of SS waves on the reef (Cheriton et al. (2016), Hoeke et al. (2013), Longuet-Higgins and Stewart (1964), Vetter et al. (2010), Becker et al. (2014)). Whereas the breaking of SS waves only depends on the ratio between wave height and water depth and thus the steepness of the waves, the stresses and wave set up induced by the breaking of SS waves influence the development of the IG wave over the reef flat (Cheriton et al., 2016).

Secondly, the amount of IG wave energy trapped on the reef flat is determined by the fore reef and its slope. Due to the sudden change in bathymetry, the fore reef acts as a barrier that causes reflection both offshore and onshore (Figure 2.5 from Buckley et al. (2018)). Due to this reflection, part of the IG wave energy that is approaching the reef is reflected offshore. Simultaneously, the wave energy that is reflected from the shoreline traveling offshore is reflected back onto the reef flat. This causes IG wave energy to be trapped on the reef flat, which may lead to an increase in wave energy at the reef flat over time (Pomeroy et al. (2012a), Péquignet et al. (2011)).

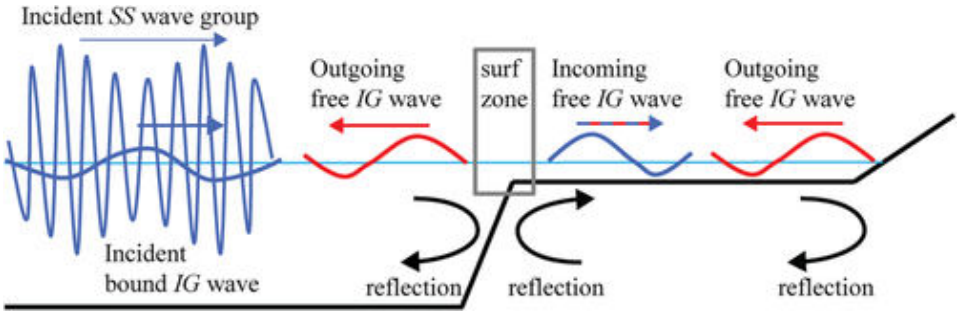

Figure 2.5: IG wave reflection of incoming and outgoing IG waves near a coral reef flat. The flat has two main reflection points: The fore reef and the shoreline. Due to the reflection of the fore reef happening in two directions, IG waves can be trapped on the reef flat. From (Buckley et al., 2018).

2.4.2. IG wave transformation on coral reef flats

When IG waves are travelling over the horizontal reef flat, they are subject to transformations due to the bathymetry of the coral reef and effects from the SS waves present.

Firstly, energy in the IG part of the spectrum is generated as it is shifted from the high frequency (SS) component to the low frequency components (Van Dongeren et al. (2013), Gawehn et al. (2016)).

Secondly, the shape of the IG waves changes as they propagate into more shallow water. The peaks become pointier and the troughs become longer and flatter. In case of low water levels and high offshore wave energy, the wave becomes asymmetrical and is pitched forward (Cheriton et al., 2016). These transformations may lead to an increase in sediment transport onshore (Pomeroy et al. (2015), Storlazzi et al. (2004)).

In case of a storm that results in an increased water level, there is more energy on the reef flat to be preserved and thus the absolute reflected wave at the beach toe is larger than for conditions in which the water level is lower. The same observations are reached when considering a shorter domain, where the distance over which friction can dissipate energy is smaller than for a wider reef (Pomeroy et al. (2015), Péquignet et al. (2009)).

2.4.3. Types of wave behaviour on reef flats

To identify and classify IG wave behaviour, Gawehn et al. (2016) studied 5 months of wave data on Roi-Namur Island in the Republic of the Marshall Islands. The four wave classes that were distinguished are: (non resonant) standing, progressive-growing, progressive-dissipative, and resonant waves.

Standing waves occur in situations where the water depth on the reef flat is large enough that the wave energy penetrates throughout the shoreline and is reflected at this location. In this situation, the total energy increases along the domain toward the shoreline.

Progressive growing waves occur in mid-range water depths without dependencies on the offshore wave periods. Though the IG wave energy increases toward the shoreline, limited reflection is happening due to the nonlinear shape of the waves. Most of the low frequency wave energy is dissipated on the shoreline.

Progressive dissipative waves occur when water levels at the reef flat are low. In these scenarios, wave energy is dissipated though bottom friction and leave little to no wave energy at the shoreline (Pomeroy et al., 2012b).

Resonant IG waves contribute 3.6 % to the total amount of IG waves considered, but due to their amplitude amplifying nature, their potential to damage the low-lying hinterland is largest of all types. In Section 2.5 this type of wave is elaborated on.

2.5. Infragravity wave resonance

As specified in Subsection 2.4.3, resonant waves have a great potential of causing overwash and damage to the low-lying hinterland. The combination of resonance and non-linear steepening of IG waves leads to bore formation, which increases the damaging potential of such waves, which could occur to storms similar to typhoon Haiyan (Roeber and Bricker (2015), Nakaza and Hino (1991)). Resonant waves have a higher chance of occurring in situations with a larger water depth (Cheriton et al., 2016; Pomeroy et al., 2012b). This increases the risk of overwash when climate change causes sea levels to rise. Events where large offshore wave heights were found resulted in a situation where the set up at the shoreline allowed for waves to propagate onto the reef flat even in low tide situations. Additionally, in resonant cases up to 16 % of offshore SS wave energy can be transferred to IG waves. This is more than when there is no resonance, for which the energy transfer is usually limited to 1% of the incoming SS value (Gawehn et al., 2016).

2.5.1. Influence of storm conditions on observed resonant characteristics

Péquignet et al. (2009) analysed the resonant forcing of tropical storm Man-Yi on the Ipan reef flat in Guam. The coral reef of this study can be schematised as seen in Figure 2.6. They concluded the following:

- Coral reef bathymetries (Figure 2.6) are subject to semi open basin eigen modes, similar to harbours;
- The eigen frequencies of the coral reef flat increase in the case of larger water depths on the reef flat. The water depth increases due set up induced by breaking of SS waves. During the observed storm, the increased water depth resulted in an increase of the natural frequencies with nearly a factor two;
- The resonant infragravity waves have the same period as incident wave groups on the reef flat;
- A water level increase also decreases the amount of wave dissipation due to friction, allowing for larger amplitudes of the wave at the shoreline;
- A larger water depth increases the possibility of IG wave resonance, as the natural frequency of a reef with a larger water depth is more in line with the period of wave groups found offshore. The associated risks may increase due to the expected sea level rise due to climate change (Pachauri, 2014).

Furthermore, Pomeroy et al. (2012b) found that the frequency at which resonance occurs does not depend on friction, but it does always depend on the water depth.

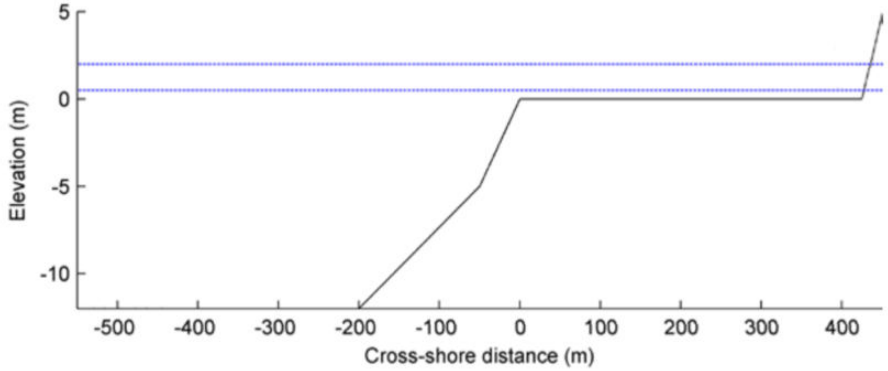

Figure 2.6: The bathymetry of t a typical coral reef at Ipan, Guam (adapted from Pomeroy et al. (2012b)). The blue lines indicate the water level, in both calm (lower line) and high-energy storm (upper line) conditions.

2.5.2. Theoretical resonance models

To determine the IG periods for which coral reefs may display resonant behaviour, the bathymetry as schematized in Subsection 2.1.2 and Figure 2.6 is treated as a harbour with an open boundary at the reef crest and a closed boundary at the onshore end of the reef flat.

Equation 2.1 gives the theoretical wave frequency $f_{n,th}$ for a simple harbour of with one open and one closed boundary (Wilson, 2000). This a function of the celerity of the wave $\sqrt{gh}$ over 4 times the width of the reef flat L. The mode with the largest amplification potential is the fundamental mode (with n = 0), since higher modes are subject to higher dissipation rates (Gawehn et al., 2016). In this mode, the wave length corresponds to four times the reef width. This function gives resonant values for a rectangular basin (Figure 2.7, black line). The red line represents the first eigen mode (n = 1 in Equation 2.1), in which the wave length corresponds to 3/4 of the reef flat width.

$$f_{n,th} = \frac{(2n+1)\sqrt{gh}}{4L} \text{ for } n = 0, 1, \dots N \tag{2.1}$$

However, the water depth typically varies over the reef flat due to set up, influencing the celerity and thus the eigen frequency $f_{n,setup}$ of the coral reef. To compensate for variations in the water depth, e.g. due to wave set up, Equation 2.1 is expanded to Equation 2.2 (Buckley et al. (2018), Gaido (2019)). x_0 represents the location at which the reef crest can be found and thus the most offshore reflection point of the wave, $h(x)$ is the water depth at location x, which varies due to wave set up.

$$f_{\text{n,setup}} = \frac{1}{4}(2n+1)\left(\int_0^{x_{\text{shoreline}}} \frac{1}{\sqrt{gh(x)}}dx\right)^{-1} \text{ for } n = 0, 1, \dots N \tag{2.2}$$

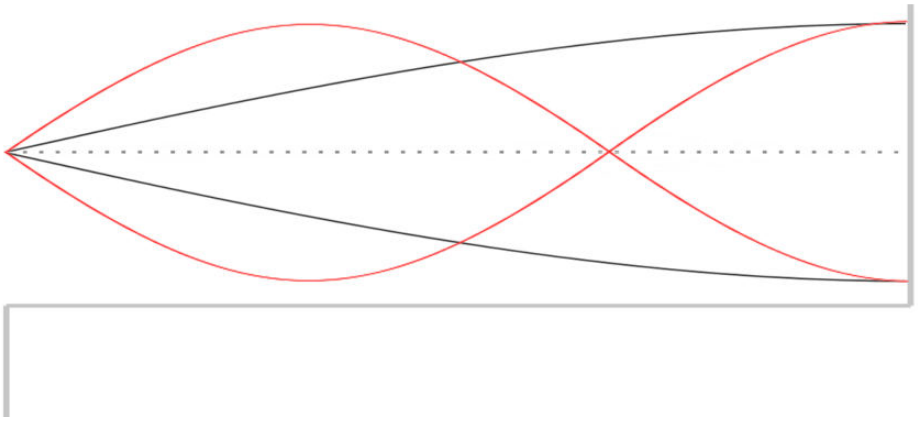

Figure 2.7: The fundamental (black) and first (red) resonance modes in a semi-enclosed basin. The resonant modes all consist of a node on the offshore side of the basin and an antinode on the shore side of the basin. Higher resonant modes are possible as long as the node - antinode requirement is fulfilled, however the lowest modes have been found to cause the largest amplification of the IG wave.

2.5.3. Resonance on coral reefs in models

It was found by Gaido (2019) and Pearson et al. (2017) that the maximum resonant amplification was found for a situation where the frequency is lower than the theoretically found resonant frequency. The deviation from the theoretical resonant period is highest for the fundamental mode (Gaido, 2019). In these cases, resonance around the fundamental mode was larger than for the first resonant mode. This includes a larger amplification as well as smaller sensitivity to the period. I.e. if a wave period was deviating with a certain percentage from the resonant mode, the amplification would be higher for the fundamental mode than for the higher modes (Gaido, 2019).

Furthermore, Gaido (2019), who looked at single incident IG waves with offshore amplitudes in the order of centimetres, found that near the fore reef decrease of the wave height was observed. It was concluded that this is likely not due to the dissipation of wave energy at this location as the friction was set to a relatively low value in this research, further insights are required to assess whether this can be attributed to reflection of the waves offshore.

Additionally, no clear relationship was found between the reduction of resonant amplification and increased skewness. Asymmetry was observed to be larger for the first resonant mode than for the fundamental mode. This factor might be a reason why the amplification is larger for the fundamental mode, as an asymmetrical shape might reduce potential for resonance. The same principle holds for larger incoming waves, which are subject to heavier steepening than smaller incoming waves. As the magnitude of the skewness of the outgoing reflected wave is larger than the incoming wave, it is concluded that steepening increases across the reef flat, even after reflection. It yet has to be concluded what the dependence of resonance is on the difference in steepness between the incoming and outgoing IG waves.

2.5.4. Qualification of resonance

To assess if certain wave behaviour classifies as resonance, various alternatives have been presented:
Pomeroy et al. (2012b) defined three conditions to be met in order for a wave to be classified as resonant:

1. A highly coherent variation in water surface elevation must be present, which indicates a standing wave pattern across the considered basin. If a propagating wave has a reasonably consistent form, this will also display high coherence. Therefore the second criteria must also be met.

2. The phase difference between waves at nodal and antinodal points must closely correspond to 0 °or 180 °.

3. Amplification of the wave signal is visible between two points. In this study, it is defined as the amplification ratio of the variance density spectra at the shore line and the crest.

Gawehn et al. (2016), who looked at the classification of IG waves, determined for which frequencies resonant conditions are present on the coral reef by looking at the energy transfer between the incident wave group envelope spectrum and the inner reef flat wave spectrum. Resonance was quantified using the ratio of low frequency energy at the reef flat over the low frequency energy at the fore reef.

Gaido (2019), who looked at resonance of a single IG wave, used the ratio between wave height at the beach toe and wave height offshore, as well as the ratio between the maximum run-up and wave height offshore to quantify resonance. Additionally, they used build-up time of the maximum wave height and the reef energy balance to assess whether resonant behaviour occurred in the numerical models.

In these studies the focus lies on the qualification of resonance rather than the quantification of resonance that allows one to compare various resonant situations with one another. Furthermore, the contribution of nearshore processes that affect the magnitude of the IG wave on the (fore) reef are not isolated. Additionally, in a perfectly resonant situation a node would be present near the location of the fore reef (Figure 2.7), which means that the energy at this location is not representative of the total energy in a non-resonant situation and thus indicates that the ratio of wave energy on the reef flat over the wave energy at the reef crest does not lend itself well for the determination of resonant amplification.

2.6. Resonant build-up over time

Understanding the build-up time of resonant behaviour and maximum amplification is of importance for the assessment of risks of flooding under certain conditions. Resonant build-up has been observed in both numerical and physical models (Gaido (2019), Nwogu and Demirbilek (2010)). In these models, a certain number of waves was required for the amplification to reach its maximum. Gaido (2019) found a number of 12 IG waves required in the numerical model with a single incident IG wave (Figure 2.8), whereas the physical experiments by Nwogu and Demirbilek (2010) showed a number of 5 IG waves needed to reach maximum amplification in the case of an incoming bichromatic wave field (Figure 2.9).

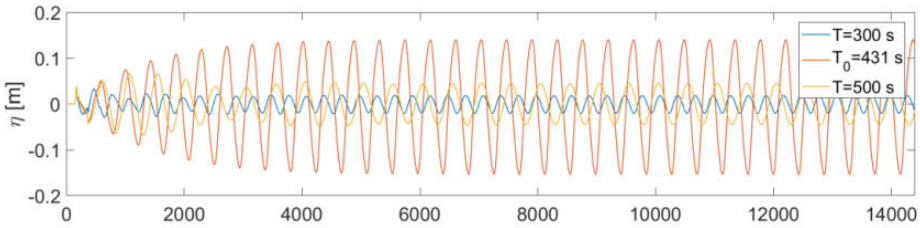

Figure 2.8: The water elevation at the beach toe over time by Gaido (2019) for normally incident IG waves with resonant (orange, T = 431 *s*) as well as non-resonant (T = 300 *s* and T = 500 *s*) periods. A stationary situation is reached in resonant conditions after 12 waves.

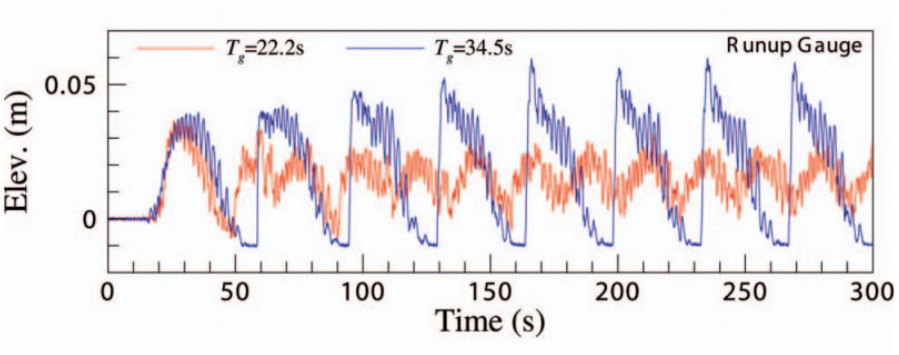

Figure 2.9: The water elevation at the run-up gauge, i.e. the most onshore point of the reef flat, by Nwogu and Demirbilek (2010). The IG waves generated by a normally incident bichromatic wave field reach a maximum amplification after 5 group periods in case of resonance (indicated by the blue line, Tg = 34.5 *s*).

3
Methodology

To answer the research questions described in Chapter 1 through numerical modelling, some things should be considered: the numerical approach; the schematization of coral reef bathymetry; the schematization of the incoming wave field; the methods for analysis. In this chapter, the basis for the model and the results evaluation in presented.

3.1. Properties and validation of the model

SWASH in an open source, robust, phase resolving model, used for simulating non-hydrostatic, free-surface rotational flows and transport phenomena in up to three dimensions. At the base lie the nonlinear shallow water equations with a non-hydrostatic pressure term, among other things the model is fit for simulating wave transformations in surf and swash zones (Zijlema et al., 2011).

The accuracy of SWASH for the simulation of waves on fringing coral reefs has been confirmed (Zijlema, 2012). In this study, laboratory conditions by Demirbilek et al. (2007) have been reproduced by the model and the results are compared by measuring the bias (Equation 3.1) and Scatter Index SI (Equation 3.2), where ϕ_{obs} is the observed wave parameter from the laboratory data and ϕ_{comp} is the corresponding value computed by SWASH. N is the total number of data points in the given data set. The statistical analysis was performed for the significant wave height and the wave-induced set up.

$$\text{bias} = \frac{1}{\mathrm{N}} \sum_{\mathrm{i}=1}^{\mathrm{N}} \left(\varphi_{\mathrm{comp}}^{\mathrm{i}} - \varphi_{\mathrm{obs}}^{\mathrm{i}} \right) \tag{3.1}$$

$$\mathrm{SI} = \frac{\sqrt{\frac{1}{N} \sum_{i=1}^{N} \left(\varphi_{\mathrm{comp}}^{\mathrm{i}} - \varphi_{obs}^{j} \right)^2}}{\frac{1}{N} \sum_{i=1}^{N} \varphi_{obs}^{i}} \tag{3.2}$$

The bias for the wave height was found to be negative and relatively small at less than 5 mm compared to a typical wave height of 5 to 10 cm. Overall, the average Scatter Index turned out to be 5.5 %, with the lowest SI being found offshore and the largest SI being found near the wave break point. The modelled wave set up was systematically lower than the observed set up, with the highest SI again being found at the break point, probably due to the way the model deals with breaking waves. Onshore of the break point, the SI for the set up averages at 17.9 %, which is deemed acceptable.

All in all, the hydrodynamics on coral reef lined coasts such as energetic wave breaking and the transfer of energy from high to low frequencies, including resonance, was captured well in the model.

3.1.1. General SWASH settings

The discretization of the horizontal momentum equations is done by the second order backward upwind BDF scheme, which is the default for horizontal advective terms. The discretization of the vertical momentum equations is done through the standard first order upwind scheme.

SWASH makes uses of a staggered grid where the water level and non-hydrostatic pressure are defined at the center of each cell, whereas the velocity components are the primary unknowns and defined at the corner of the cell (Figure 3.1). To determine the bottom level of the bathymetry at the center of the cell, the mean between the values at the cell corners is computed. For steep slopes (which is the case for coral reef lined coasts), this is something to be aware of as this might influence flooding and drying.

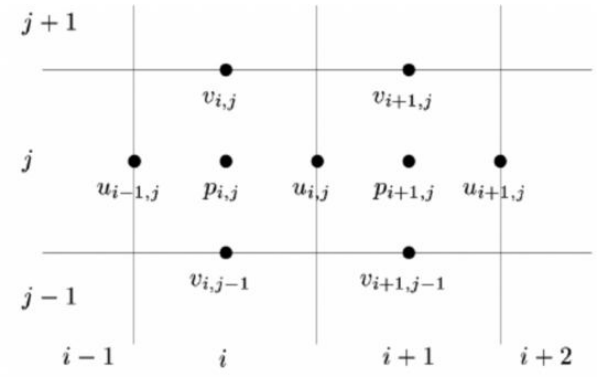

Figure 3.1: An example of what a staggered grid looks like. At the center of the cell, the water level and the non-hydrostatic pressure term are defined. The primary unknowns, the velocity components, are defined at the corner of the cells. From Scheidegger et al. (2004).

3.1.2. Numerical integration, discretization and implementation

There are various options for time integration of the continuity and momentum equations in SWASH, for instance with the second order leapfrog scheme. This scheme does not alter the wave amplitude while the numerical dispersion is favourable for wave propagation. Another option for time discretization is the explicit time stepping for horizontal advective and viscosity terms and semi-implicit time stepping using the $\theta-$method for both surface level and pressure gradients as well as the free-surface condition. If the time stepping is chosen to be semi-implicit, this induces unconditional stability for the propagation of waves, as the gradient of the water level in the momentum equations and the velocity divergence in the continuity equation are discretized implictly. This allows for larger time steps compared to the conditionally stable leapfrog scheme, yet the time step is still restricted due to the explicit integration of the horizontal advective terms.

For this project the time integration is chosen to be explicit, for simplicity reasons. This induces a time step restriction based on a maximum value for the Courant number. Since the area of interest lies with high waves, wave-wave interactions and wave breaking, the maximum Courant number is set to 0.5, as to properly capture wave behaviour. The bottom grid is set to structured, i.e. each interior cell is surrounded with an equal number of cells. Furthermore, 2 vertical layers are employed as to properly account for frequency dispersion of the waves. The horizontal grid size Δx is set at 1 m so a fine enough resolution is realised for the required data near the coral reef and beach toe, where the most transformations are expected to occur. Based on the value for Δx in the input grid and the Courant number, SWASH determines an appropriate Δt.

An overview of the settings used in the simulations for this project can be found in Table 3.1. In Appendix B the full SWASH file can be found that is used as the base for each of the simulations.

SWL	k	min depth	background viscosity	offshore boundary	breaking type	max Courant	Δx
1.6 m	2	0.005 m	0.0001	weakly reflective	non-hydrostatic	0.5	1 m

Table 3.1: The settings as chosen in SWASH. The full SWASH file of the base case can be found in Appendix B. The parameter k corresponds to the number of vertical layers in the simulation.

3.1.3. Initial and boundary conditions

Initial and boundary conditions can be imposed in SWASH in various ways. The longer the simulation time, the more significant the effects of the boundary conditions are compared to the initial conditions, which are often only of importance in the first stages of the simulation. However, a good correspondence between the initial and boundary conditions reduces the time it takes for the model to spin up and thus leads to a shorter required simulation time.

The initial condition imposed on the simulations is a water level of 1.6 m above the reef flat, which corresponds to the mean water level in the domain.

In order to ensure the waves are generated in a realistic manner, the waves should behave linearly at the location of the wave maker. A measure for the linearity of the waves is the dimensionless Ursell parameter (Equation 3.3), which is the ratio between the wave height over the water depth ($\frac{H}{h}$), times the ratio of the wave length over the water depth squared ($\frac{\lambda^2}{h^2}$) (Ursell, 1953). If waves are generated as specified in Section 3.3 in a water depth of 21.6 m, the Ursell number stays well below 25 and thus it can be assumed that the waves

are linear.

$$U = \frac{H\lambda^2}{h^3} \tag{3.3}$$

The ADDBOUNDWAVE command is used at the wave maker boundary to generate IG waves as a result of the incoming wave field. As the waves at the offshore boundary are located in intermediate water, the command is used to generate weakly nonlinear IG waves based on the work of Hasselmann (1962). Should the boundary be located in the surf zone (where the waves are strongly nonlinear) or in deep water (where a linear approximation suffices), the usage of this command should be reconsidered.

At the wave maker, a weakly reflective boundary is imposed as to allow for outgoing waves and to avoid artificial reflection. This radiation condition has been shown to lead to good results. (Zijlema et al., 2011)

Various options are available for the onshore boundary of the domain. If the bathymetry as shown in Figure 3.3 is imposed, no additional information is required for SWASH to recognize the boundary as 'closed' and thus as fully reflective. Alternatively, if a non-reflective boundary is required, the user can opt for a sponge layer or a Sommerfeld radiation condition. Both of these boundaries serve the purpose of absorbing the waves, representing a situation where the waves can freely leave the domain. More information about absorbing boundary conditions can be found in Section 3.4 and Appendix A.

3.2. Schematization of coral reef bathymetry

On Roi-Namur Island in the Republic of the Marshall Islands, a five-month field study was conducted to analyse the behaviour of low frequency waves on coral reef lined coasts (Cheriton et al., 2016). This field study has been the base for various analyses on long wave propagation on coral reef lined coasts (Gawehn et al. (2016), Quataert et al. (2020), Pomeroy et al. (2012b)). The schematized and simplified results from this analysis and its bathymetry lie at the base of the numerical approach of this research.

Various measuring stations were deployed on the reef (Figure 3.2). The bathymetry can roughly be characterized by a fore reef with a slope of 1/6 starting at 20 m below the reef flat, followed by a more gentle slope of 1/15 before reaching the reef crest. In total, the fore reef is 180 m wide. The reef flat is nearly horizontal at a slope of 1/700 and the distance between outer and inner locations of the reef flat is 270 m. Onshore of the reef flat a beach with a slope of 1/6 is found (Gawehn et al., 2016).

In this research, a further schematization of the bathymetry on Roi-Namur Island is made (Figure 3.3). The most offshore part is characterised by a horizontal bed at 21.6 m below mean water level (MWL) and 20 m below the reef flat. Offshore of the reef flat, the fore reef with a slope of 1/6 is found. The reef flat is a horizontal section stretching 270 m until the beach with a slope of 1/6 is reached at the onshore end. The reef crest is the transition from fore reef to reef flat and is located at 1.6 m below MWL. The beach toe is the transition between the reef flat and the beach and is also located at 1.6 m below MWL. For this bathymetry, the fundamental resonant period is found to be 272 s, neglecting possible set up due to wave breaking. The start of the fore reef is located at x = -120 m, the reef crest is located at x = 0 m and the beach toe is located at x = 270 m.

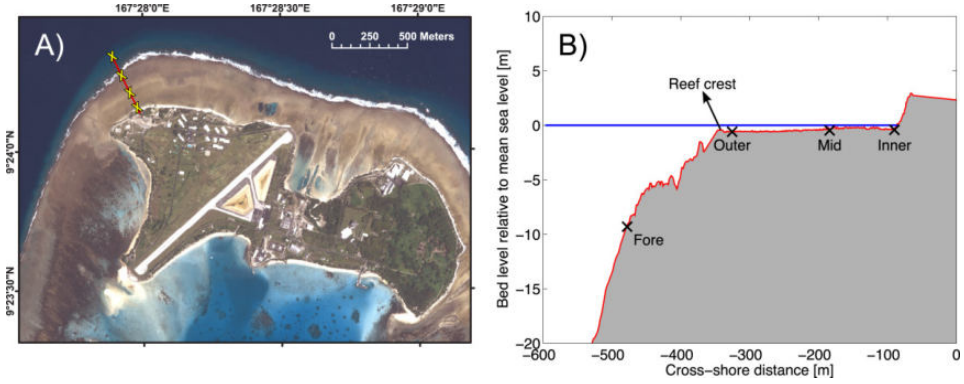

Figure 3.2: The site for the measuring devices as they were deployed on Roi-Namur Island during the 5 month field study. The figure on the left shows an aerial image of the site, the right figure displays a cross section of the bathymetry.

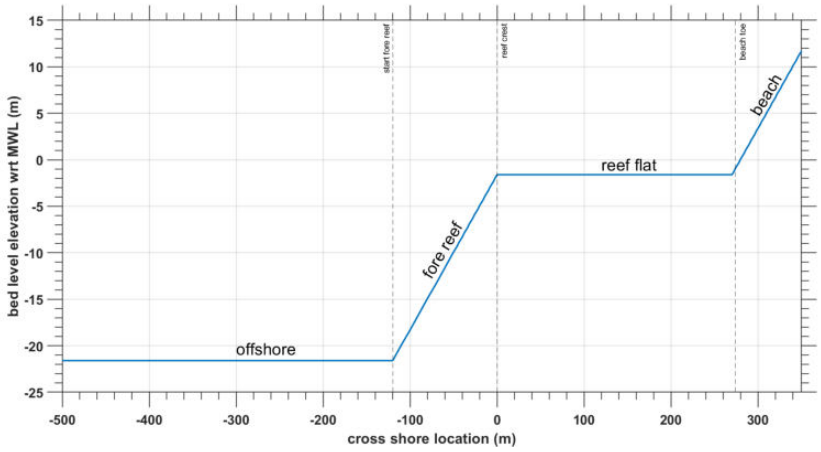

Figure 3.3: The schematization of the bathymetry as found on Roi-Namur Island. The schematization consists a 21.6 m deep offshore stretch, followed by a steep 1/6 fore reef onshore (starting at x = -120 m). The fore reef is separated from the horizontal reef flat by the reef crest (at x = 0 m). On the onshore boundary of the reef flat the beach toe is found (at x = 270 m), followed by a steep 1/6 beach. The reef flat has a still water depth of 1.6 m.

3.3. Schematization of the incoming wave field

To assess the behaviour of the coral reef flat under realistic conditions that the area is subject to, the statistics of the offshore field data by Cheriton et al. (2016) are used as a starting point (Table 3.2). To ensure the incoming wave energy in the model is in good correspondence with the wave energy that can be expected at coral reef lined coasts, the measured incoming SS energy is used as a starting point for this research. In Table 3.2, the variance var and H_{mean} are determined through Equations 3.4 and 3.5, and the data obtained through the field campaign.

$$H_s = 4\sqrt{var} \tag{3.4}$$

$$H_{mean} = \sqrt{2\pi var} \tag{3.5}$$

The statistics of this field study are the base of the bichromatic wave field that is imposed at the offshore boundary of the domain in this study. Having an incident bichromatic wave field allows for easy control of the wave group and IG characteristics.

In Table 3.2, the mean variance is given based on the mean value for the significant wave height H_s = $1.6m$. A larger variance corresponds to a more energetic wave field, whereas a smaller variance denotes a less energetic wave field. For the model, storm conditions are considered, i.e. rather energetic conditions compared to the mean values. These conditions have been shown to more often lead to resonance than more calm, non-storm conditions (Péquignet et al., 2014).

In Section 3.7.1, the parameters as imposed in SWASH are presented and elaborated on. Figure 3.4 gives an overview of the physical representation of considered variables.

$H_{s,mean}$	range H_s	$T_{s,mean}$	range T_p	$H_{max,mean}$	mean variance	range variance	H_{mean}
$1.6m$	$0.7-4.0m$	$10.9s$	$5.0-18.3s$	$2.9m$	$0.16m^2$	$0.03-1m^2$	$1.0m$

Table 3.2: Offshore field data obtained by Cheriton et al. (2016) at Roi-Namur island for regular, non-storm conditions (left of the double line). $H_{s,mean}$ and $T_{s,mean}$ correspond to the mean values of the significant wave height and the corresponding period, respectively. The data on the right of the double line is extracted of the presented data through Equations 3.4 and 3.5.

3.4. Analysis of the results

To distinguish between situations in which resonance does and does not occur, a method that quantifies resonant amplification must be applied. For this goal, resonant conditions must be compared to non-resonant conditions under the same circumstances. An overview of the qualification methods of resonance from other studies is given in Subsection 2.5.4. In this study, the focus lies on the comparison of various resonant modes

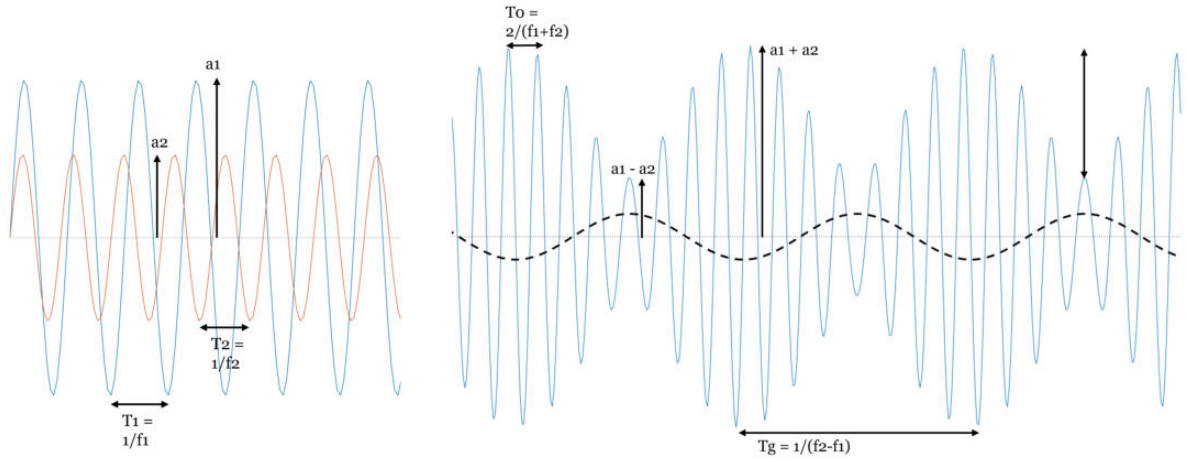

Figure 3.4: The individual waves of the incoming bichromatic wave field and their characteristics (left) along with the resulting bichromatic wave field (right) and its induced IG wave (dashed line, not to scale). T1, T2, a1 and a2 are defined as inputs of the model. It is always valid that a1 > a2 and T1 > T2. As a result, the highest amplitude of the wave group is a1 + a2, the frequency of the SS waves is the mean of the individual frequencies. The group frequency is the difference in frequencies of the two waves of the bichromatic wave field. The modulation is defined as the difference between the largest and smallest amplitudes of the waves in the wave group and is thus only dependent on a2.

to one another. Therefore, the quantification of resonance as presented in Subsection 2.5.4 does not suffice and additional quantification methods must be considered.

3.4.1. Quantifying resonance

To assess whether resonance on the reef flat occurs and to what extent, a method to distinguish resonant from non-resonant waves is required. For this purpose, a comparison is made for the incoming energy in the IG wave band between a simulation with a reflective beach, where resonance can occur, and a simulation with an absorbing boundary, where resonance cannot occur. Because of the complex nearshore processes and the largely unpredictable effects on the behaviour of both SS and IG waves, this method is used to account for these nearshore processes that are present in both resonant and non-resonant situations.

Equation 3.6 gives the amplification ratio (AR) that is used to determine the extent to which resonance occurs at the beach toe. It is defined as the ratio of the incoming IG wave energy at the beach toe for a simulation with a reflective beach ($E_{BT,R}$) over the energy at the beach toe for a simulation that has an absorbing onshore boundary ($E_{BT,A}$).

$$AR = \frac{E_{BT,R}}{E_{BT,A}} \tag{3.6}$$

If this AR is larger than 1, there is more energy at the beach toe for a reflective boundary than an absorbing boundary and thus resonance is expected to occur. For AR ≤ 1, no resonance is expected to be present on the reef flat.

Equation 3.7 gives the wave energy (E) as a function of the wave height.

$$E = \frac{1}{8}\rho g H_{IG,in,BT}^2 \tag{3.7}$$

In this analysis, the energy of the incoming IG wave at the beach toe is used for the AR (wave $H_{IG,in,BT}$). Therefore, AR is only representative of the incoming energy at the beach toe.

3.4.2. Resonant behaviour in total and incoming wave height

Regardless if resonance is occurring, a fully reflected standing wave results in an IG wave height (at the antinode at the beach toe) of twice the incoming IG wave. In case of resonance on the reef, energy is trapped on the coral reef flat, increasing the height of the incoming wave over time (Figure 3.5, left panel). In case of a non-resonant standing wave, stationary conditions are expected to be reached sooner as there is no energy trapped on the reef flat, the incoming IG wave is therefore similar to the wave height in the situation of an absorbing boundary condition.

When stationary conditions have been reached, the incoming IG wave height is larger for resonant conditions than for non-resonant conditions (Figure 3.5, right panel). Non-resonant conditions can be due to a non-resonant standing wave or an absorbing boundary at the onshore end of the reef flat.

Equations 3.8 to 3.12 can be used to determine the incoming ($\eta_{IG}^{in}(t)$) and outgoing ($\eta_{IG}^{out}(t)$) contribution to the instantaneous IG water elevation ($\eta_{IG}(t)$) based on the celerity of the incoming and outgoing waves (c_{in} and c_{out}, respectively) and the IG velocity component (u_{IG})(Guza et al. (1984), Lashley et al. (2020)). In this case, the IG waves are assumed to be travelling in shallow water and are bound to the wave group as they enter the domain.

$$\eta_{IG}(t) = \eta_{IG}^{in}(t) + \eta_{IG}^{out}(t) \tag{3.8}$$

$$\eta_{IG}^{in}(t) = \frac{\eta_{IG}(t) \cdot c_{in} + u_{IG}(t) \cdot h}{c_{in} + c_{out}} \tag{3.9}$$

and

$$\eta_{IG}^{out}(t) = \frac{\eta_{IG}(t) \cdot c_{out} - u_{IG}(t) \cdot h}{c_{in} + c_{out}} \tag{3.10}$$

where

$$c_{\text{in}} = \begin{cases} c_g & x < x_b \\ \sqrt{gh} & x \geq x_b \end{cases} \tag{3.11}$$

$$c_{out} = \sqrt{gh} \tag{3.12}$$

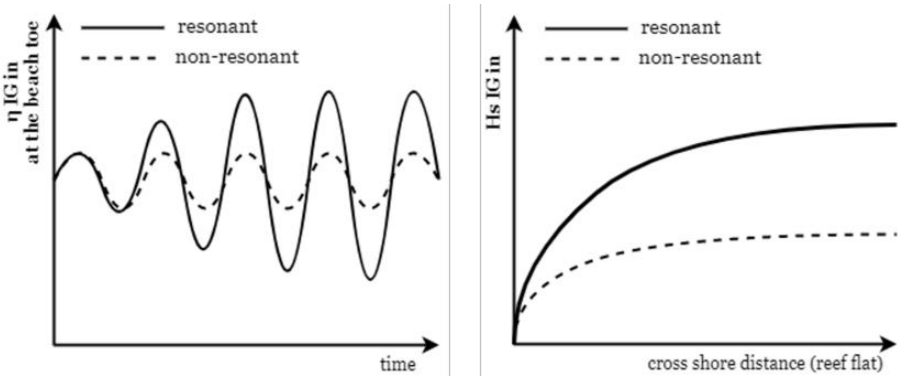

Figure 3.5: The behaviour of resonant (solid line) incoming IG waves compared to non-resonant (dashed line) incoming IG waves. Left: the development of the incoming IG wave over time. Right: the cross shore evolution $H_{s,IG,in}$ on the reef flat once stationary conditions are reached.

3.5. Filtering of the generated data

To assess the properties and behaviour of the waves on the reef flat, the acquired data set should representative of reality, accounting for spin-up time and filtering.

3.5.1. Removing the spin-up time

The model takes some time to spin up: it takes time for the wave conditions imposed at the boundary to reach the location of which the measurements are taken, as well as for the model itself to reach stationary conditions under the imposed boundary conditions (Figure 3.6). Therefore, the first 700 s of the model are removed to ensure no spin-up time is taken into account in the statistical analysis of the results.

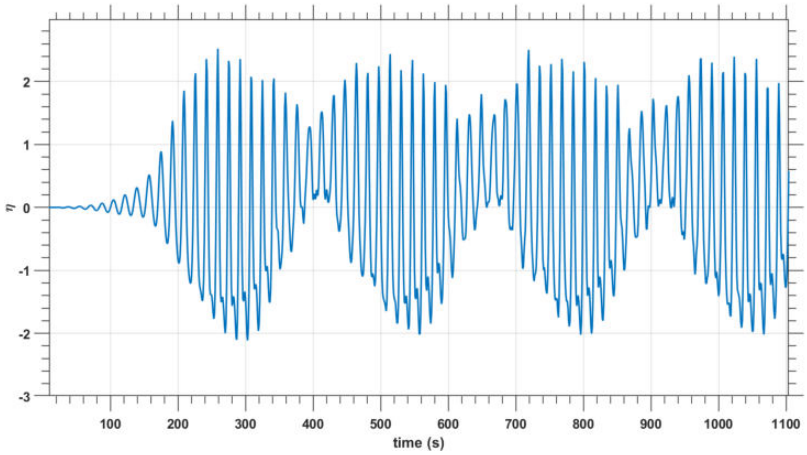

Figure 3.6: Total water elevation for a simulation with a group period of the bichromatic wave field of Tg = 127.5 s (non-resonant, T1 = 17 s, T2 = 15 s), a1 = 1.37 m, a2 = 0.72 m, and the fore reef has a slope of 1/6. The data displayed is retrieved from x = -260 m, 260 m offshore of the reef crest. The skewed behaviour of the wave is due to the non-linear behaviour of the wave at this location.

3.5.2. Fast-Fourier transformation and numerical artefacts

To analyse the behaviour of the IG waves on the reef flat and offshore, the IG component must be isolated from the total elevation signal. This is done through a fast Fourier transformation with a cutoff frequency $f_{cut} = 0.015\,s^{-1}$, which is 1/4 of the smallest SS wave frequency. A fast Fourier transformation has been shown to adequately work for a bichromatic wave field (van Dongeren et al., 2007).

After filtering, the water level at the beginning and end of the simulation does not correspond with what is expected or the stationary conditions of the middle of the time series (Figure 3.7). Therefore, an extra 100 s is to be removed from the beginning and end of the time series.

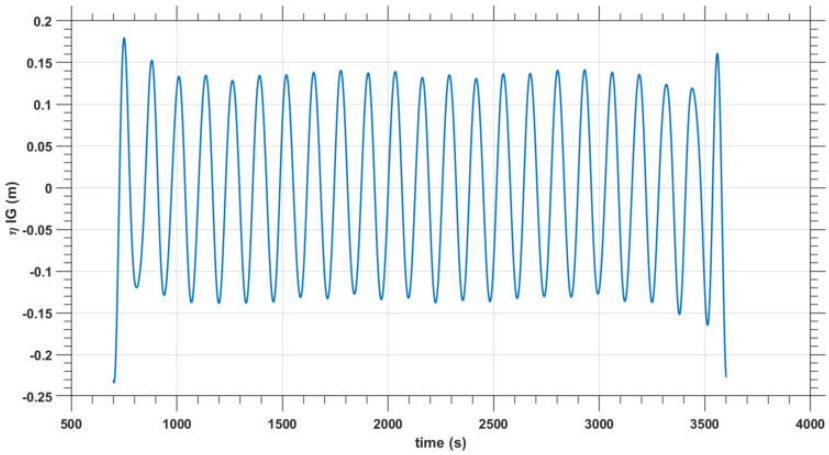

Figure 3.7: The IG water elevation as a function of time after the spin up time is removed. The total water elevation is split using a fast Fourier transformation, which induces artefacts at the beginning and end of the time series. Tg = 127.5 s, T1 = 17 s, T2 = 15 s, a1 = 1.37 m, a2 = 0.72 m and the fore reef has a slope of 1/6. The data displayed is retrieved from x = -260 m, 260 m offshore of the reef crest.

3.6. Absorbing onshore boundary condition

To quantify resonance at the beach toe, a situation with and without a reflective beach is compared, i.e. a sponge layer (a built-in option in SWASH) is imposed at the onshore boundary, which absorbs any incoming energy and prohibits reflection at this location. Therefore, no energy can build up over the reef flat. Thus, under the same circumstances as for a reflective beach at the onshore location, this could serve as a comparison between resonant and progressive situations, taking into account nearshore processes present on the reef (Figure 3.8).

In SWASH, the sponge layer is defined as an exponential decay function on the momentum equations in the domain of the sponge layer to dissipate both wave height and velocity (Zou and Zhang, 2013). The sponge layer starts at x = 270 m and has a width of 200 m.

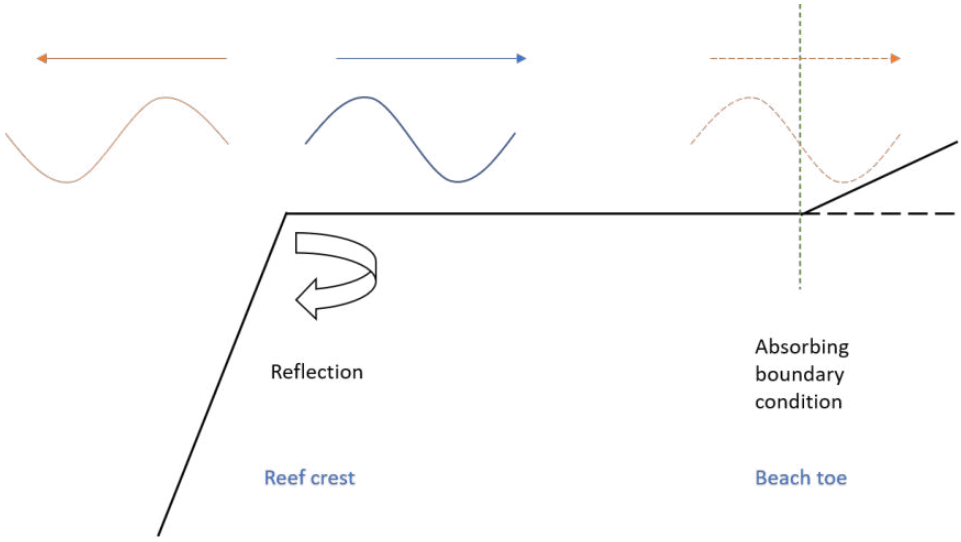

Figure 3.8: Schematization of the reef in case an absorbing boundary condition is imposed at the location of the beach toe (dashed line). This implies no energy is reflected at this location, so there cannot be a build up of energy on the reef flat. For a situation with a beach (solid line), reflection and therefore the trapping of IG wave energy is possible on the reef flat

3.6.1. Performance of the sponge layer

The incoming IG wave height varies based on the periods of the individual waves of the incoming bichromatic wave field, this is visible in simulations with both a beach boundary and a sponge layer boundary (Figure 3.9. The ratio of the incoming IG wave height at the beach toe does not vary as a function of the wave period of the bichromatic wave field and remains constant between 0.79 and 0.87 (right). The closer this ratio is to 1, the better the correspondence of non-resonant behaviour between the beach boundary and the sponge layer boundary simulation. Therefore, a value as close to unity as possible is desired.

The incoming IG wave height decreases for a higher value for a1 (Figure 3.10), this can be explained by considering the fact that the variance of the bichromatic wave field is at a constant value. Thus, as a1 increases, a2 must decrease and there is a smaller modulation, thus less IG wave energy present. The ratio between the incoming IG wave height at the location of the beach toe for the beach versus sponge layer boundary remains constant between 0.81 and 0.86 (Figure 3.10, left).

In general, the mean ratio of $\frac{H_{s,IG,in,beach}}{H_{s,IG,in,sponge}}$ is 0.85 and the standard deviation of the ratio is found to be 0.055. This statistical data is based on the data seen in Figure 3.9, Figure 3.10 and data from the simulations presented in Chapter 4 for a non-resonant group period of 127.5 s. In Appendix A, detailed results are shown for the performance of the sponge layer compared to the beach boundary as well as alternative absorbing boundary conditions.

In Chapter 4 the evolution of the incoming wave is shown for various group periods under different circumstances. From this chapter, it is evident that there appears to be resonant amplification even for very large values of Tg. Therefore, only small values of Tg are taken into account for the assessment of the performance of the sponge layer. Figure 3.11 displays the absorbing quality of the sponge layer for both small and large values of Tg. However, uncertainties should be considered when the sponge layer is considered for large values of Tg.

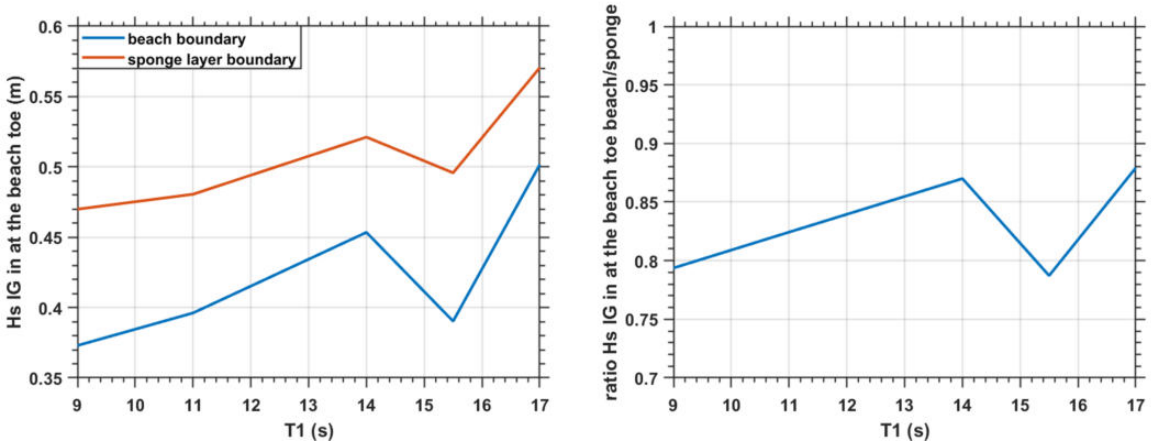

Figure 3.9: The incoming significant IG wave height at the beach toe (left) for simulations with a beach boundary (blue) and a sponge layer boundary (orange) and the ratio of these wave heights (right). Tg = 127.5 *s* (non-resonant). The varying parameters are T1 and T2. The ratio of the incoming IG wave height for the two boundaries is somewhat constant ranging between 0.79 and 0.87.

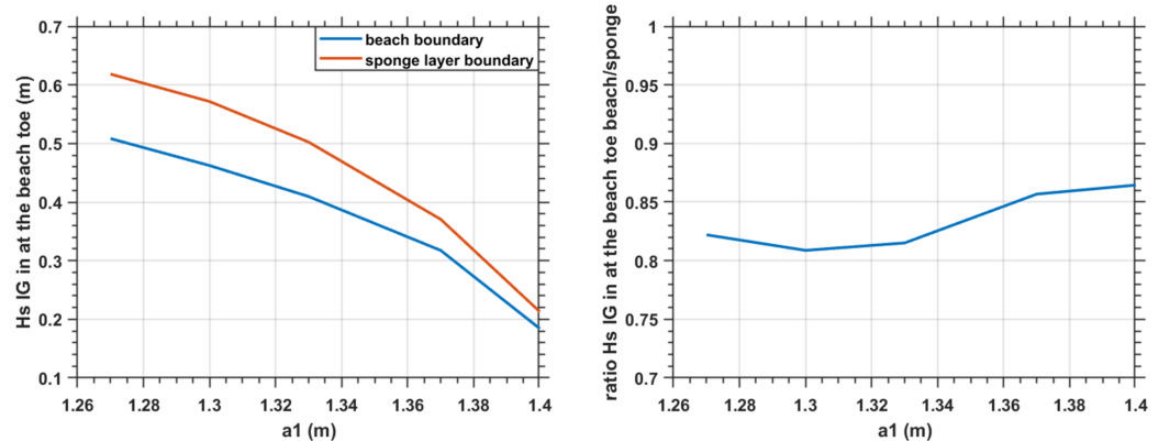

Figure 3.10: The incoming significant IG wave height at the beach toe (left) for simulations with a beach boundary (blue) and a sponge layer boundary (orange) and the ratio of these wave heights (right). Tg = 127.5 *s* (non-resonant). The varying parameters are a1 and a2, while the variance is kept constant.The ratio of the incoming IG wave height for the two boundaries is somewhat constant ranging between 0.81 and 0.86.

3.6.2. Reflection coefficient

To assess the absorbing properties at individual locations, a reflection coefficient (RC) is considered (Equation 3.13). It is defined as the ratio of the square of the outgoing significant wave height ($H^2_{s,out}$) over the square of the incoming significant wave height ($H^2_{s,in}$). The RC can be considered at various locations on the domain, as well as for the different components of the wave (SS and IG).

$$RC = \frac{H^2_{s,out}}{H^2_{s,in}} \tag{3.13}$$

The absorbing sponge layer boundary absorbs all IG and SS wave energy (Figure 3.11, blue dots). For a reflective beach boundary, IG waves are nearly fully reflected (Figure 3.11, left panel, red dots), whereas the SS waves are partially reflected and partially dissipated on the beach (Figure 3.11, right panel, red dots).

3.7. Numerical set up

To answer the research questions defined in Chapter 1, various series of simulations are conducted. The base of each simulation evaluated in this project is the same, these conditions are shown in Table 3.3. Since the analysis is done for different group periods Tg, the value for T2 is varied accordingly.

The effects of the change in a2 (thus modulation of the bichromatic wave field), a1 (the energy of the

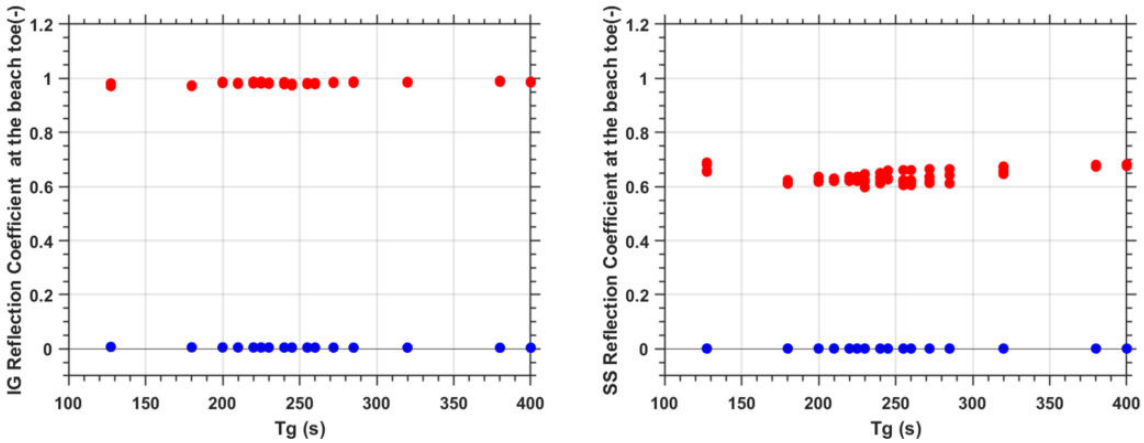

Figure 3.11: The Reflection Coefficient for IG waves (left) and SS waves (right) at the location of the beach toe for various group periods. Each group period contains two data points: one for a beach boundary (red) and one for a sponge layer boundary (blue)

a1	a2	Hmean	Hs	var	T1	fore reef slope	Manning friction	MWL
1.37	$0.72m$	2.74 m	4.73 m	1.2 m^2	17 s	1/6	0 $m^{-1/3}/s$	1.6 m

Table 3.3: The values for the conditions of the simulations in a reference case. T2 is varied in such a way to achieve the desired group period of the incoming bichromatic wave field.

incoming SS wave field without altering the modulation), individual wave period T1 of the incoming bichromatic wave field and the fore reef slope are assessed by considering the resonant behaviour induced by each of the variables as a function of wave group period.

Table 3.4 displays the values of the incoming wave periods and their frequencies, as well as the mean frequency f0 and its period T0. When variations in a2, a1 and the fore reef slope are considered, all variables are subject to each of the conditions found in Table 3.4. If the effect of variations in T1 is under consideration, the values for T2 change accordingly. This is elaborated on in Subsection 3.7.1.

T1 (s)	f1 ($1/s$)	T2 (s)	f2 ($1/s$)	T0 (s)	f0 ($1/s$)	Tg (s)	fg ($1/s$)
17	0.0588	15	0.0667	15.94	0.0627	127.5	0.0078
		15.53	0.0644	16.23	0.0616	180	0.0056
		15.67	0.0638	16.31	0.0613	200	0.0050
		15.73	0.0636	16.34	0.0612	210	0.0048
		15.78	0.0634	16.37	0.0611	220	0.0045
		15.81	0.0633	16.39	0.0610	225	0.0044
		15.83	0.0632	16.40	0.0610	230	0.0043
		15.88	0.0630	16.42	0.0609	240	0.0042
		15.9	0.0629	16.43	0.0608	245	0.0041
		15.94	0.0627	16.46	0.0608	255	0.0039
		15.96	0.0627	16.47	0.0607	260	0.0038
		16	0.0625	16.49	0.0607	272	0.0037
		16.04	0.0623	16.51	0.0606	285	0.0035
		16.14	0.0620	16.56	0.0604	320	0.0031
		16.27	0.0615	16.63	0.0601	380	0.0026
		16.31	0.0613	16.65	0.0601	400	0.0025

Table 3.4: The values for T1, f1, T2, f2, T0, f0, Tg anf fg that each of the variations in parameters is subject to. The theoretical fundamental period of the reef flat, without considering set up, is 272 s.

3.7.1. Parameter spaces

Figure 3.12 depicts the parameter spaces for the variations in a2 (left) and a1 (right). Tables 3.5 and 3.5 display the implications of the variations in a1 and a2 for the incoming bichromatic wave field, respectively. All

variations in a1 and a2 are subject to the mean and group periods presented in Table 3.4. The variables are implemented at the offshore boundary of the numerical domain.

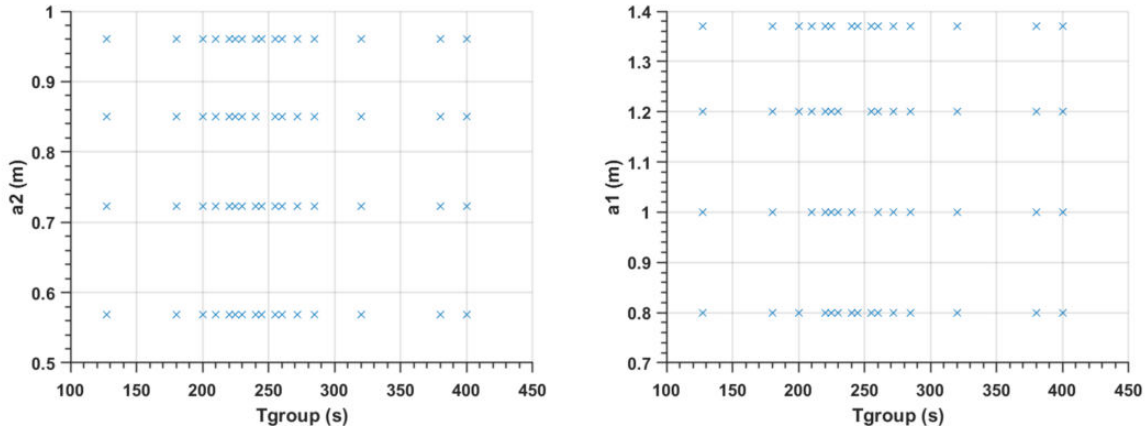

Figure 3.12: The parameter space for the simulations that assess the influence of the amplitudes of the incoming SS wave field on resonance on the reef flat. A2 is varied from 0.57 m to 0.96 m (left). An increase in the value for this parameter results in an increased energy of the reef flat (variance of 1.1 m^2 to 1.4 m^2, respectively) as well as an increased modulation. A1 is varied from 0.8 m to 1.37 m (right). This parameter does not influence the modulation of the incoming wave field.

varied parameter	**a2** (m)	**a1** (m)	**Hmean** (m)	**var** (m^2)	**Hs** (m)
a2	0.57	1.37	2.63	1.1	4.2
	0.72		2.75	1.2	4.38
	0.85		2.86	1.3	4.56
	0.96		2.97	1.4	4.73

Table 3.5: The variations in the value for a2 to assess the behaviour of this parameter under different conditions and incoming wave groups. All four values of a1 are combined with the variations in T2 and Tg as presented in Table 3.4.

varied parameter	**a2** (m)	**a1** (m)	**Hmean** (m)	**var** ($m2$)	**Hs** (m)
a1	0.7233	0.8	1.91	0.58	3.05
		1.0	2.19	0.76	3.49
		1.2	2.48	0.98	3.96
		1.37	2.75	1.2	4.73

Table 3.6: The variations in the value for a1 to assess the behaviour of this parameter under different conditions and incoming wave groups. All four values of a1 are combined with the variations in T2 and Tg as presented in Table 3.4.

Figure 3.13 gives the parameter spaces under consideration for the variation in T1 (left) and fore reef slope (right). When the fore reef slope is considered, this has no implications for the incoming wave field offshore of the coral reef. The variations in fore reef slope are subject to the parameters presented in Table 3.3. Figure 3.14 gives a visualisation of the different fore reef slopes under consideration.

Table 3.7 shows the parameter ranges under considered for when the effect of variations in T1 is assessed. The ranges in T2, f2, T0 and f0 indicate the minimum and maximum values of each parameter, in total each value of T1 is subject to 16 variations in T2 and thus T0.

3.8. The mean water level on the reef flat and theoretical resonant modes

The theoretical eigenperiod of the coral reef is determined by the integration of the water depth over the reef flat (Equation 2.2). As the mean water level varies in each situation, a representative mean water level is chosen. In Section 4.1, the cross shore evolution of the mean water level for the various situations is treated more extensively.

varied parameter	T1 (s)	f1 ($1/s$)	T2 (s)	f2 ($1/s$)	T0 (s)	f0 ($1/s$)
T1	19	0.053	16.54 - 18.14	0.060 - 0.055	17.70 - 18.52	0.056 - 0.054
	17	0.059	15.0 - 16.31	0.067 - 0.061	15.87 - 16.67	0.063 - 0.060
	14	0.071	12.61 - 13.53	0.079 - 0.074	13.33 - 13.79	0.075 - 0.073
	11	0.091	10.13 - 10.71	0.099 - 0.93	10.53 - 10.87	0.095 - 0.092

Table 3.7: The variations in the value for T1 to assess the behaviour of this parameter under different conditions and incoming wave groups. The simulations for each of these values are subject to the values for Tg presented in Table 3.4.

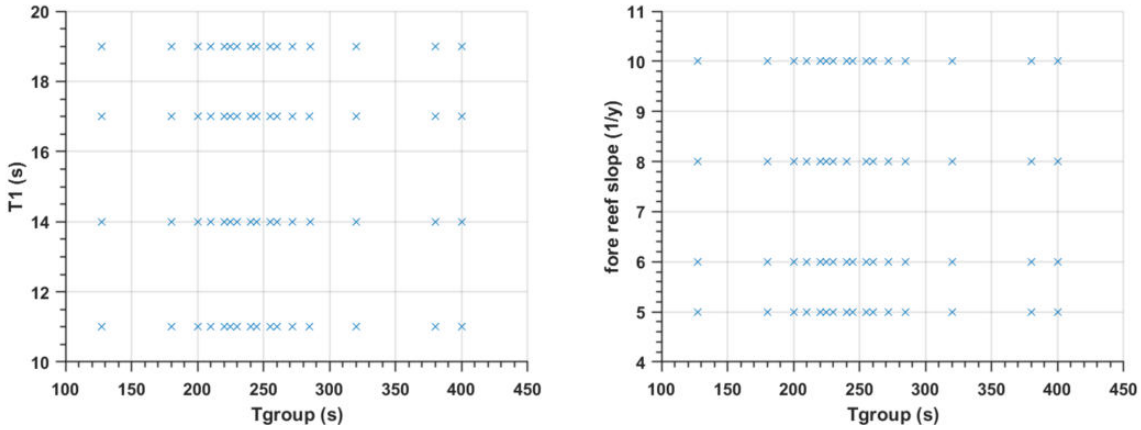

Figure 3.13: The parameter space for the simulation that assess the influence of the SS wave period (T1, left) and the fore reef slope (right). T1 is varied from 11 s to 17 s, the fore reef slope is varied from a steep slope of 1/5 to a gentle slope of 1/10.

3.8.1. Mean water level for different SS group periods

The mean water level at the beach toe increases slightly when the group period increases for all variations in a1 (Figure 3.15). Additionally, a slight 'bump' is visible near the most theoretically found group periods (around Tg = 250 s). However, all these variations over Tg are deemed to be small compared to the variations of MWL at the beach toe for different a1. Therefore, the mean water level that is used to determine the theoretical eigenperiods is chosen at a single value for Tg around the period for which maximum amplification occurs (Tg = 240 s, see also Chapter 4).

Additionally, it can be seen that the MWL at the beach toe is larger for larger values of a1. This is due to the increased SS wave energy that enters the reef flat, breaks, and thus induces a large set-up (Section 4.1).

3.8.2. Water depth integration over the reef flat

To determine the theoretical period for which resonance occurs, the water depth over the reef flat is integrated (Equation 2.2). When the coral reef bathymetry is approached as harbour-like, thus semi-open (Figure 2.7), the node of the resonant wave form is located at the reef crest. However, this might not be the actual location of the node of the resonant IG wave.

The smallest IG wave height for the resonant reference case is located just offshore of the reef crest (Figure 3.16). This location is used as the offshore point of water depth integration for determination of the theoretical fundamental eigenperiod. Equation 2.2 is extended to Equation 3.14.

$$f_{\text{node}} = \frac{1}{4}\left(\int_{x_{\text{Hs,IG,min}}}^{x_{\text{shoreline}}} \frac{1}{\sqrt{gh(x)}}\,dx\right)^{-1} \tag{3.14}$$

This approach increases the theoretical fundamental eigenperiod by 0.8 to 3%, which leads to better correspondence between the observed and theoretical resonant periods (see Section 4.6, as the observed resonant period is always larger than the theoretically found resonant period).

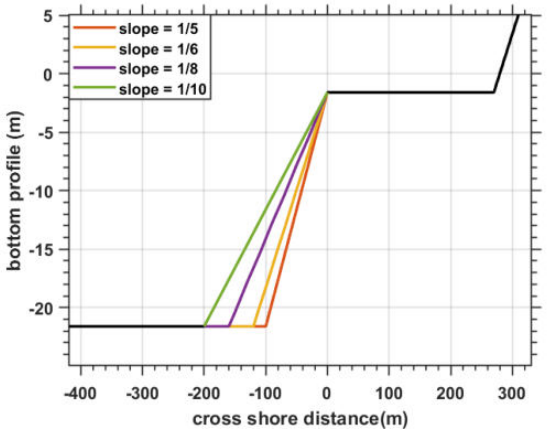

Figure 3.14: A visualisation of the effect of the variations in fore reef slope on the bathymetry under consideration. The black line corresponds to the common bathymetry which is valid in all the considered circumstances.

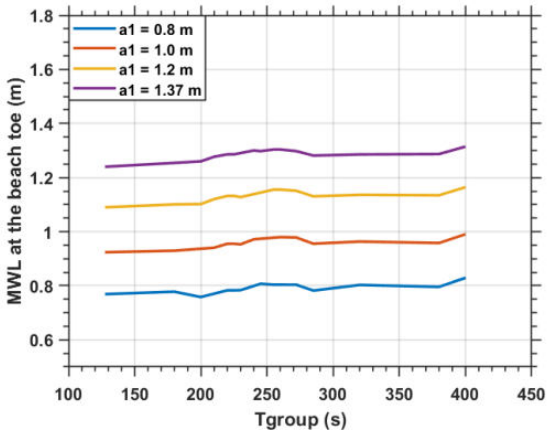

Figure 3.15: The mean water level (MWL) at the beach toe for different values of incoming wave amplitude a1 under different group periods. A2 = 0.72 m, T1 = 17 s and the fore reef has a slope of 1/6. The MWL is shown with respect to the still water level of 0 m, which is 1.6 m above the reef flat.

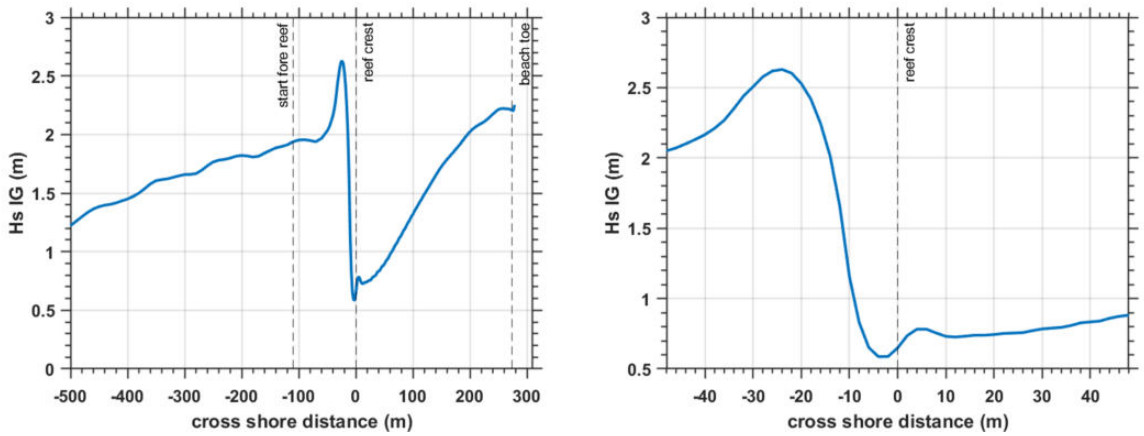

Figure 3.16: The cross shore evolution of the IG wave for the reference case, with a resonant group period of Tg = 240 s. T1 = 17 s, a1 = 1.37 m, a2 = 0.72 m and the fore reef has a slope of 1/6. The right panel shows the same information zoomed in on the area around the reef crest.

4
Results

This chapter deals with the results of the numerical simulations. It contains the non-resonant behaviour of the mean water level, the SS wave component and the IG component; the sensitivity of the maximum wave height to the varied parameters; the maximum relative and absolute amplification under various circumstances; the period for which maximum amplification occurs; and IG and SS behaviour over time.

4.1. Sea swell wave and mean water level behaviour

In this section, the non-resonant cross shore evolution of the SS wave component and the mean water level are presented for variations in the parameters a2, a1, T1 and the fore reef slope. As discussed in Subsection 2.2.2, the expected set up on coral reefs due to SS wave breaking is higher than the set up on sandy sloping beaches under the same conditions.

4.1.1. SS wave and MWL behaviour for variations in a2

Offshore of the start of the fore reef, oscillations in SS wave height are visible due to wave reflection (Figure 4.1, left panel). At this location, the larger incoming wave amplitude a2 results in a larger offshore wave height. On the fore reef the waves can be seen to shoal. When the SS waves travel on the reef flat, they break and the wave energy is dissipated from this part of the wave spectrum. The wave height on the reef flat is similar for the different values of a2.

The mean water level on the reef flat does not vary a lot based on the value for the incoming wave amplitude a2 (Figure 4.1, right panel). A large value for a2 results in a large value for the maximum wave amplitude of the bichromatic wave field, yet since a2 < a1, a large a2 also decreases the the wave height of the smallest wave of the wave group. The variations in H_{mean} are limited if a2 is varied (Table 3.5). From Equation 3.4 it follows that an increase in a2 positively affects the variance, thus the energy approaching the reef flat.

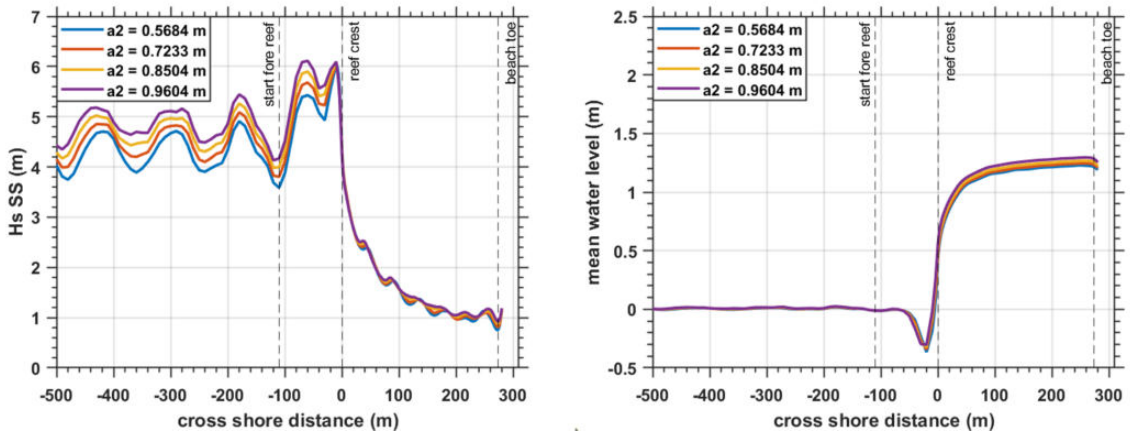

Figure 4.1: The cross shore MWL (left) and significant SS wave height (right) dependent on the offshore wave amplitude a2. Tg = 127.5 *s*, T1 = 17 *s*, T2 = 15 *s*, a1 = 1.37 *m* and the fore reef has a slope of 1/6.

4.1.2. SS wave and MWL behaviour for variations in a1

For all variations in a1, the cross shore evolution of the SS wave height displays a standing pattern offshore of the fore reef, after which the waves shoal up until the reef crest, and dissipate their energy on the reef flat (Figure 4.2, left panel). Similar as to the results for variations in a2, a larger value for the incoming wave height results in a larger offshore SS wave height.

he set up on the reef can be seen to be highest for the simulations where a1 is largest (4.2, right panel) . The set up is less for the smaller values of a1, the difference between set up is similar for each difference in a1, indicating a constant relationship between set up and amplitude a1.

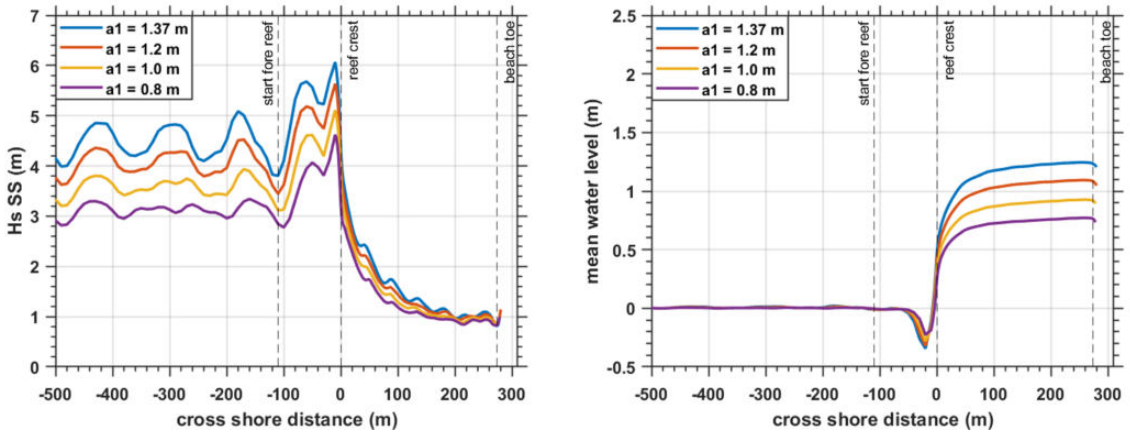

Figure 4.2: The cross shore MWL (left) and significant SS wave height (right) dependent on the offshore wave amplitude a1. Tg = 127.5 *s*, T1 = 17 *s*, T2 = 15 *s*, a2 = 0.72 *m* and the fore reef has a slope of 1/6.

4.1.3. SS wave and MWL behaviour for variations in T1

Offshore of the reef crest, the SS wave height can be seen to be largest for the largest values of T1 (Figure 4.3, left panel). Cross shore oscillations in SS wave height are present due to reflection on the fore reef. The range of the maximum offshore SS wave height varies from 4.8 *m* for T1 = 11 *s*, to 5.0 *m* for T1 = 19 *s*, which is all in the same order of magnitude. Onshore of the reef crest, on the reef flat, the behaviour of the SS waves with a longer period differs from the behaviour of the shorter waves by the rate at which energy is dissipated. At the reef crest, the significant wave height is similar for all cases, when propagating shoreward the SS wave energy is dissipated faster for the shorter waves. At any given point on the reef flat, the significant SS wave height is larger for the longer wave periods, this may be due to the reduced steepness of the wave: a longer period leads to a longer wave length.

The set up is largest for the largest value of T1 and smallest for the smallest value of T1. This in accordance with findings by Gourlay (1996), as the SS wave period influences the relative set-up parameter (Subsection 2.2.2). The difference in set up between two values for T1 is not constant, accounting for the non-equal value of $\Delta T1$.

4.1.4. SS wave and MWL behaviour for variations in the fore reef slope

For a steep fore reef slope, cross shore oscillations due to reflections are visible offshore of the fore reef (Figure 4.4, left panel). For a more gentle fore reef slope, this standing wave pattern is less pronounced. Moreover, SS waves approaching a gentle fore reef start to shoal and break more offshore than the waves approaching a steeper fore reef, due to the fore reef stretching further offshore (Figure 3.14). On any given location on the reef flat, the significant SS wave height is larger for the simulations with a steep fore reef than when a more gentle fore reef is considered.

The mean water level on the reef flat is highest for the steeper fore reef slope of 1/5 than for a more gentle fore reef slope of 1/10 (Figure 4.4, right panel), which corresponds to larger SS waves being present on the reef flat for steeper slopes. Furthermore, the maximum set down on the fore reef is largest for the steeper slopes. The location at which maximum set down occurs for the steepest fore reef slopes is more onshore than the for the cases with a more gentle fore reef slope.

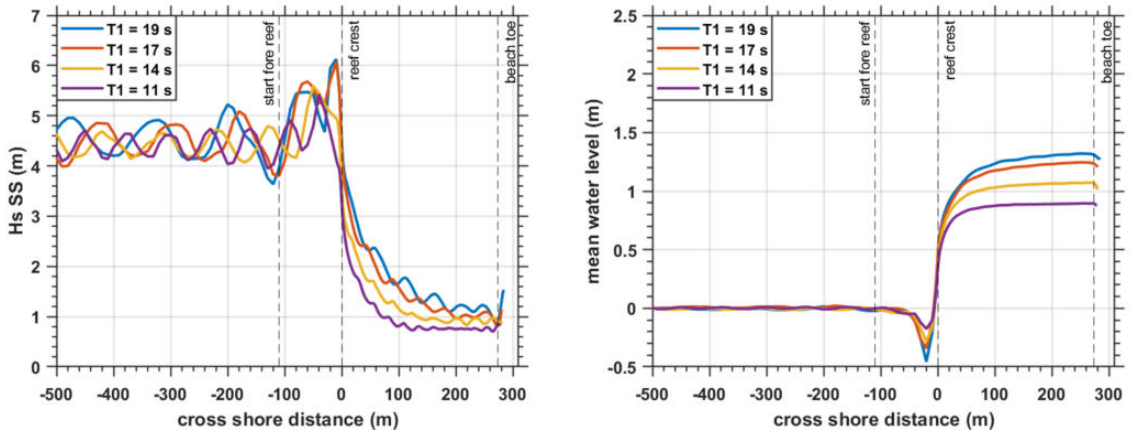

Figure 4.3: The cross shore MWL (left) and significant SS wave height (right) dependent on SS wave period T1. Tg = 127.5 s, a2 = 0.72 m, a1 = 1.37 m and the fore reef has a slope of 1/6.

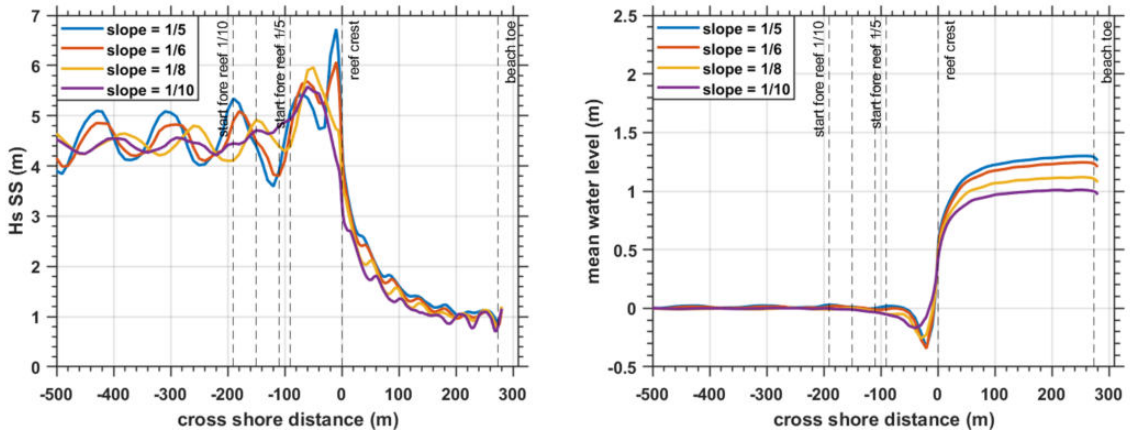

Figure 4.4: The cross shore MWL (left) and significant SS wave height (right) dependent on the fore reef slope. Tg = 127.5 s, T1 = 17 s, T2 = 15 s, a2 = 0.72 m and a1 = 1.37 m

4.2. Non-resonant IG wave behaviour

To assess the amplification of the IG waves on the reef flat due to resonance, the behaviour of IG waves without resonance must be understood. For this purpose, the cross shore evolution of the incoming IG wave is assessed for a beach boundary simulation where a non-resonant Tg is imposed (Tg = 127.5 s) as well as the value of the incoming significant IG wave height ($H_{s,IG,in}$)at the beach toe for various values of Tg when a sponge layer boundary is imposed at the onshore end of the domain.

4.2.1. Total, incoming and outgoing IG wave height

In the total cross shore IG wave signal (Figure 4.5, left panel), nodes are visible at x = -360 m and at x = 120 m. These nodes are a results of the interaction between the incoming and outgoing wave, resulting in a standing wave pattern in the total IG wave.

In the incoming IG wave (Figure 4.5 right panel, blue line), a clear increase in the wave height is visible on the fore reef. Just offshore of the reef crest, the incoming IG wave decreases in height and gradually increases again over the reef flat. The outgoing IG wave (Figure 4.5, right panel, orange line) is more constant throughout the domain, with a wiggle near the reef crest.

Offshore of the start of the fore reef, the height of the incoming IG wave is equal to the bound long wave. On the fore reef, the incoming IG wave signal is determined by the shoaling of the released bound long wave and the IG wave generated in positive x direction through break point forcing. On the reef flat, the incoming IG wave height is determined by the incoming IG wave that is able to propagate onto the reef flat, consisting of both the released bound long wave and the break point generated IG wave. However, these two components

have a phase difference of 180°(see also Subsection 2.3.2 and Section 4.5). Additionally, on the reef flat the outgoing IG wave that is reflected onshore at the reef crest is also contributing to the incoming IG wave height.

On the reef flat, the outgoing IG wave is equal to the reflected IG wave at the beach toe. Offshore of the reef crest, the outgoing IG wave is composed of the seaward propagating outgoing IG wave, the reflected released bound wave and the IG wave generated in negative x direction by break point forcing.

In Appendix C the contribution of the shoaled free IG wave compared to the break-point generated wave height is elaborated on.

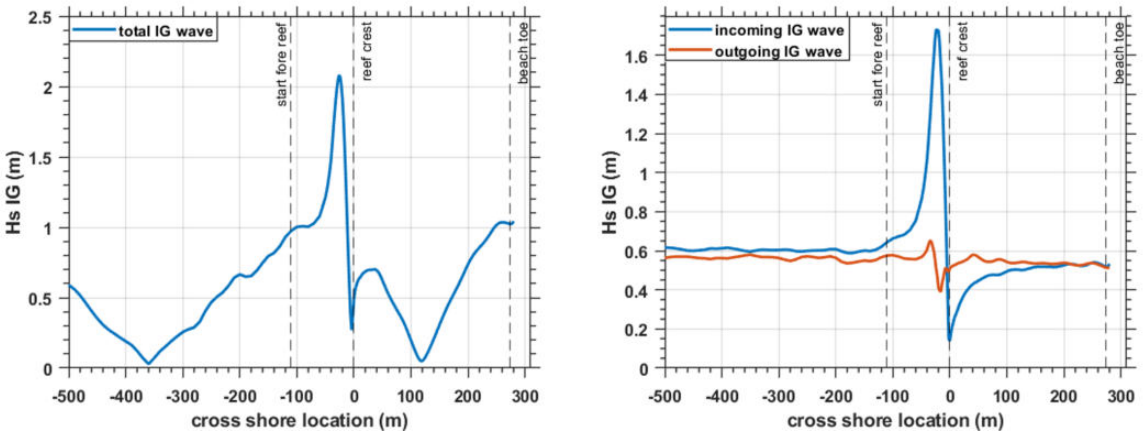

Figure 4.5: The cross shore evolution of the total significant IG wave height (left) and the incoming and outgoing component of the IG wave (right). T1 = 17 s, a1 = 1.37 m, a2 = 0.72 m and the fore reef has a slope of 1/6. The incoming wave group has a period of 127.5 s and is thus non-resonant.

4.2.2. Effects of the variations of the amplitudes of the SS waves

For variations in a1 and a2, offshore of the reef crest the incoming IG wave height is determined by the amount of SS wave energy entering the domain (Figure 4.6). At this location, the IG wave height is solely determined by the bound long wave. The waves are travelling in intermediate water, thus the IG wave height is dependent on the modulation of the bichromatic wave (a2, left panel), as well as the mean height of the wave field (a1, right panel) as this determines the deviation of a sinusoidal wave in this region of intermediate water depth, thus the difference in momentum transported by the largest waves and smallest waves of the bichromatic wave field (Figure 4.6).

As the IG wave approaches the fore reef, the wave height increases to a 'spike' just offshore of the reef crest in all cases. Due to the nature of the separation mechanism the accuracy of the actual height of the incoming wave is doubtful in this area (see also Section 3.1). It should be noted that for the situations where a1 is varied (Figure 4.6, right panel), the modulation of the incoming bichromatic wave field is the same for all cases, as this is solely determined by a2. The magnitude of the modulation determines the amplitude of the cross shore oscillations of the break point. The mean location of the oscillations is determined by the energy of the incoming bichromatic wave field, as higher waves break further offshore (Symonds et al., 1982).

A larger value of a2 leads to a larger incoming IG wave on the reef flat (Figure 4.6, left panel). This can be explained by the fact that the magnitude of a2 determines the modulation and this lies at the base of IG wave generation (Section 2.3). For the variations in a1,a larger value of a1 leads to less incoming IG energy on the reef flat (Figure 4.6, right panel). For the three lower values of a1, the incoming IG wave height on the reef flat is in the same order of magnitude.

Additionally, the relation in the magnitude of the incoming IG wave on the reef flat seems to have a dependence on the modulation (a2) that is non-linear. For larger values of the modulation, where the values of a1 and a2 are closer, the difference in the incoming IG wave height is smaller than for a smaller modulation (Figure 4.6, left panel). Practically: the incoming IG wave height for a2 = 0.72 m is much larger than for a2 = 0.57 m compared to the difference in IG wave height for a2 = 0.96 m and a2 = 0.85 m. The difference in variance between two successive variations in a2 is 0.1 m^2.

Thus, it can be seen that offshore of the reef crest, where the bound long wave is considered, the incoming IG wave height is dependent on the incoming energy of the SS component of the wave field. However, on the reef flat, the size of the incoming IG wave is predominantly determined by the modulation, thus the value of

a2. When a1 is varied, different mechanisms appear to play a role that result in a lower incoming IG wave height for larger values of a1.

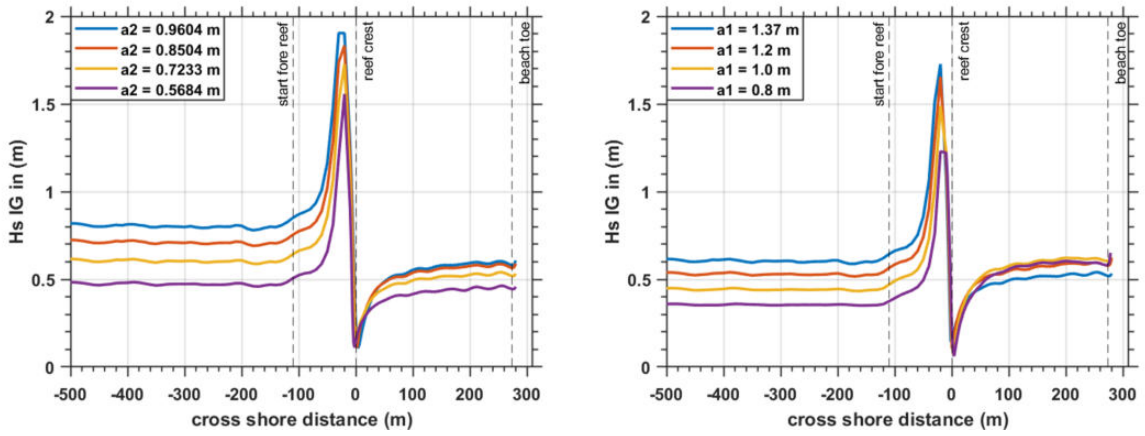

Figure 4.6: The cross shore evolution of the incoming significant IG wave height for variations in amplitude of the smallest wave of bichromatic wave field (a2, left) and the largest wave of the bichromatic wave field (a1, right). The group period is non-resonant at 127.5 *s*, T1 = 17 *s* and the fore reef has a slope of 1/6. A larger a2 means that the ratio of a2/a1 is larger. In the situations where a1 is varied, a2 is constant at 0.72 *m*. Therefore, a larger value of a1 means a smaller value of a2/a1. When a2 is varied, a1 is constant at 1.37 *m*.

4.2.3. Effects of the variations in incoming SS wave period

Offshore of the reef flat the incoming IG wave height increases as periods of the SS waves increase (Figure 4.7, left panel). The largest offshore IG waves also corresponds to the largest wave at the location near the reef crest. The incoming IG wave height as a function of the group period depends on the incoming SS wave period (Figure 4.7, right panel). For small values of Tg, T1 = 11 *s* leads to the smallest incoming IG wave. For large values of Tg, T1 = 14 *s* leads to the smallest incoming IG wave. It should be noted that the relation between incoming SS wave period and incoming IG wave height at the beach toe differs qualitatively for beach and sponge layer boundary conditions. This is elaborated on in Subsection 5.4.1.

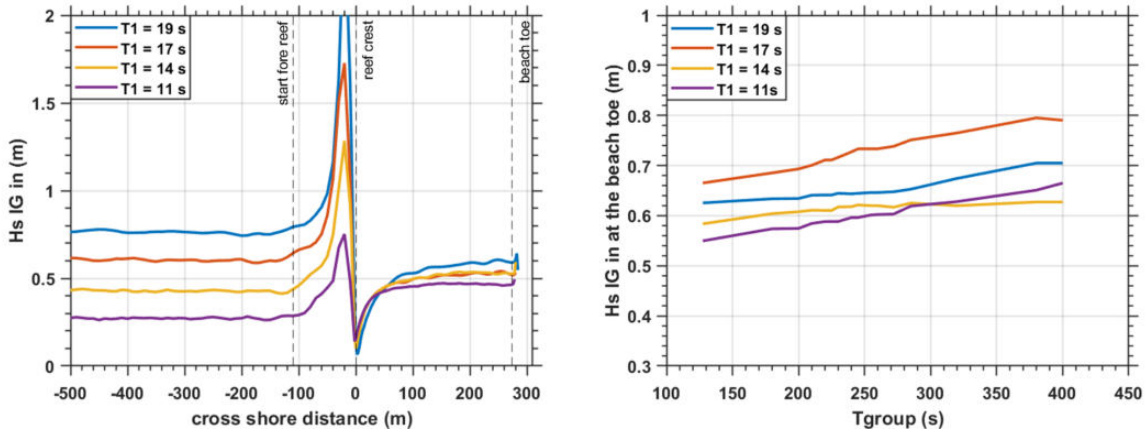

Figure 4.7: The cross shore variations of the incoming significant IG wave height for variations in T1 for a non-resonant group period with an onshore beach boundary (Tg = 127.5 *s*) (left). The non-resonant incoming IG Hs at the beach toe for various group periods is determined by defining a sponge layer boundary on the onshore end of the domain (right). The incoming bichromatic wave field has amplitudes a1 = 1.37 *m* and a2 = 0.72 *m*. The fore reef has a slope of 1/6.

4.2.4. Effects of the variations in fore reef slope

A steeper slope can be seen to generate more IG wave energy and allows for more IG wave energy to be present on the reef flat (Figure 4.8, left panel). The IG wave fully reflects at the beach toe, as the outgoing IG wave height at this location is equal to the incoming IG wave height (Figure 4.8). The offshore outgoing wave,

which consists of the wave reflected at the reef crest as well as the wave that is reflected at the beach toe and then leaves the reef flat, is largest for a steep fore reef. The offshore outgoing wave for a gently sloping fore reef is higher than the outgoing wave on the reef flat.

A steeper fore reef slope results in more IG wave energy being generated at this location (Figure 4.8, left panel). This IG wave energy then partially reflects offshore and partially propagates onto the reef flat. As more IG wave energy is generated for a steeper sloping fore reef (also found by Masselink et al. (2019)), more IG wave energy can be found on the reef flat.

Furthermore, it can be seen that growth of the IG wave height for different steepnesses of the fore reef holds a non-linear relationship with the steepness (Figure 4.9). For the two most gently sloping fore reefs (with steepnesses 1/10 and 1/8), the incoming IG wave at the beach toe varies greatly depending on this fore reef slope. For the steeper fore reef slopes (1/5 and 1/6), this sensitivity is less and the incoming IG wave height at the beach toe is in the same of order of magnitude.

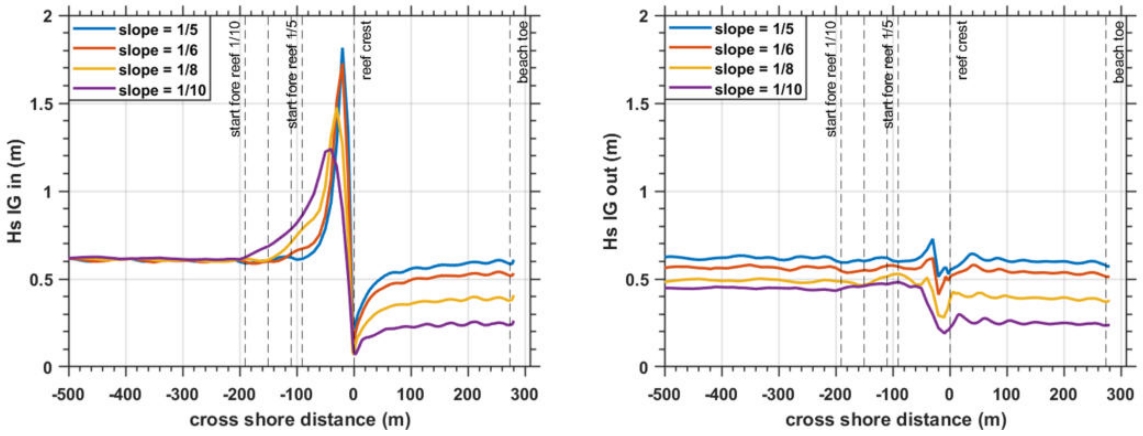

Figure 4.8: The cross shore development of the incoming (left) and outgoing (right) significant IG wave for variations in the fore reef slope for a non-resonant group period of 127.5 s. A1 = 1.37 m, a2 = 0.72 m, T1 = 17 s.

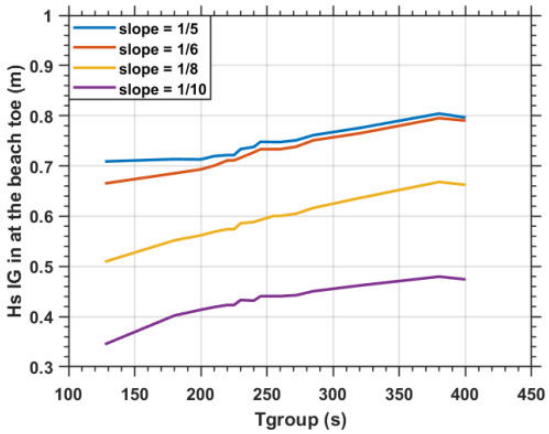

Figure 4.9: The incoming significant IG wave at the beach toe for simulations of various group periods where a sponge layer is imposed on the onshore boundary and the fore reef slope is varied. T1 is set to 17 s, a1 = 1.37 m and a2 = 0.72 m.

4.3. Low energy SS and IG wave behaviour

In this chapter, a distinction is made between highly energetic and low energetic conditions. The rest of the chapter deals with highly energetic conditions to assess the behaviour of the IG component of the wave field, as well as the SS component and the MWL. This section deals with the behaviour of the wave field under low energetic conditions. The wave amplitudes of the incoming waves are a1 = 0.15 m and a2 = 0.05 m

Offshore of the reef crest, the low energetic SS wave can be seen to display cross shore oscillations due

to reflection at the reef crest (Figure 4.10, left panel), with a maximum significant wave height of 0.55 m and a minimum significant wave height of 0.42 m. As the SS waves approach the coral reef, they start shoaling on the fore reef until they reach a maximum height of 1.03 m at the reef crest. On the reef crest, some of the waves break yet most of the SS wave energy is preserved and then reflected on the beach. This results in a standing wave on the reef flat with a shorter wave length than the standing wave offshore of the reef crest.

Offshore of the reef crest, the bound IG wave has an amplitude of 0.5 cm (Figure 4.10, right panel). On the fore reef the height of the IG wave increases to 0.05 m (5 cm). On the reef flat, the incoming IG wave has a value of around 0.022 m, which increases near the beach toe where more of the SS wave height is dissipated.

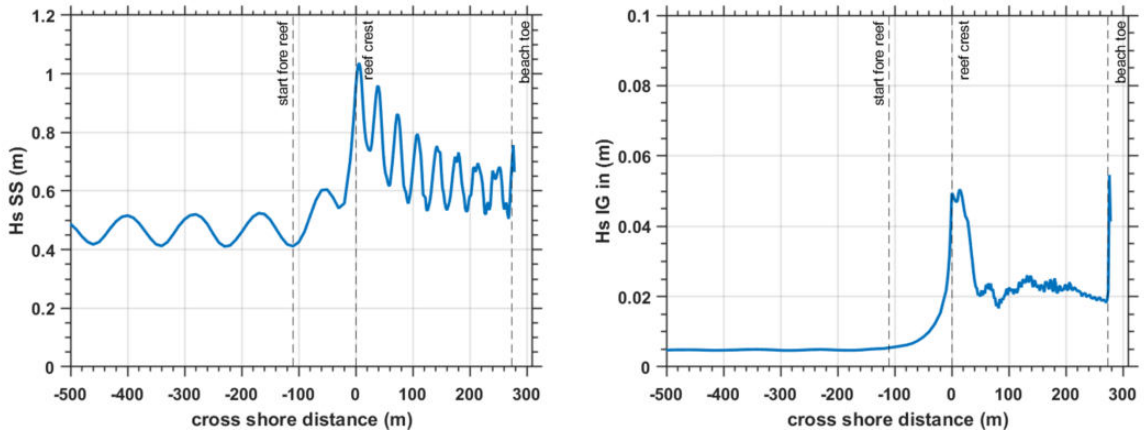

Figure 4.10: The cross shore evolution of the SS wave height (left) and the incoming IG wave height (right) under low energetic conditions with offshore values of a1 = 0.15 m and a2 = 0.05 m. T1 = 17 s, Tg = 127.5 s (thus non-resonant) and the fore reef has a slope of 1/6.

4.4. Amplification of the IG wave for different conditions

This section presents the amplification of the incoming IG wave under different characteristics of the incoming SS wave field and the bathymetry of the fringing reef.

4.4.1. The dependence of IG amplification on SS wave amplitudes

A larger value of a2 corresponds to a larger AR (Figure 4.11, left panel). If the group period of the bichromatic wave field is smaller than the most resonant period (Tg up to 200 s), the AR is of the same magnitude for all values of a2. If the considered group period is larger than the most resonant period (Tg from 250 s), a larger a2 leads to a larger AR.

A large value of a1 leads to less amplification at the beach toe compared to small values of a1 (Figure 4.11, right panel). This indicates that there is a negative relationship between the size of the incoming offshore wave a1 and IG amplification. This phenomenon is treated more extensively in Sections 4.5 5.2. Furthermore, when the variations in a1 are considered, the behaviour for non-resonant values of Tg is similar to when a2 is varied: for short Tg (up to 200 s), the AR is independent of a1; for long Tg (from 250 s), the AR 'lingers' and does not approach zero the way it does for short values of Tg.

The shapes of the incoming significant IG wave height for variations in a2 and a2 are similar to the shapes of their respective AR curves (Figure 4.12). It can be seen that for large a1 for the considered range of amplitudes (right panel), the IG wave height at the beach toe is small. The opposite is true for largen a2 (left panel). As this parameter also affects the modulation of the incoming SS wave field, a larger value for a2 leads to a larger height of the incoming IG wave at the beach toe.

4.4.2. The dependence of IG amplification on SS wave periods

The largest amplification under these circumstances occurs for T1 = 14 s, followed by T1 = 11 s and then T1 = 19 s and T1 = 17 s (Figure 4.13, left panel). The difference in AR for the various values of T1 is larger than the difference in height of the incoming IG wave (Figure 4.13, right panel). It can also be deduced that for T1 $\neq$ 14 s, the incoming IG wave height does not vary much with T1. The value of this wave height is slightly larger for smaller values of T1.

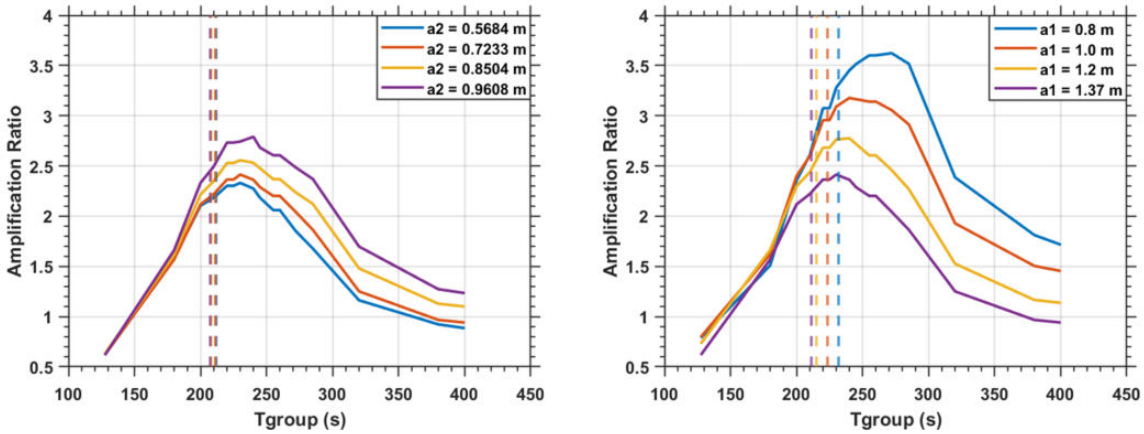

Figure 4.11: The amplification ratio (AR) for different offshore a2 (left) and offshore a1 (right) based on different values for Tg. The theoretical resonant period is dependent on the incoming wave amplitudes and is depicted by the dashed lines. For all simulations the fore reef slope is 1/6, T1 = 17 s. If a2 is varied, a1 = 1.37 m. If a1 is varied, a2 = 0.72 m.

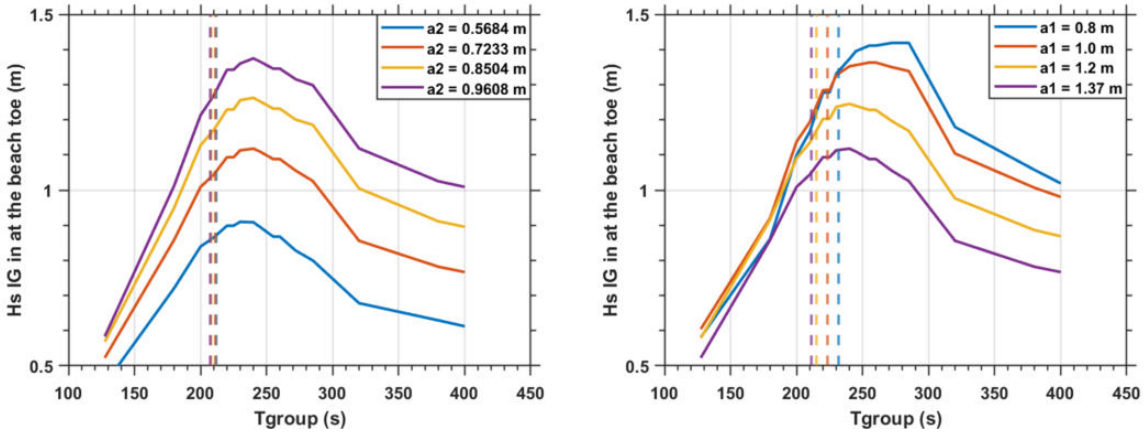

Figure 4.12: The incoming significant IG wave height ($H_{s,IG,in}$) at the beach toe for variations in a2 (left) and a1 (right). The dashed lines indicate the theoretically found fundamental resonant period. For the simulations T1 = 17 s and a fore reef slope of 1/6 is used. If a2 is varied, a1 = 1.37 m. If a1 is varied, a2 = 0.72 m.

4.4.3. The dependence of IG amplification on the fore reef slope

The largest amplification occurs for the mildest slope for the considered conditions (Figure 4.14, left panel). The AR for slopes of 1/5 and 1/6 is pretty similar in terms of maximum value as well as shape. Furthermore, for the gentle slopes, the resonant peak is more enhanced: for group periods much shorter (Tg up to 200 s) or longer (Tg from 320 s) than the resonant period, the amplification occurring on the reef flat preceded by a gentle slope is less than for a steeper slope.

If height of the incoming IG wave at the beach toe is considered, a steeper fore reef slope results in a higher incoming significant IG wave at the beach toe under these circumstances (Figure 4.14). Additionally, the difference in the height of the incoming significant wave is less between slopes in the steeper regime than in the more gentle regime.

4.5. Time variation and phase shifts in the IG wave

There is a phase shift of around 180 °in the incoming IG wave around the reef crest (Figure 4.15). This is an indicator that the height of the incoming IG wave offshore of the reef crest is indeed determined by the bound IG wave travelling out of phase with the SS wave group. Beyond the reef crest, the height of the incoming IG wave is dominated by the break point forcing generated IG wave, as this wave is in phase with the incoming SS wave group (see also Subsection 2.3.2). However, on the reef also the onshore propagating incoming IG wave that is released from the wave group is present, which is not reflected at the reef crest and is thus able to

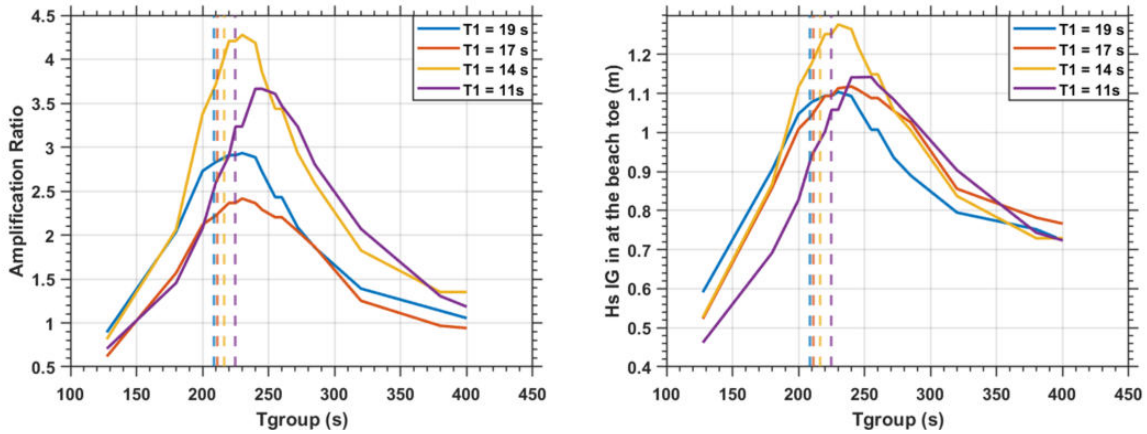

Figure 4.13: The amplification ratio (AR) at the beach toe (left) and the absolute height of the incoming IG wave(right) for various group periods and periods of the individual waves that make up the SS wave field. The theoretical resonant period is shown through dashed lines. For all simulations the fore reef slope is 1/6, a1 = 1.37 m and a2 = 0.72 m.

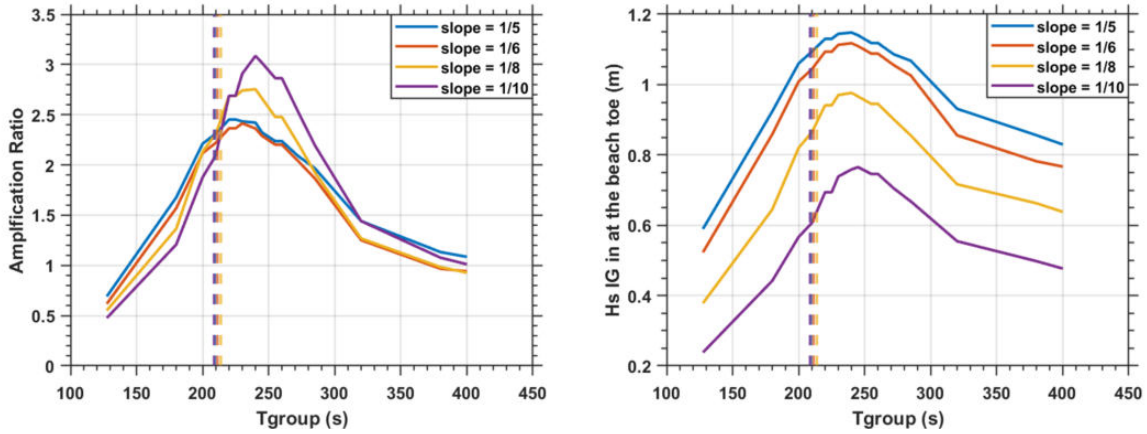

Figure 4.14: The amplification ratio (AR) at the beach toe (left) and incoming significant IG wave height at the beach toe for different values of the fore reef slope depending on the group period. The dashed lines correspond to the theoretical value of the fundamental resonant mode. The incoming bichromatic wave field has characteristics T1 = 17 s, a1 = 1.37 m, a2 = 0.72 m.

propagate further onshore. Interactions of these two incoming IG wave components can have a reducing effect on the total incoming IG wave height due to the 180 °phase difference. The outgoing IG wave (Figure 4.15, right panel) on the reef flat is in phase with the outgoing IG wave offshore of the fore reef. The outgoing IG wave height offshore of the reef flat is larger than on the reef flat, due to the contributions of the reflected released bound long wave and the break point generated IG wave travelling in negative cross shore direction.

The presence of SS waves does not appear to inherently enhance or limit the height of the IG wave on the reef flat (Figure 4.16, shown by the absence of correlation between the SS wave presence on the reef flat and the height of the incoming IG wave, both in resonant and non-resonant conditions).

4.6. The IG wave period for which maximum amplification occurs

In this section, the processes governing the period for which maximum amplification occurs are highlighted.

Table 4.1 gives the maximum amplification ratio (AR_{max}), the theoretically found resonant period ($T_{res,t}$, which is determined through Equation 3.14), the observed resonant period ($T_{res,o}$, the group period for which AR is largest), and the deviation of the observed resonant period from the theoretical resonant period ($\frac{T_{res,o}-T_{res,t}}{T_{res,t}}$). The data over which the observed resonant period is found, is based on the interpolation of the numerical data, to account for the relatively large ΔTg between simulations.

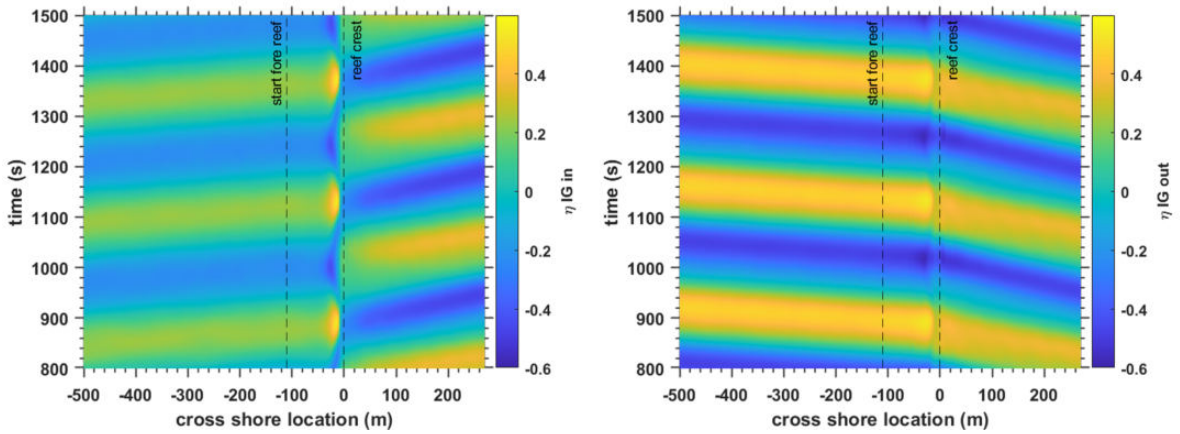

Figure 4.15: The cross shore evolution of the water elevation for the incoming (left) and outgoing (right) IG component over time. The simulation shown is the reference case with T1 = 17 s, a1 = 1.37 m, a2 = 0.72 m and a fore reef slope of 1/6. The group period is 240 s, thus conditions are resonant.

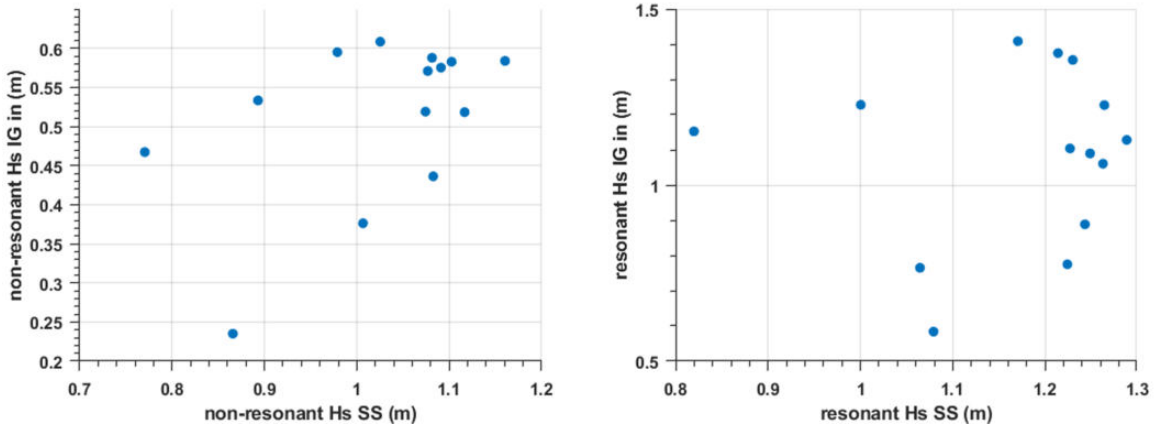

Figure 4.16: The values of the significant SS wave height at the reef flat and the corresponding incoming significant IG wave height at the reef flat for non-resonant (Tg = 127.5 s, left) and resonant (Tg = 240 s, right) conditions.

From Table 4.1 it follows that, considering variations in a2, the AR is largest for the largest value of a2, AR is smallest for the smallest values of a2. A large value for a2 (thus AR) coincides in this parameter space with a large deviation of the observed resonant period from the theoretical resonant period.

If the parameter a1 is under consideration, it is evident that a smaller wave amplitude leads to a larger AR. Furthermore, both the corresponding $T_{res,t}$ and $T_{res,o}$ are longest for the smallest values of a1, due to the energy in the SS wave spectrum being lower, which leads to a smaller set up on the reef flat. A small value of a1 (thus large AR) corresponds to a large deviation of the observed resonant period from the theoretical resonant period.

For the variations in T1 the largest value of AR, which corresponds to a T1 of 14 s, corresponds to the smallest deviation of observed from theoretically found resonant period for the values of T1 under consideration. The second largest AR, corresponding to a T1 of 11 s, shows a deviation of 8.6 %. For the smaller values of AR that correspond to the larger values of T1, the deviation is significantly larger (11.2 and 11.0 % for T1 = 19 s and T1 = 17 s, compared to 7.3 and 8.6 % for T1 = 14 s and T1 = 11 s, respectively).

The last variable influencing AR and the period for which resonance occurs is the fore reef slope. It is evident that a more gentle slope leads to a larger AR under these conditions. Furthermore, there is no clear relationship visible between the fore reef slope and the deviation of theoretical from observed resonant group period. The resonant period however increases as the slope becomes gentle, as the MWL over the reef flat is lower (see Section 4.1).

	base	**a2 (m)**			**a1 (m)**			**T1 (s)**			**slope**		
		0.57	**0.85**	**0.96**	**1.2**	**1**	**0.8**	**19**	**14**	**11**	**1/5**	**1/8**	**1/10**
AR_{max}	2.41	2.33	2.56	2.79	2.76	3.18	3.62	2.93	4.27	3.66	2.45	2.75	3.08
$T_{res,t}$ (s)	207.5	208.5	206.5	205.6	213.5	221.5	229.9	206.7	214.6	221.3	205.8	211.8	215.8
$T_{res,o}$ (s)	230.3	229.8	230.3	239.8	230.3	240.3	271.9	229.8	230.3	240.3	220.2	239.8	239.8
dev (%)	11.0	10.2	11.5	16.6	7.9	8.5	18.3	11.2	7.3	8.6	7.0	13.2	11.1

Table 4.1: The maximum AR along with the theoretically found fundamental resonant period (calculated using Equation 3.14) and the observed period for which amplification occurs, for all simulation sets. The deviation of the observed resonant period from the theoretically found resonant period is determined by $\frac{T_{res,o}-T_{res,t}}{T_{res,t}}$. The data is also presented visually in Figures 4.11 to 4.14. The reference (or base) case corresponds to a simulation with a2 = 0.72 m, a1 = 1.37 m, T1 = 17 s and a fore reef slope of 1/6

4.7. The amplification for combinations of SS wave periods and fore reef slope

For large values of T1 (15.5 to 19 s), the AR is relatively small for all slopes under consideration and there is not a distinct relationship between the slope and the incoming SS wave period T1 (Figure 4.17).

For T1 in the range 13.5 to 14 s the AR can clearly be seen to increase for more gentle slopes. The largest amplification of the circumstances under consideration can be seen to occur at T1 = 13.5 s and a fore reef slope of 1/10.

If the T1 is considered below this latter range, in the range of 11 to 12 s, an inverse relationship is found and the AR is larger for a steeper fore reef slope under the same incident wave field.

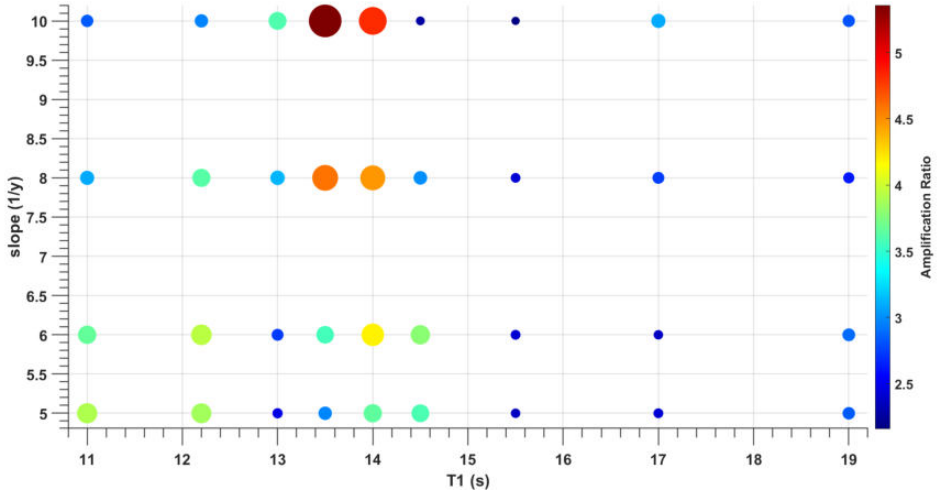

Figure 4.17: The amplification ratio displayed by color and by size, for different values of T1 combined with different values for the fore reef slope. In all simulations Tg = 240 s (thus conditions are resonant), a1 = 1.37 m, a2 = 0.72 m. The size and colour of the data point represents the AR in the parameter space.

4.8. The behaviour of the IG component of the water elevation over time

The situation that is most amplified for highly energetic conditions, with Tg = 240 s displays no build up behaviour, the second wave can even be seen to be lower than the first wave (Figures 4.18). For the simulation where the group period is much lower than the resonant period at Tg = 127.5 s, the first wave of the signal is much higher than the second and following waves. The opposite is true for the simulation where Tg = 380 s. In this case, the second wave is higher than the first wave. This case is however not in the resonant region of the considered parameter space. The fact that there are some properties present in the start of the time series for short Tg of 127.5 s that are yet to be understood, evident from the high first peak, indicates that some other processes might play a role in this part of the simulation.

Similar to high energy results (Figures 4.18) no clear build-up is visible for the low energetic cases considered (4.19). For the lowest present wave energy at a1 = 0.15 m and a2 = 0.05 m, the second peak is slightly higher than the first peak.

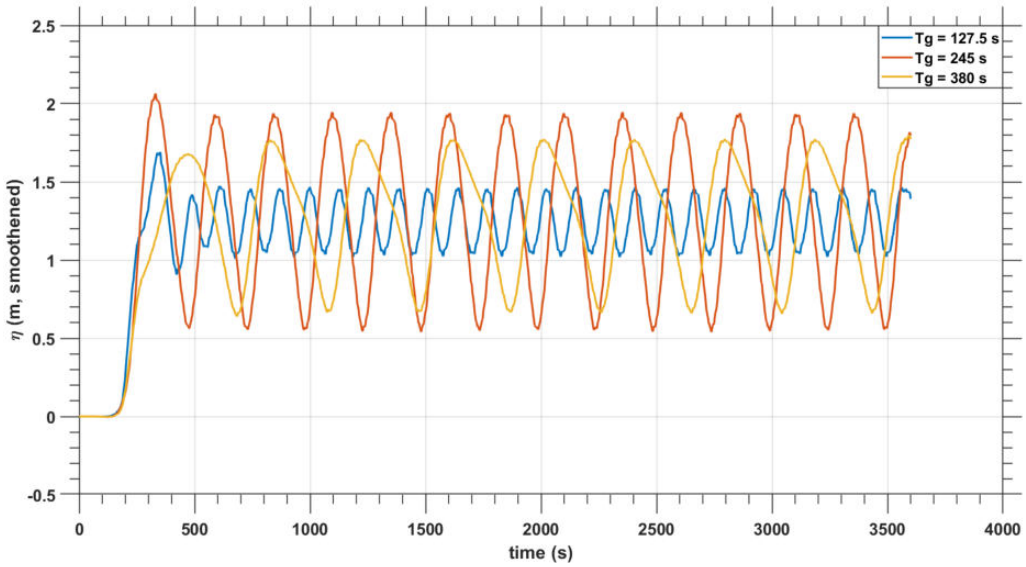

Figure 4.18: The evolution of the water level at the beach toe (smoothened over 70 *s*) for simulations where T1 = 17 *s*, the fore reef has a slope of 1/6, a1 = 1.37 *m* and a2 = 0.72 *m*. The three group periods considered are Tg = 127.5 *s* (non-resonant), Tg = 240 *s* (resonant) and Tg = 380 *s* (non resonant). The signal is unsplit, unfiltered and the spin-up time is not cut off.

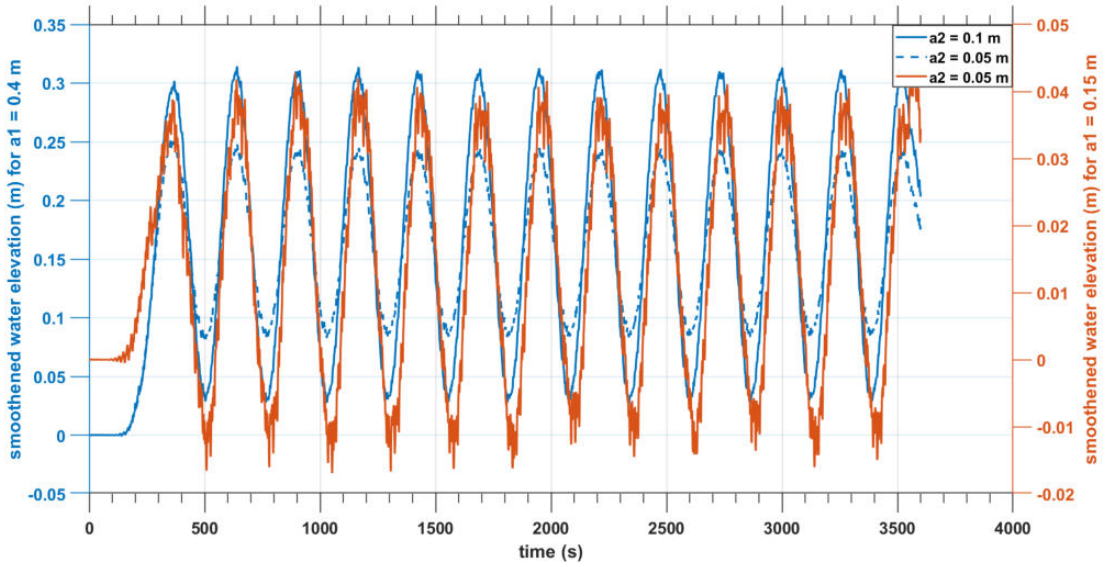

Figure 4.19: The evolution of the water level at the beach toe (smoothened over 100 *s*) for simulations where a1 = 0.4 *m* (blue lines) and a1 = 0.15 *m* (orange line). A2, which determines the modulation is 0.1 *m* (blue solid line) or 0.05 *m* (blue dashed line and orange line). The signal is unsplit, unfiltered and the spin-up time is not cut off.

5
Discussion

In this chapter, the results presented in Chapter 4 are discussed, along with their implications and limitations.

5.1. Results discussion

The results from Chapter 4 are discussed in this section.

5.1.1. Generation and presence of IG wave energy

Offshore of the reef flat, higher energetic conditions lead to higher incoming IG waves. Since the fore reef slope and the reef itself have no impact on the incoming wave height at this location, the incoming IG energy is determined by the bound long wave that travels with the wave group. This IG wave height is dependent on the characteristics of the SS wave field: more incoming SS wave energy leads to larger bound long waves; longer SS wave periods, thus fewer waves per wave group, also lead to more IG wave energy offshore.

On the reef flat, the incoming IG wave height is determined by the amount of IG wave energy generated by break point forcing on the fore reef and the amount of IG energy that is able to travel from offshore onto the reef flat without being reflected back offshore by the fore reef.

The former, IG wave generation through break point forcing, is determined by various parameters:

1. The modulation of the reef flat, the value of the smallest amplitude of the incoming bichromatic wave field: The larger the modulation of the incoming wave group, the stronger the break point generation mechanism and thus the more IG wave energy is generated at this location.

2. The period of the individual waves of the incoming bichromatic wave field: A greater wave period leads to more generation of IG wave energy for the same energetic conditions. This is in line with observations and derivations for a gently sloping bottom by Herbers et al. (1995) and Elgar et al. (1992).

3. The slope of the fore reef, offshore of the reef crest: A steeper slope leads to more IG wave generation. This is in accordance with the findings by Masselink et al. (2019).

The latter, the ability of the IG waves to enter the reef flat, depends on the fore reef slope and the amount of SS wave energy present on the reef flat. A steeper fore reef slope allows for more SS and IG wave energy to travel onto the reef flat. For gently sloping beaches, a steeper slope generally means more reflection present, however due to the steep nature of the fore reefs under consideration, the IG waves are always fully reflected under these circumstances (determined with Schiereck (2012)).

A mechanism may play a role that relates the presence of the bound IG wave released from the wave group and break point generated IG wave to the total height of the incoming IG wave on the reef flat (Section 4.5). As the phase difference between the (released) bound long wave and the break point generated wave IG wave is 180 °(Subsection 2.3.2), the presence of the onshore propagating released bound long wave may decrease the total incoming IG wave height, if the break point generated IG wave is largest and independent of the incoming SS energy and water level on the reef flat. Therefore, more reflection at the reef crest and thus smaller onshore propagating IG waves may lead to a higher total incoming IG wave. For both non-resonant and resonant conditions, the value for $H_{s,IG,out} - H_{s,IG,in}$ is largest for small a1, indicating that the reflected wave is largest for these cases (Figure 5.1 left and right panel, respectively).

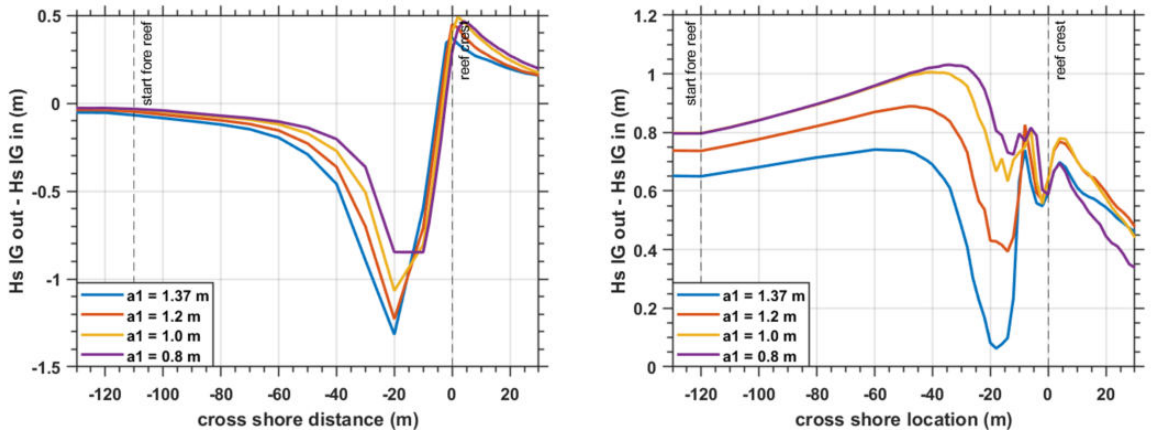

Figure 5.1: The difference between the outgoing and incoming significant IG wave on the fore reef for non-resonant (Tg = 127.5 *s*, left) and resonant (Tg = 240 *s*, right) conditions. T1 = 17 *s*, a2 = 0.72 *m* and the fore reef has a lope of 1/6.

At the base of this mechanism lies the theory that the generation of IG wave energy through break point forcing is determined only by the modulation of the SS wave field (Symonds et al., 1982). This is however not displayed explicitly in the results obtained for this thesis.

Furthermore, a larger water depth may reduce the reflective properties of the fore reef, thus allowing for more released bound long wave energy to propagate onto the reef flat. The water depth on the reef flat is positively influenced by the incoming SS wave height (Section 4.1), therefore the presence of SS wave. When the smallest wave of the bichromatic wave field (wave 2) is increased, the modulation is larger, more IG wave energy is generated through break point forcing. A large modulation of the wave field does increase the total energy on the reef flat and thus the set up, which may negatively impact the total incoming IG wave height on the reef flat. However, the behaviour of the IG wave on the reef flat is dominated by the effects of modulation as an increased value for a2 leads to a greater IG wave on the reef flat.

The time evolution of the outgoing IG wave does not provide additional information on the contribution of the released bound IG wave and the outgoing break point generated IG wave, see Appendix D.

5.1.2. Variations in amplification

The amplification ratio (AR), defined as the ratio in incoming IG wave energy at the location of the beach toe for reflective and absorbing boundary conditions, varies depending on the incoming wave field and the fore reef slope.

For nearly all simulations, regardless of the conditions present offshore, the amplification ratio stays well below a value of 4, which implies a doubling of the incoming IG wave height. The exception is a situation where the fore reef slope and period of the individual waves of the waves are both varied, which leads to an AR of maximum 5.

It should be noted that the deviation of the incoming IG wave for the sponge layer boundary and a reflective beach boundary is not compensated for in the calculation of the AR. Therefore, the AR in reality may be higher than is displayed due the fact that the incoming significant IG wave height is always larger for the sponge layer boundary (Section 3.6.1).

Both the maximum value of AR as well as the behaviour of AR for different Tg varies depending on the characteristics of incoming SS wave field and the coral reef bathymetry:

1. A greater modulation of the incoming SS wave field leads to a larger value for the AR at the beach toe.
2. An increase in SS wave energy (without an increase in modulation of the wave field) leads to a smaller AR.
3. With regard to the SS wave periods, there is no straightforward relation between the number of waves per wave group and the amplification of the incoming IG wave at the beach toe.
4. The AR is largest for the most gentle slopes, for the considered SS characteristics.

In Subsection 5.1.3 it is discussed how this relates to the incoming IG wave height.

Furthermore, different combinations of fore reef slopes and individual wave periods of the incoming wave field lead to different amplifications. For instance, the difference in amplification ratio for different slopes is highest when the mean period of the incoming waves is around 13.5 s, ranging from AR = 2 for the steepest slope under consideration to AR = 5 for the most gentle slope. For shorter incoming SS periods, this relation is reversed as the larger amplification for these conditions occur when a steep slope is considered. This suggest that there is a dependence of the amplification at the beach toe on the combination of the SS wave period and the fore reef. It could be that there are optimal incoming wave periods for a certain steepness of the fore reef slope. Furthermore, the variations in AR for different fore reef slopes is not the same for different incoming SS wave periods, i.e. the slope of the vertical 'lines' in Figure 4.17 is not constant. This holds for Tg = 240 s.

5.1.3. Variations in the amplified incoming IG wave height

The incoming IG wave height at the beach toe varies based on the characteristics of the incoming SS wave field as well as the coral reef bathymetry. In this section, a few differences between the shape of the curves for the amplification ratio and the height of the incoming significant IG wave are highlighted. It should be noted that in this section, the incoming IG wave is considered. The wave height relevant for flooding is twice as high due to the fully reflective regime of the beach for IG waves.

First of all, the effects of the incoming SS wave periods on the incoming IG wave height at the beach toe compared to the AR are considered. There is a difference between the shapes of the AR and the incoming significant IG wave height at the beach toe for variations in T1 (Figure 4.13). Whereas large differences in amplification are visible, the differences in the heights of the incoming IG wave are smaller. This is due to the fact that greater periods of the SS waves, so fewer waves per wave group, lead to a greater generation and presence of IG wave energy on the reef flat (Subsection 4.2.3). However, it is still evident that for these particular circumstances and bathymetry, a T1 of 14s creates the largest incoming IG wave. For the other SS wave periods under consideration, the maximum value of the incoming IG wave is around the same value. An increase in amplification for the lower values of T1 compared to larger incoming SS periods is compensated by a smaller amount of IG wave energy on the reef flat for shorter SS wave periods under these circumstances.

The relationship between the variations in the slope of the fore reef and the height of the incoming IG wave is clear, as a steeper slope results in a larger incoming IG wave for both resonant and non-resonant conditions. Furthermore, the steeper the fore reef slope, the smaller the differences in wave height become as a function of steepness. This implies that the sensitivity of the incoming IG wave height to the fore reef slope is larger in the more gentle regime.

5.1.4. Group period for which resonant amplification occurs

In general, the period for which maximum amplification occurs is higher than the theoretically found fundamental period. The theoretical resonant period is determined by an integration of the mean water level over the reef flat, from the point of the minimum height of the IG wave near the reef crest to the beach toe. This increases the distance over which is integrated compared to the distance from the reef crest to the beach toe. This deviation between $T_{res,t}$ and $T_{res,o}$ is similar to results found by Gaido (2019) and Pearson et al. (2017). This deviation is in the order of 10%, with outliers up to 18%, which is smaller than what is found in the aforementioned literature. This can be due to the different methods to determine the theoretical eigenperiod: taking the integration from the minimum IG wave height offshore to the beach toe instead of reef crest to the beach toe. The period for which maximum amplification occurs does not vary much based on the modulation of the incoming wave field, as this does not have a large effect on the set up on the reef flat. If the 'base' for the bichromatic wave field (a1) is varied, the set up on the reef increases as a1 increases, thus the resonant period decreases. For the periods of the incoming SS waves and the steepness of the fore reef, the resonant period varies based on the set up that is induced by these conditions. A smaller set up on the reef flat means a larger group period for which resonance occurs.

The maximum amplification varies throughout the parameter space for different values of Tg. For all group periods longer than the resonant period (Tg from 250 s), the amplification is larger for larger modulations. A greater modulation of the incoming SS wave field thus induces a larger risk of flooding than less modulated incoming SS wave fields for long non-resonant group periods. For periods shorter than the most resonant period (Tg up to 200 s), the risk of flooding due to amplification is independent on the modulation or the the energy of the incoming SS wave field. The differences in incoming significant IG wave height for variations in offshore SS amplitudes are smaller than the differences in IG wave height for variations in the group period.

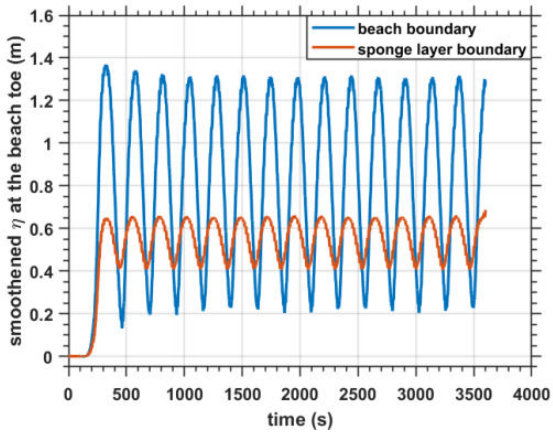

Figure 5.2: The IG component of the water elevation (filtered by smoothening the total signal over an interval of 40 seconds) for the most resonant case under consideration with a2 = 0.72 m, a1 = 1.37 m, T1 = 13.5 s, Tg = 240 s and a fore reef slope of 1/10. The blue line depicts the IG water elevation in the simulation of an onshore beach boundary, the orange line depicts the same simulation but with a sponge layer boundary at the onshore end.

As the period of the incoming SS waves and the slope of the fore reef have a great influence on the set up on the reef flat, the values for which the risk of flooding is largest highly depend on the group period under consideration. For group periods that are below the most resonant peak (Tg up to 200 s), the greatest amplification occurs for the longest incoming SS waves and the steepest fore reef slope. At the other side of the resonant peak, where longer group periods are considered (Tg from 320 s), the largest amplification occurs for shorter wave periods and more gentle fore reef slopes. It should be noted that the height of the incoming IG wave with IG periods larger than the resonant period does not vary a lot with incoming SS wave period. For the fore reef it holds that a steeper slope always results in a larger incoming IG wave height, regardless of the group period. Thus, steeper slopes pose a greater risk of flooding than more gentle slopes.

In assessment of the set up induced by SS wave breaking through SWASH modelling, it should be noted that the results generated by SWASH display a lower mean water level than can be observed in physical models under the same circumstances (see Section 3.1). This can lead to an overestimation of the theoretical IG period for which resonance occurs.

5.1.5. Build-up time of resonant behaviour

The build-up time of resonant behaviour as found Gaido (2019) and Nwogu and Demirbilek (2010) is not visible in the time series that follow from the data as produced by SWASH. The value for maximum amplification is reached within the first wave period, which is contradicting the theory that resonance occurs through amplification and excitation over time (Section 4.8). Given the value of the amplification ratio of approximately 4 (which means a doubling of the incoming IG wave height), logically it would take at least two waves and thus two wave periods for maximum amplification to be reached in the case of full reflection at the beach toe and reef crest. This behaviour is not visible.

The beach boundary induces a far larger water elevation on the beach toe than the sponge layer for the most resonant simulation (Figure 5.2), yet no build up of this water elevation is visible. As this AR is nearly 5, more than 2 waves would be required to reach this maximum AR.

Some (numerical) artefacts are present at the beginning of the simulation for some (non-resonant) cases, such as the larger first wave for both the Tg = 127/5 s case and the Tg = 245 s case (Figure 4.18). This could prevent the resonant build up time from being visible in the time series, due some numerical or physical processes dominating at this location. In numerical (Gaido, 2019) and physical (Nwogu and Demirbilek, 2010) experiments, the first wave height of the long wave component has been observed to be larger than the second wave (Figures 2.8 and 2.9).

5.2. Structure of the resonant IG wave

In Section 3.8.2 the base for the determination of the theoretical resonant period is explained. In Section 4.6 it is discussed how the period for which resonance occurs varies for each of the parameters. It is evident that the deviation of the observed IG period for which resonance occurs from the theoretically determined

resonant period is significant for all variables under consideration.

The observed period for which resonance occurs is always longer than the theoretically found fundamental resonant period. This can indicate that the length over which resonance occurs is in reality greater than the distance between the minimum of the IG wave to the shoreline (as used in Equation 3.14). In this section, two alternatives are discussed for the determination of the theoretical resonant period: integration from the point of maximum IG wave reflection to the shoreline, and integration from the most offshore point of the oscillation of the break point.

5.2.1. Reflection of the IG wave near the reef crest

On the fore reef, there is a sudden shift in behaviour of the incoming and outgoing IG waves (Figure 5.3, left panel). In the IG RC, a clear peak is visible slightly offshore of the reef crest, indicating the largest value of the ratio of the outgoing IG wave over the incoming IG wave (Figure 5.3, right panel). When this point of maximum reflection is used as the offshore boundary of the water depth integration to find the theoretical fundamental eigenperiod, the deviation of the observed resonant period from the theoretical resonant period is reduced by 50% compared to the deviation found by the method described in Section 3.8.2 (approximately 5% deviation compared to 10% deviation). However, the point of maximum reflection varies greatly depending on the group period Tg (Figure 5.4). Additionally, the wave height changes for the incoming and outgoing component are extremely sudden, which compromises the reliability of the separation mechanism that is used. Therefore, though this method leads to better results regarding the deviation of the observed from the theoretical eigenperiod, it is not used in this analysis.

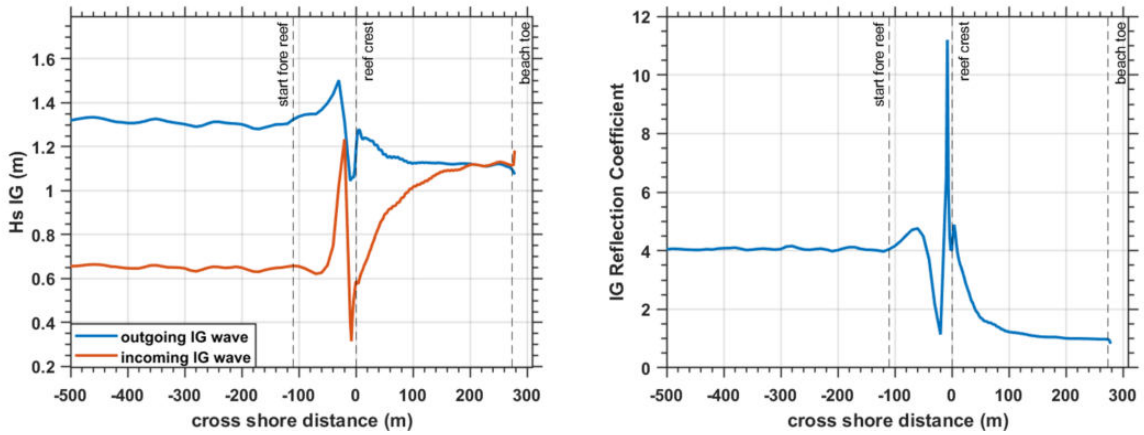

Figure 5.3: The cross shore evolution of the incoming (orange) and outgoing (blue) IG wave (left) and the RC of the IG component (right). The simulation shown is the reference case with T1 = 17 *s*, a1 = 1.37 *m*, a2 = 0.72 *m* and a fore reef slope of 1/6. The group period is 240 *s*, thus conditions are resonant.

5.2.2. Time-varying SS and IG behaviour

In Section 2.3 it is discussed that the dominant IG wave generation mechanism on coral reef lined coasts is likely to be the oscillation of the break point. In the incoming SS wave signal, a clear cross shore variation of the largest water elevation is visible over time (Figure 5.5, left panel).

The offshore location of this shoaling region corresponds to the onshore location of the region over which the depth must be integrated to calculate the theoretical fundamental eigenperiod to match the observed resonant period. This is true for most, however not all, resonant cases under consideration. It is expected that forcing of the IG wave happens at this location. This oscillating signal is also visible in the incoming IG component of the total water elevation (Figure 5.5, right panel). The offshore location of the integrated water depth as discussed in Section 3.8.2 roughly corresponds to the most onshore location of this oscillation.

The variation in the region where breaking occurs over time may explain the phenomenon that the observed resonant period is longer than the theoretically calculated resonant period due to the fact that reflection of the IG wave happens at a location further offshore than anticipated on. This information of the oscillation is lost in the time-averaging of the signal.

However, the deviation of the observed resonant period from the theoretical eigenperiod is also visible in simulations where a single free long wave is present (Gaido, 2019), without a bichromatic wave field and thus

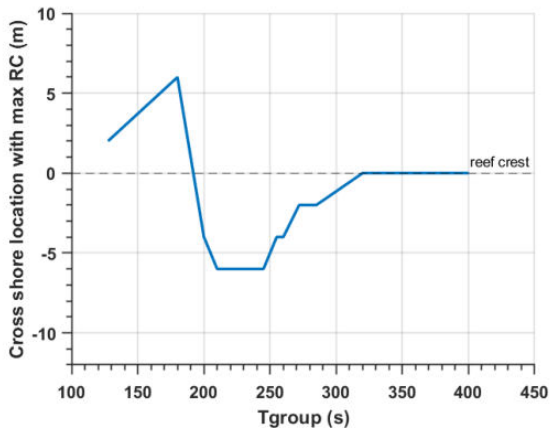

Figure 5.4: The cross shore location of the point of maximum IG reflection for various group periods. The location of the reef crest is indicated by a horizontal dashed line. The simulation shown is the reference case with T1 = 17 *s*, a1 = 1.37 *m*, a2 = 0.72 *m* and a fore reef slope of 1/6.

without a time varying break point. More research is required into the exact processes governing the location of reflection of the resonant IG wave.

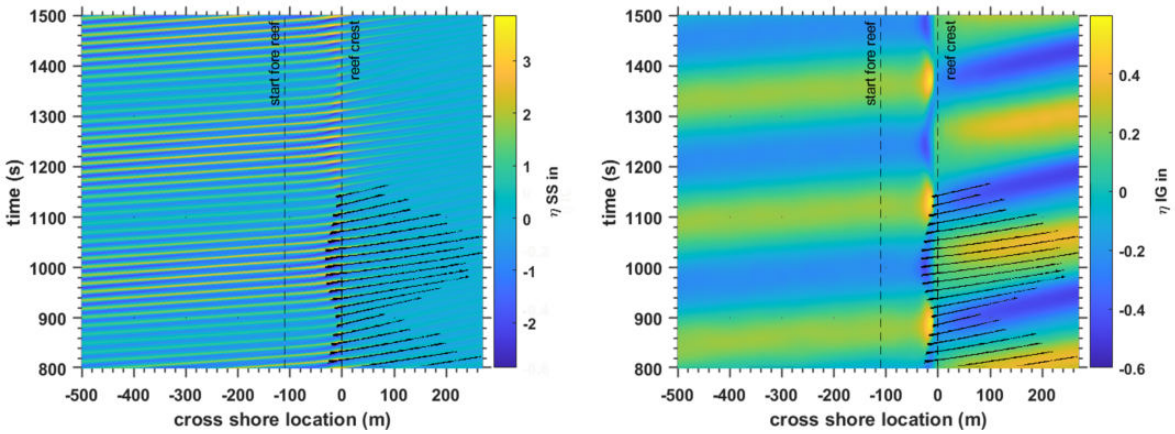

Figure 5.5: The cross shore evolution of the water elevation for the incoming SS (left) and IG (right) component over time. The black lines in the first half of the shown time series indicate the locations where breaking occurs as found by the computation. The simulation shown is the reference case with T1 = 17 *s*, a1 = 1.37 *m*, a2 = 0.72 *m* and a fore reef slope of 1/6. The group period is 240 *s*, thus conditions are resonant.

5.3. Comparison to Literature

To asses the applicability and the relevance of this research within the existing literature, a comparison is made between findings.

5.3.1. Qualification and quantification of resonance

In Subsection 2.5.4 different methods to assess resonance are presented according to Pomeroy et al. (2012b), Gawehn et al. (2016) and Gaido (2019). In these researches, the focus was predominantly on the qualification rather than quantification of resonance. Especially in the former two, the goal was to separate resonant- from non-resonant conditions rather than comparing the extent to which resonance occurs under various circumstances. In this research, the focus lies on comparing various resonant modes with one another rather than the individual classification of resonant waves. Thus, a different approach is developed that allows for inter comparing resonant modes for the considered condition.

5.3.2. General behaviour of IG waves

In the approach of the IG wave to the reef flat over the fore reef, the incoming IG wave height should increase due to shoaling once the bound long wave is released. However, additional IG wave energy can be found at this location due to break point forcing (see Appendix C). This is indeed in line with theory that suggests that for steep slopes, break point forcing is a dominant IG wave generation mechanism compared to the shoaling of the bound IG wave (Pomeroy et al., 2012b). This sudden decrease in IG wave height near the reef crest has been observed by Buckley et al. (2018) and Péquignet et al. (2014), albeit unexplained (though the value of IG wave height only increased little or not at all across the reef flat, probably due to wave breaking and frictional dissipation).

5.3.3. Behaviour of resonant IG waves

It was found through numerical simulations by Gaido (2019) and Pearson et al. (2017) that the group period for which resonance occurs is generally larger than the theoretically found resonant period on the reef flat. The results of this thesis correspond to those findings. For most communities living near fringing coral reefs this can be perceived as positive, as the theoretical fundamental resonant period of coral reefs is often on the long end of the naturally occurring group periods in the area. An increase in the period for which resonance occurs therefore reduces the risk of resonance occurring compared to the theoretical models. Furthermore, a good understanding of the deviation of these periods may be used for predictive models. With regard to observations in nature, findings by Pomeroy et al. (2012b) based on work by Péquignet et al. (2009) display similar behaviour, though less pronounced (Pomeroy et al. (2012b), Figure 2).

5.4. Research limitations

Factors that should be taken into account in the assessment of the results are discussed in this section.

5.4.1. Deviation in non-resonant behaviour for sponge layer and beach boundaries

In Section 3.6.1 the performance of the sponge layer under the variation of different parameters is presented. The deviation of 20% in significant wave height for the cases with a sponge layer boundary compared to the cases with a beach boundary translates to a deviation in the order of 40% in the amplification ratio (AR). This deviation is significant compared to the maximum AR of 4. Since the value for the incoming IG wave height is larger for the sponge layer simulation, the expectation is the AR is underestimated through the usage of the sponge layer as non-resonant reference case.

In the assessment of the performance of the sponge layer, group periods much lower than the theoretical resonant period are considered. In the figures presented in Section 4.4 it can be seen that for group periods much higher than the theoretically found resonant period, the AR does not appear to converge to a certain value for each variable. This suggests that on the high side of the group periods considered, resonance is still present to some degree. Another option is that the deviation of sponge layer from beach boundary results is simply larger for long Tg, but this has to be explored further.

Furthermore, for some cases the sponge layer behaviour is qualitatively different from the non-resonant behaviour for simulations with a beach boundary. For instance non-resonant behaviour for a beach boundary for different values of T1 for non-resonant conditions (Figure 4.7). At the beach toe, the incoming significant IG wave height can be seen to be largest for the longest value of T1 and smallest for the shortest T1. This does not line up with the data visible in the right panel at Tg = 127.5 s, where the simulation with T1 = 17 s results in the largest incoming IG wave at the beach toe. A similar mismatch holds where the difference between the heights of the incoming significant IG wave for a slope of 1/5 and 1/6 is larger when a beach boundary is present than when a sponge layer boundary is present (Figure 4.8). However, this is a quantitative error rather than a qualitative error.

The mismatch between the incoming IG wave and for the two boundary conditions is within an error margin that is deemed acceptable, yet should be taken into account when quantitatively assessing the results.

5.4.2. Incoming wave height and shoaling

Though the incoming wave height is in accordance with the offshore values for wave height as found by Cheriton et al. (2016), both the SS and the free IG component of the waves increase greatly due to shoaling on the fore reef. As a result, the total significant wave height at the location of the reef crests are higher than would intuitively be possible under these conditions. These high waves can cause disturbances or phenomena that would not normally be observed, which can dominate the signal.

5.4.3. Resources and parameter space

Within the scope and time frame of this research, not all combinations of parameters are considered. Predominantly the effects of one variable are considered with respect to variation in group period. This rules out any effects that interactions of these variables may have.

In the situation that two input variables are both varied, the SS wave period and the fore reef slope, only one group period is considered. It is evident that the behaviour of all variables changes depending on the group period, thus the results may be very different for these different group periods.

5.4.4. Model limitations

The numerical model used to obtain the results presented in this thesis is 2D without taken into account any alongshore or directional effects that occurs on the reef. Furthermore, in the z-direction only 2 layers are present in the model, so the depth-dependent processes are not fully captured. Additionally, it has been shown that IG wave generation and behaviour is sensitive to topographic variations (Torres-Freyermuth et al., 2012), as well as the incident wave angle of the (SS) wave field (Herbers et al., 1995).

6
Conclusions

In this chapter, the research questions presented in Chapter 1 are answered and conclusions are drawn based on the results and discussion from Chapters 4 and 5. The main question that requires answering is:

What processes and conditions influence the characteristics of infragravity wave resonance on coral reef lined coasts?

This question is split up into sub questions:

What is the influence of incoming SS wave heights on IG wave resonance?

The wave heights of the incoming sea swell (SS) wave field lie at the base of two components that influence the height of the infragravity (IG) wave: the modulation (or envelope) of the wave field, and the total variance found in the SS wave spectrum.

The modulation of the wave field influences the amount of IG energy generated at the fore reef. A large modulation means that a lot of IG wave energy is generated at the fore reef. Furthermore, a large modulation also positively influences the maximum value for the amplification ratio (AR).

Highly energetic offshore SS waves correspond to limited presence and amplification of IG waves on the reef flat. Though the IG wave offshore of the reef crest is largest for energetic SS waves, the opposite is true on the reef flat itself. This may be due to interactions of the released bound long wave and the break point generated IG wave that have a phase difference of 180 °.

In the end, the strongest resonant amplification as well as the largest incoming IG wave height at the beach toe occurs for a SS wave field that is strongly modulated yet not highly energetic.

What is the influence of the incoming SS wave periods on IG wave resonance?

The period of the incoming SS wave influences the maximum amplification of the IG wave found on the reef flat. There is not a clear universal relationship between incoming SS wave period and AR. The behaviour of the SS waves with respect to the fore reef slope is one of the factors that influence for what incoming SS wave periods the amplification ratio is largest.

Moreover, the height of the IG wave at the beach toe does not clearly depend on the incoming SS wave period. A larger amplification for certain variations in incoming wave period coincides with the lower incoming IG wave. This implies that regardless of the period of the incoming SS waves, the risk of flooding is similar.

What is the influence of the fore reef slope on IG wave resonance?

The most resonant amplification of the incoming IG wave is largest for the most gentle slope under consideration. For IG wave periods that deviate from the most resonant period, a steeper slope leads to more amplification.

The height of the resonantly amplified incoming IG wave is always largest for the steeper slope regime, therefore the risk of flooding is largest for steep fore reef slopes. Additionally, the risk of flooding is also larger for steep fore reef slopes if IG periods are considered that fall outside of the resonant regime.

How is the period for which maximum amplification occurs shaped by the characteristics of the incoming SS wave field and the bathymetry of the coral reef?

The observed resonant period is always longer than the theoretical resonant period.

The wave heights of the incoming SS wave field influence the period for which maximum amplification occurs in such a way that an increase in incoming SS wave energy increases the set up on the reef flat. A large set up leads to both a shorter theoretically resonant period as well as the observed resonant period. The stronger the modulation of the incoming SS wave field, the greater the deviation between the observed and theoretical resonant periods. With respect to the dependence of the deviation from observed and theoretical resonant period when the SS wave height is considered, a stronger amplification corresponds to a larger deviation.

The theoretical resonant period of the IG wave depends on the incoming SS periods in the sense that a longer SS wave period leads to a larger set up and thus a shorter theoretical resonant period. Moreover, there is no clear relationship between the deviation of the observed resonant period from the theoretical resonant period and the wave periods of the incoming SS waves. A larger AR based on the incoming SS wave periods corresponds to a smaller deviation in theoretical versus observed resonant period.

Between the slope of the fore reef and the IG wave period for which resonance occurs, the relationship is found that a steeper fore reef slope leads to a shorter theoretical resonant period, due to a larger set up on the reef flat. The deviation of the observed resonant period depends on the slope and no straightforward relationship is found.

7
Recommendations

In this chapter, recommendations and suggestions for further research are given.

7.1. Application of the acquired insights

Aside from forming a base for further research into the topic of IG wave resonance, the obtained results and gained insights might serve as an argument to enhance the protection of the small island states.

7.1.1. Using the obtained results

The results and conclusions obtained in this thesis suggest that for highly energetic conditions, the risk of waves being larger than predicted without resonance is significant for small islands. The indicators of resonance as well as the variability of the amplification based on variations in the conditions considered may serve as a base for site specific models made to assess and interpret the risk for small island states under certain forcing.

7.1.2. Climate change

Climate change leads to an increase in sea level, which increases the water depth on the reef flat as well as diminishes the energy dissipating features of the coral reef. Therefore, through climate change the risks of damaging resonance occurring increases. Pomeroy et al. (2012b) have shown that the amplification on coral reefs increases for fundamental and higher order resonant periods in the case of water depth increase.

Furthermore, climate change leads to a degradation of coral reefs and their contribution to the high friction environment waves are subject to. The combination of higher water levels and decrease in friction can have a devastating effect to the communities living near fringing reef environments. Therefore, monitoring of the health and properties of the coral reefs is of vital importance to the safety of communities living in small-island states.

7.2. Change in incoming wave field

In this thesis, a limited range of incoming SS wave characteristics are treated and analysed. To better understand IG wave resonance on coral reefs, a larger range of characteristics must be assessed.

7.2.1. Irregular offshore waves

Irregular waves provide a more accurate representation of reality than a bichromatic wave field. Doing similar simulations could give insight into the generation mechanisms of IG wave energy under irregular SS wave forcing. Furthermore, the propagation of the IG wave on the reef flat and its amplification has been shown to lead to different results under different incoming SS wave energies as well as modulations. Therefore, an irregular wave field may influence these parameters as well and can provide better insight into the real-life behaviour of IG waves on fringing coral reefs.

7.2.2. Shorter group periods to asses higher modes

In this thesis, the focus has predominantly been on IG wave behaviour near the fundamental resonant period. The behaviour of the IG wave for lower resonant period has not been considered in-depth. It has been shown that though the fundamental period leads to the largest amplification and largest absolute value of the IG wave, the higher resonant modes also lead to amplification of the IG wave (Gaido (2019)). As the periods of these higher modes are shorter (Equation 2.1), these periods may occur more often, especially for longer reef

flats. Higher modes may therefore pose a greater risk of flooding and damage to low-lying coral reef islands and should thus be understood.

7.2.3. Less energetic incoming SS waves

The results presented and discussed in Chapters 4, 5 and 6 are based on highly energetic wave conditions. In Section 4.3, the behaviour of the SS and IG waves under low energy conditions are presented and these can be seen to differ greatly from the highly energetic conditions. As the conditions considered lie at the high end of the storm spectrum regarding incoming wave characteristics, these conditions might not be the most realistic representation of what can be expected at the locations of low-lying fringing reef islands. Furthermore, less energetic conditions might provide better insight in what is happening over time when resonance is present.

7.2.4. Ramping of the wave climate

In the simulations under consideration, the wave climate is imposed at the offshore boundary instantly, without wave ramping. In general, the focus has been mostly on the characteristics of the SS and IG waves once stationary conditions have been reached. Ramping, i.e. letting the offshore SS wave develop over a certain period of time, could provide new insights on how resonance is triggered by the incoming wave field: what the threshold in incoming SS wave energy is for resonant amplification; from what values of SS wave heights the resonance is damped by the presence of the SS waves; what the delay in IG wave amplification is with regard to the characteristics of incoming SS waves.

Furthermore, one of the potential causes of the absence of build-up time in resonant behaviour (Section 4.8) is that the energetic incoming wave field is in such high contrast with the still water conditions at the beginning of the simulation that the stationary conditions are reached immediately. To assess the impact of resonance-inducing conditions compared to the system under similar, though non-resonant, forcing in terms of energy, the wave climate can be imposed in two steps. For instance, first the 'base' of the wave field is imposed on the offshore boundary so that the system can reach new stationary conditions. Then the modulation of the wave field can be imposed, so that the impacts of IG wave can be determined separately from the impacts of the highly energetic conditions.

7.3. Change in the characteristics of the coral reef

The bathymetry of the considered reef flat is heavily schematized for the purpose of this thesis. An exploration of the different characteristics of reefs as found on atolls, fringing reefs and other low-lying islands could help identify which areas are under increased risk under certain circumstances.

7.3.1. Non-homogeneous reef flat

The schematized fringing reef under consideration is consists of two homogeneous areas: the steep fore reef slope and the horizontal reef flat. In reality, coral reefs can have other shapes and distinct features, such as elevated reef crests and lagoons. These features could potentially alter the resonant behaviour of fringing coral reefs (Masselink et al., 2019). Research into the resonant behaviour for different coral reef bathymetries could help predict which reefs are under increased risk of flooding under which circumstances.

7.3.2. Friction on the fore reef and reef flat

Coral reefs have the distinct feature of high friction compared to sandy beaches due to the nature and structure of corals. A large value of friction can lead to more dissipation on the reef flat of different components of SS and IG waves. Furthermore, the friction on the fore reef is generally higher than that on the reef flat. This can lead to different nearshore processes dominating, which may affect resonant amplification or the generation of IG wave energy at this location.

7.3.3. Combination of variables

In Section 4.7 different values for the amplification ratio are given for the combination of fore reef slope and incoming SS wave period variation. To better understand the behaviour of IG waves under different conditions, further research into the combined effects of bathymetry and SS wave characteristics is recommended. In addition to different behaviour for a single considered group period, changes in the SS wave field and the bathymetry might alter the period for which maximum amplification occurs.

7.4. Numerical set up

The numerical set up can give insights into the resonant behaviour of IG waves on coral reefs by assessment of the right input parameters as well as the analysis of the data

7.4.1. Separation and filtering methods

In the analysed data, the total signal of the incoming and outgoing significant wave height is presented. For each of the signals, no distinction is made between the released bound long wave and the IG wave energy generated through break point forcing. Janssen et al. (2003) presented a way to distinct the correlation between the low-pass filtered surface elevation time series and the envelope of the SS waves using Hilbert-Huang transformation. This could provide more insights on the location of IG wave generation compared to shoaling, which often occurs in same areas for steep slopes. A generally better understanding of IG wave generation and transformation leads to better basis for numerical modelling as well as better understanding of the risks of flooding.

7.4.2. 2D or 3D simulations

The SWASH simulations are done using a 2D model with 2 vertical layers, which does not accurately describe the vertical velocity profile in the domain. An increased vertical resolution would lead to better insights and more accurate results regarding IG wave transformation and amplification on the reef flat. However, this does negatively affect the stability and the computational time of the simulations.

Furthermore, IG wave generation is highly dependent on the incident angle of the SS wave field (Herbers et al., 1995). Additionally, nearshore IG wave dynamics are highly sensitive to reef geometry (Torres-Freyermuth et al., 2012) Therefore, for specific coral reef environments a 3D simulation might be worthwile to assess the specific risks and processes occurring at certain locations. It has been shown that taking into account directional spreading in the assessment of risks of overwash on coral reefs, the run up is generally lower, thus a 1D or 2DV model makes a conservative assessment of risks (Veldt, 2019). However, it is not known whether and how this can be applied to resonance.

7.4.3. Sponge layer performance

Though a sponge layer boundary has been observed to fulfill its purpose in simulations regarding a coral reef in terms of absorption of IG and SS waves (Section 3.6.2), a mismatch is found in non-resonant conditions for a beach boundary and a sponge layer. In an ideal situation, the (incoming IG) wave heights in two similar simulations with a different onshore boundary condition should be the same, however this is not the case (Section 3.6.1). This leads to an uncertainty in both quantitative and qualitative assessment of the results. The reason behind this mismatch is not completely understood and required more in-depth research.

7.4.4. Separation of the IG wave components

Much is yet to be understood about the contribution of the released bound IG wave and the break point generated IG wave to the total incoming IG wave. Information about this could provide insights into what processes dominate at for which circumstances, since the total IG wave signal is a combination of various separately generated components. This can be done by looking at the phase shifts in the IG wave over the reef flat, as well as the cross shore and temporal evolution of the IG wave under different circumstances. Furthermore, energy transfer near the reef crest can give an indication of how much energy is reflected and how much energy is propagating onto the reef flat

A

Absorbing boundary condition

In this appendix, the properties of the sponge layer are shown. Furthermore, some alternatives to the sponge layer as absorbing boundary are presented.

A.1. Absorbing boundary conditions in SWASH

Figure A.1 shows the outgoing IG wave height (left) and the IC RC (right) for three boundary conditions in SWASH: a reflective beach boundary (blue); a sponge layer boundary (red); and a Sommerfeld radiation condition (yellow). The reflective beach boundary serves as a comparison method, the simulation where reflection is free to occur. The sponge layer boundary is clear to absorb the incoming IG wave as the outgoing IG wave height goes to 0 m, furthermore the IG RC is 0 over almost the entire reef flat.

The Sommerfeld radiation condition does not appear to absorb the IG wave, as the outgoing IG wave is even higher than the reference wave height of the beach boundary simulation. Furthermore, the IG reflection coefficient is not 0 over the reef flat, which further emphasizes the lack of absorbing properties for this boundary condition.

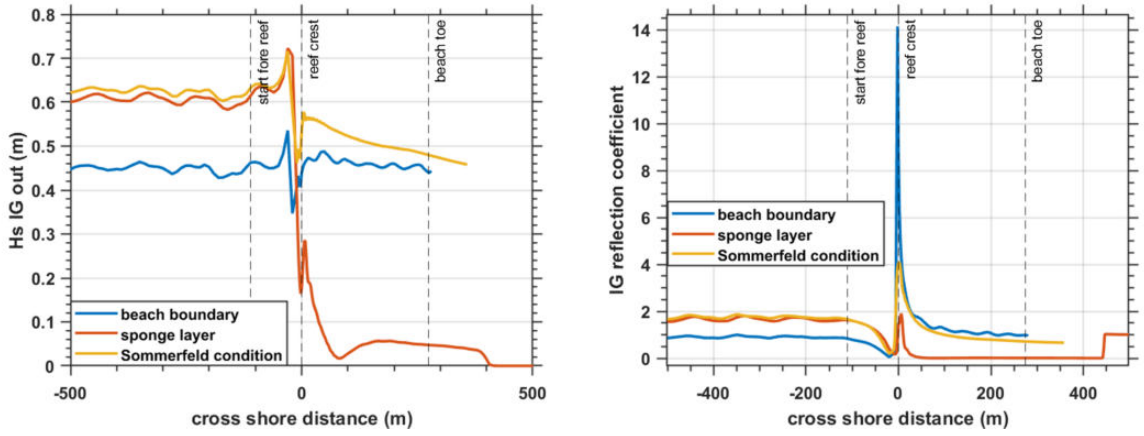

Figure A.1: The outgoing IG wave (left) and the IG reflection coefficient (right) for various onshore boundaries in SWASH. The group period is non-resonant at Tg = 127.5 s. Furthermore, a1 = 1.06 m, a2 = 0.53 m, T1 = 17 s and the fore reef slope has a steepness of 1/6. The locations of the start of the fore reef, reef crest and the beach toe are indicated through vertical dashed lines.

A.2. Properties of the Sponge layer

Figure A.2 shows the cross shore mean velocity (left) and mean water level (right). The simulation with a beach boundary shows two distinct negative peaks in mean velocity: a strong undertow near the reef crest and at the beach toe, at locations where the waves break. This is in line with expectations. For the sponge layer, the mean velocity throughout the domain is positive, reaching values of up to 1.7 m/s on the reef flat. This velocity goes to zero in the sponge layer, which starts onshore of the beach toe. The positive mean velocity indicates the outflow of water from the domain, which is in line with the practical implementation of the sponge layer of a function of exponential decay on the momentum equations. However, water flowing out of the domain is not physically accurate for the situation under consideration.

The right panel of Figure A.2 shows the mean water level for a simulation with a beach boundary compared to a simulation with a sponge layer boundary. It is evident that the mean water level at any cross shore location is higher for the beach boundary simulation than for the simulation with a sponge layer boundary. This difference in water level may lead to an increase in shoaling coefficient for the simulations with a sponge layer boundary or other effects.

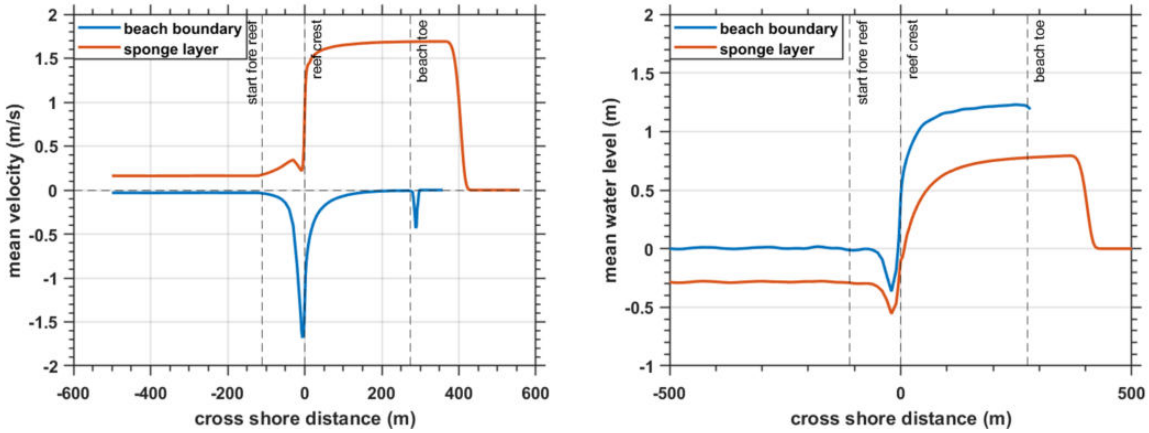

Figure A.2: The cross shore mean velocity (left) and the mean water level (right) for a beach boundary and a sponge layer boundary in SWASH. The group period is non-resonant at Tg = 127.5 s. Furthermore, a1 = 1.06 m, a2 = 0.53 m, T1 = 17 s and the fore reef slope has a steepness of 1/6. The locations of the start of the fore reef, reef crest and the beach toe are indicated through vertical dashed lines.

A.3. Other alternatives

Figure A.3 shows the incoming (left) and outgoing (right) significant IG wave height for various (absorbing boundary conditions). With regard to $H_{s,IG,in}$, the match with the beach boundary is largest for the regular sponge layer, the sloping beach with friction and the modified sponge layer with friction. However, in the right panel it can be seen that only the regular sponge layer absorbs the IG which can be seen by the absence of an outgoing IG wave on the reef flat. The other alternatives might show a different match with the beach boundary with respect to the incoming IG wave, yet absorbing properties are crucial for the goal of the research, since in the non-resonant case no energy may be trapped on the reef flat.

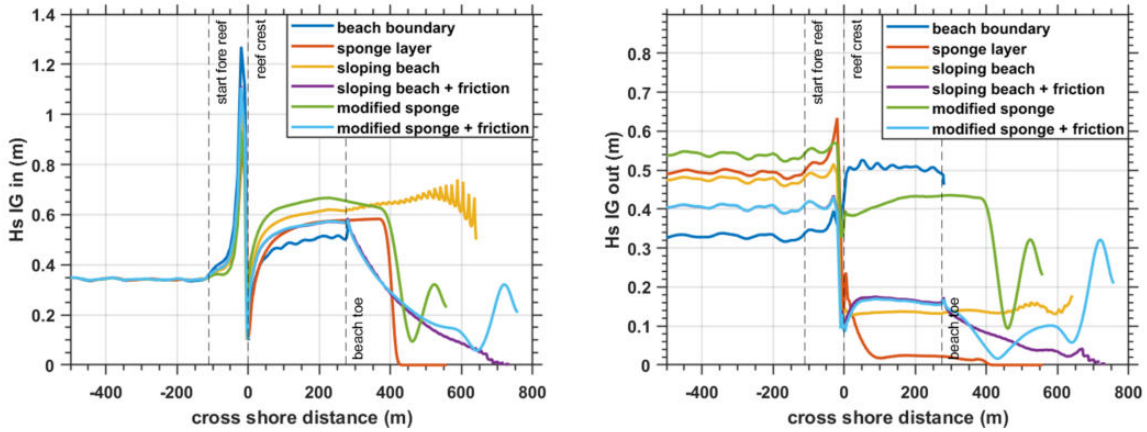

Figure A.3: The incoming (left) and outgoing IG wave (right) for various onshore boundaries in SWASH. The group period is non-resonant at Tg = 127.5 s. The beach boundary (dark blue) is the reference case that should induce resonance for the right group periods. The beach has a slope of 1/6. The sponge layer boundary (red) is the regular sponge layer which implements exponential decay functions on the velocity and water level in domain of the sponge layer. The gently sloping beach (yellow) consists of a frictionless beach with a slope of 1/163 to dissipate any incoming wave energy. The purple line corresponds to a similar beach, but with a Manning friction of 0.3 $m^{-1/3}/s$ on the beach. The modified sponge layer (green) utilizes an exponential decay function of the velocity much like the regular sponge layer, yet the exponential decay of the water level is removed. The same goes for the light blue line, but this boundary condition also has a Manning friction of 0.3 $m^{-1/3}/s$ in the domain of the sponge layer. Furthermore, a1 = 1.06 m, a2 = 0.53 m, T1 = 17 s and the fore reef slope has a steepness of 1/6. The locations of the start of the fore reef, reef crest and the beach toe are indicated through vertical dashed lines.

B

SWASH file

```
$*************HEADING*************************************
$
PROJ 'Reef' 'FR'
$
$ Finding bichromatic resonance
$
$
$***********MODEL INPUT*********************************
$
SET LEVEL=1.6
$
MODE NONSTATIONARY ONED
CGRID REG -500.00 0.00 0.00 860.00 0.00 1720 0
$
VERT 2
$
INPGRID BOTTOM REGULAR -500.00 0.00 0.00 860 0 1.00 0.00
READ BOTTOM 1.00 'BOTTOM_PROFILE_0001.bot' 1 0 FREE
$
INIT zero
$
SET DEPMIN =0.005
SET BACKVISC 1.00e-04
$
BOU SIDE W CCW BTYPE WEAK HYPER SMOO 45.0 SEC ADDBoundwave CON FOUR 0.00 1.370 0.370 0.000
0.568 0.419 0.000
$
FRIC MANNING 0.00
BREAK
NONHYDROSTATIC
$
DISCRET UPW UMOM HOR BDF
DISCRET UPW UMOM VERT FIRST
DISCRET UPW WMOM HOR BDF
DISCRET UPW WMOM VERT FIRST
DISCRET CORRDEP MUSCL
$
TIMEI METH EXPL 0.20 0.60
$
$************ OUTPUT REQUESTS ************************
$
$ locations
POINTS 'points' FILE 'LOCATIONS_0001.loc'
$
```

```
$ surface elevation
QUANT XP HEXP 10.
$
TABLE 'points' NOHEAD 'bichromatic_0001.tab' TSEC XP DEPTH BOTL WATL
VEL OUTPUT 000000.000 1 SEC
$
$TEST 1 0
COMPUTE 000000.000 0.05 SEC 010000.000
STOP
```

C
IG wave shoaling

In the highly energetic situation (Figure C.1) the incoming IG wave height increases on the fore reef more than would be expected due to shoaling alone. However, on the reef flat a lot of the IG wave energy is dissipated again. In the resonant case (right), break-point generated IG waves appear to be suppressed for the first few meters of the fore reef, where the observed IG wave height is lower than the wave would be due to shoaling. Halfway across the fore reef however, the IG wave height suddenly increases which is likely due to break-point forcing. On the reef crest, the incoming IG wave height suddenly drops, for it to increase again toward the beach toe. On the fore reef, the incoming IG wave is higher in the non-resonant (left) situation than in the resonant situation (right). On the reef flat, the incoming IG wave height is larger for the resonant situation.

It can be seen that for low energy case (Figure C.2) there is a lot more IG wave energy on the fore reef slope than would be expected just due to shoaling. Therefore, it can be derived that the dominant mechanism for the generation of IG wave energy at this location is break-point shifting. For the non-resonant case (left), the energy over the reef flat decreases again beyond the reef crest, to increase again near the beach toe. For the resonant situation (right), the energy increases over the reef flat.

It is yet unclear what mechanisms drive the offshore difference in break-point generated IG waves for resonant and non-resonant conditions.

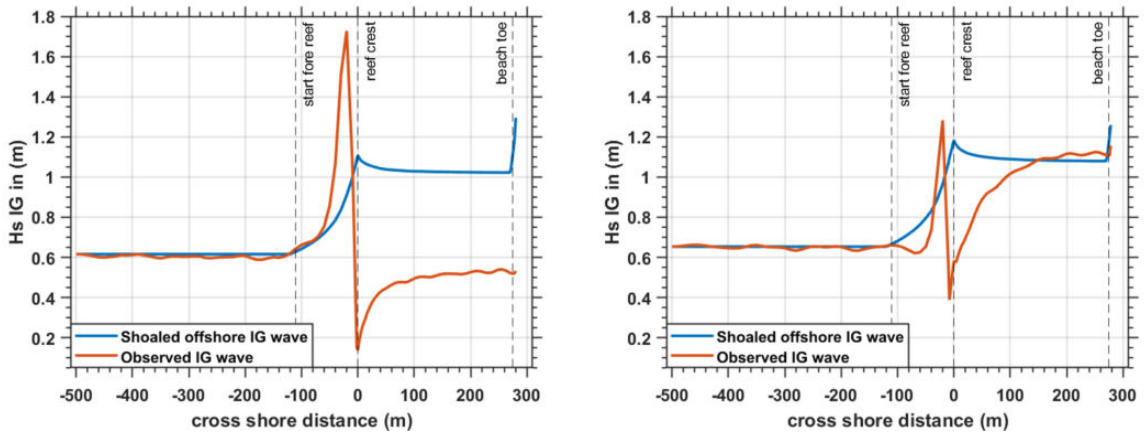

Figure C.1: The cross shore significant incoming IG wave height in a non-resonant (Tg = 127.5 *s*, left) and resonant (Tg = 240 *s*, right) highly energetic case. The orange line corresponds to the observed value of the incoming IG wave, the blue line represents the theoretical IG wave height due by taking the offshore wave height and shoaling it in shallow water conditions. A1 = 1.37 *m*, a2 = 0.73 *m* and the fore reef has a slope of 1/6.

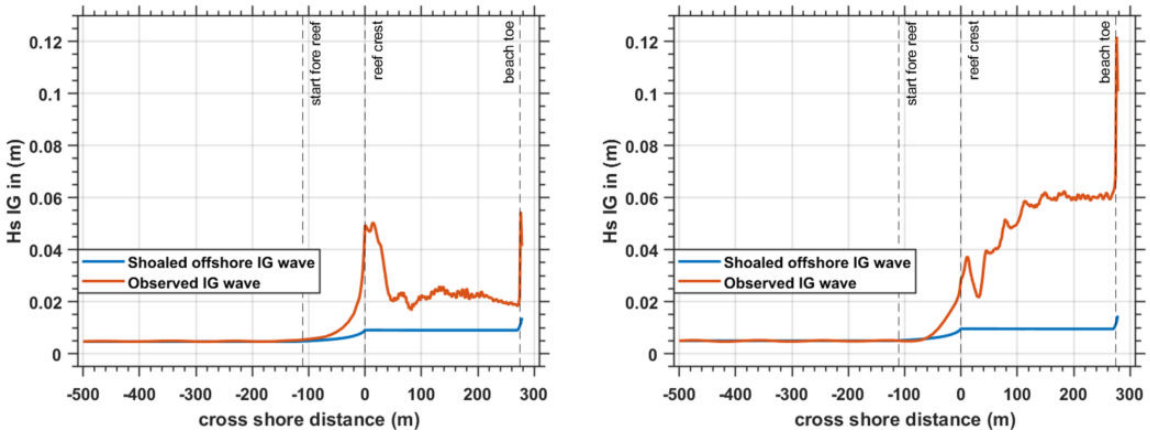

Figure C.2: The cross shore significant incoming IG wave height in a non-resonant (Tg = 127.5 *s*, left) and resonant (Tg = 240 *s*, right) low energetic case. The orange line corresponds to the observed value of the incoming IG wave, the blue line represents the theoretical IG wave height by taking the offshore wave height and shoaling it in shallow water conditions. A1 = 0.15 *m*, a2 = 0.05 *m*, T1 = 17 *s* and the fore reef has a slope of 1/6.

D

Time evolution of the outgoing IG wave

Offshore of the reef flat, the outgoing IG wave consists of three components: the reflected IG wave released from the wave group; the break point generated IG wave in negative x direction and the offshore propagating IG wave that is reflected at the beach toe.

In the water elevation signal of the outgoing IG wave (Figure D.1), no phase shifts are visible near the reef crest. The bound IG wave is 180°out of phase with the incoming wave group, so is the break point generated IG wave in negative x direction (Contardo et al., 2018). The break point generated IG wave is in phase with the wave group, however as the reef flat is 1/4 of the length of the IG wave, the outgoing IG wave that is reflected at the beach toe is 180°out of phase with the incoming IG wave at the reef crest. Therefore, all components of the outgoing IG wave field are in phase with each other (being 180°out of phase with the incoming SS wave field) and no distinction can be made about the dominance of the different components.

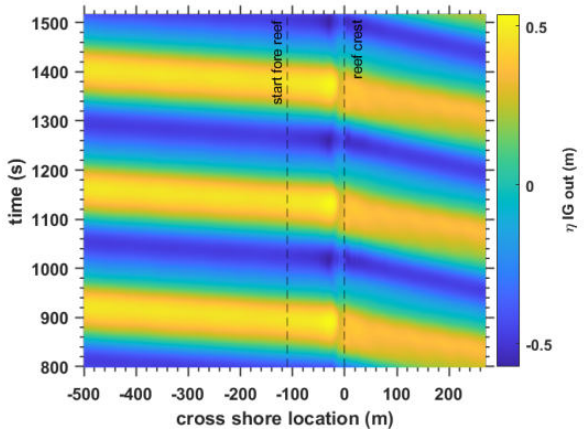

Figure D.1: The cross shore and temporal evolution of the outgoing IG wave. Reference case conditions are displayed: T1 = 17 s, a1 = 1.37 m, a2 = 0.72 m and the fore reef has a slope of 1/6. The group period Tg is 240 s, thus the conditions are resonant.

Bibliography

Baldock, T. E., Huntley, D. A., Bird, P. A., O'Hare, T., and Bullock, G. N. (2000). Breakpoint generated surf beat induced by bichromatic wave groups. *Coastal Engineering*, 39(2-4):213–242.

Battjes, J. A. (1974). Copmputation of set-up, longshore currents, run-up and overtopping due to wind-generated waves. Technical report.

Battjes, J. A., Bakkenes, H. J., Janssen, T. T., and van Dongeren, A. R. (2004). Shoaling of subharmonic gravity waves. *Journal of Geophysical Research: Oceans*, 109(2).

Becker, J. M., Merrifield, M. A., and Ford, M. (2014). Water level effects on breaking wave setup for Pacific Island fringing reefs. *Journal of Geophysical Research: Oceans*, 119(2):914–932.

Becker, J. M., Merrifield, M. A., and Yoon, H. (2016). Infragravity waves on fringing reefs in the tropical Pacific: Dynamic setup. *Journal of Geophysical Research: Oceans*, 121(5).

Bertin, X., de Bakker, A., van Dongeren, A., Coco, G., André, G., Ardhuin, F., Bonneton, P., Bouchette, F., Castelle, B., Crawford, W. C., Davidson, M., Deen, M., Dodet, G., Guérin, T., Inch, K., Leckler, F., McCall, R., Muller, H., Olabarrieta, M., Roelvink, D., Ruessink, G., Sous, D., Stutzmann, , and Tissier, M. (2018). Infragravity waves: From driving mechanisms to impacts.

Birkeland, C. (2018). Global status of coral reefs: In combination, disturbances and stressors become ratchets. In *World Seas: An Environmental Evaluation Volume III: Ecological Issues and Environmental Impacts*.

Buckley, M. L., Lowe, R. J., Hansen, J. E., Van Dongeren, A. R., and Storlazzi, C. D. (2018). Mechanisms of wave-driven water level variability on reef-fringed coastlines. *Journal of Geophysical Research: Oceans*, 123(5).

Cheriton, O. M., Storlazzi, C. D., and Rosenberger, K. J. (2016). Observations of wave transformation over a fringing coral reef and the importance of low-frequency waves and offshore water levels to runup, overwash, and coastal flooding. *Journal of Geophysical Research: Oceans*, 121(5).

Cheriton, O. M., Storlazzi, C. D., and Rosenberger, K. J. (2020). In situ Observations of Wave Transformation and Infragravity Bore Development Across Reef Flats of Varying Geomorphology. *Frontiers in Marine Science*, 7.

Contardo, S. and Symonds, G. (2013). Infragravity response to variable wave forcing in the nearshore. *Journal of Geophysical Research: Oceans*, 118(12):7095–7106.

Contardo, S., Symonds, G., and Dufois, F. (2018). Breakpoint Forcing Revisited: Phase Between Forcing and Response. *Journal of Geophysical Research: Oceans*, 123(2):1354–1363.

Demirbilek, Z., Nwogu, O. G., and Ward, Donald L. (Donald Leslie), . (2007). Laboratory study of wind effect on runup over fringing reefs, Report 1: Data report. *This Digital Resource was created from scans of the Print Resource*.

Elgar, S., Herbers, T. H., Okihiro, M., Oltman-Shay, J., and Guza, R. T. (1992). Observations of infragravity waves. *Journal of Geophysical Research*, 97(C10).

Ferrario, F., Beck, M. W., Storlazzi, C. D., Micheli, F., Shepard, C. C., and Airoldi, L. (2014). The effectiveness of coral reefs for coastal hazard risk reduction and adaptation. *Nature Communications*, 5.

Field, M., Cochran, S., and Evans, K. (2002). U.S. Coral Reefs–Imperiled National Treasures.

Gaido, C. (2019). Dynamics of resonant low-frequency waves over a schematized fringing coral reef. Technical report.

Gawehn, M., van Dongeren, A., van Rooijen, A., Storlazzi, C. D., Cheriton, O. M., and Reniers, A. (2016). Identification and classification of very low frequency waves on a coral reef flat. *Journal of Geophysical Research: Oceans*, 121(10).

Gourlay, M. R. (1996). Wave set-up on coral reefs. 2. Set-up on reefs with various profiles. Technical report.

Guza, R. T., Thornton, E. B., Asce, M., and Holman, R. A. (1984). SWASH ON STEEP AND SHALLOW BEACHES. Technical report.

Hassan, R. (2005). Ecosystems and Human Well-being : Current State and Trends , Volume 1. *Current*.

Hasselmann, K. (1962). On the non-linear energy transfer in a gravity-wave spectrum Part 1. General theory. *Journal of Fluid Mechanics*, 12(4):481–500.

Herbers, T. H., Elgar, S., and Guza, R. T. (1995). Generation and propagation of infragravity waves. *Journal of Geophysical Research*, 100(C12).

Hoeke, R. K., McInnes, K. L., Kruger, J. C., McNaught, R. J., Hunter, J. R., and Smithers, S. G. (2013). Widespread inundation of Pacific islands triggered by distant-source wind-waves. *Global and Planetary Change*, 108:128–138.

Janssen, T. T., Battjes, J. A., and van Dongeren, A. R. (2003). Long waves induced by short-wave groups over a sloping bottom. *Journal of Geophysical Research: Oceans*, 108(8).

Kleypas, J. and Gattuso, J.-P. (2006). Coral Reefs.

Lashley, C. H., Bricker, J. D., Meer, J. v. d., Altomare, C., and Suzuki, T. (2020). Relative Magnitude of Infragravity Waves at Coastal Dikes with Shallow Foreshores: A Prediction Tool. *Journal of Waterway, Port, Coastal, and Ocean Engineering*, 146(5):04020034.

Lee, T. T. and Black, K. P. (1978). The Energy Spectra of Surf Waves on a Coral Reef. In *Coastal Engineering 1978*, pages 588–608, New York, NY. American Society of Civil Engineers.

Longuet-Higgins, M. S. and Stewart, R. W. (1962). Radiation stress and mass transport in gravity waves, with application to 'surf beats'. *Journal of Fluid Mechanics*, 13(4).

Longuet-Higgins, M. S. and Stewart, R. w. (1964). Radiation stresses in water waves; a physical discussion, with applications. *Deep-Sea Research and Oceanographic Abstracts*, 11(4):529–562.

Lowe, R. J. (2005). Spectral wave dissipation over a barrier reef. *Journal of Geophysical Research*, 110(C4):C04001.

Masselink, G. (1995). Group bound long waves as a source of infragravity energy in the surf zone. *Continental Shelf Research*, 15(13):1525–1547.

Masselink, G., Tuck, M., McCall, R., van Dongeren, A., Ford, M., and Kench, P. (2019). Physical and Numerical Modeling of Infragravity Wave Generation and Transformation on Coral Reef Platforms. *Journal of Geophysical Research: Oceans*, 124(3).

Merrifield, M. A., Becker, J. M., Ford, M., and Yao, Y. (2014). Observations and estimates of wave-driven water level extremes at the Marshall Islands. *Geophysical Research Letters*, 41(20):7245–7253.

Nakaza, E. and Hino, M. (1991). Bore-like surf beat in a reef zone caused by wave groups of incident short period waves. *Fluid Dynamics Research*, 7(2):89–100.

Ning, Y., Liu, W., Sun, Z., Zhao, X., and Zhang, Y. (2019). Parametric study of solitary wave propagation and runup over fringing reefs based on a Boussinesq wave model. *Journal of Marine Science and Technology (Japan)*, 24(2).

NOAA (2021). Coral Reefs.

Nwogu, O. and Demirbilek, Z. (2010). Infragravity Wave Motions and Runup over Shallow Fringing Reefs. *Journal of Waterway, Port, Coastal, and Ocean Engineering*, 136(6).

Oberle, F. K., Swarzenski, P. W., and Storlazzi, C. D. (2017). Atoll groundwater movement and its response to climatic and sea-level fluctuations. *Water (Switzerland)*, 9(9).

Osinga, R., Schutter, M., Griffioen, B., Wijffels, R. H., Verreth, J. A., Shafir, S., Henard, S., Taruffi, M., Gili, C., and Lavorano, S. (2011). The Biology and Economics of Coral Growth.

Pachauri, R. K. (2014). Climate Change 2014: Synthesis Report. Contribution of Working Groups I, II and III to the Fifth Assessment Report of the Intergovernmental Panel on Climate Change | EPIC.

Pearson, S. G., Storlazzi, C. D., van Dongeren, A. R., Tissier, M. F. S., and Reniers, A. J. H. M. (2017). A Bayesian-Based System to Assess Wave-Driven Flooding Hazards on Coral Reef-Lined Coasts. *Journal of Geophysical Research: Oceans*, 122(12):10099–10117.

Péquignet, A. C., Becker, J. M., Merrifield, M. A., and Boc, S. J. (2011). The dissipation of wind wave energy across a fringing reef at Ipan, Guam. *Coral Reefs*, 30(SUPPL. 1).

Péquignet, A. C. N., Becker, J. M., and Merrifield, M. A. (2014). Energy transfer between wind waves and low-frequency oscillations on a fringing reef, Ipan, Guam. *Journal of Geophysical Research: Oceans*, 119(10).

Péquignet, A. C. N., Becker, J. M., Merrifield, M. A., and Aucan, J. (2009). Forcing of resonant modes on a fringing reef during tropical storm Man-Yi. *Geophysical Research Letters*, 36(3):n/a–n/a.

Pomeroy, A., Lowe, R., Symonds, G., Van Dongeren, A., and Moore, C. (2012a). The dynamics of infragravity wave transformation over a fringing reef. *Journal of Geophysical Research: Oceans*, 117(C11):n/a–n/a.

Pomeroy, A. W., Lowe, R. J., Van Dongeren, A. R., Ghisalberti, M., Bodde, W., and Roelvink, D. (2015). Spectral wave-driven sediment transport across a fringing reef. *Coastal Engineering*, 98:78–94.

Pomeroy, A. W., Van Dongeren, A., Lowe, R. J., Van Thiel De Vries, J. S., and Roelvink, J. (2012b). Low frequency wave resonance in fringing reef environments. In *Proceedings of the Coastal Engineering Conference*.

Quataert, E., Storlazzi, C., van Dongeren, A., and McCall, R. (2020). The importance of explicitly modelling sea-swell waves for runup on reef-lined coasts. *Coastal Engineering*, 160.

Quataert, E., Storlazzi, C., Van Rooijen, A., Cheriton, O., and Van Dongeren, A. (2015). The influence of coral reefs and climate change on wave-driven flooding of tropical coastlines. *Geophysical Research Letters*, 42(15).

Roeber, V. and Bricker, J. D. (2015). Destructive tsunami-like wave generated by surf beat over a coral reef during Typhoon Haiyan. *Nature Communications*, 6(1):1–9.

Roelvink, F. (2019). Coral Restoration for Coastal Hazard Risk Reduction. Technical report.

Scheidegger, C. E., Jo~, J., Luiz, J., Comba, D., Dias, R., and Cunha, D. A. (2004). Navier-Stokes on Programmable Graphics Hardware using SMAC.

Schiereck, G. (2012). Introduction to bed, bank and shore protection (2nd edition). *Collegedictaat CIE4310*.

Shimozono, T., Tajima, Y., Kennedy, A. B., Nobuoka, H., Sasaki, J., and Sato, S. (2015). Combined infragravity wave and sea-swell runup over fringing reefs by super typhoon Haiyan. *Journal of Geophysical Research: Oceans*, 120(6):4463–4486.

Storlazzi, C., Reguero, B. G., Cole, A. D., Lowe, E., Shope, J. B., Gibbs, A. E., Nickel, B. A., McCall, R. T., van Dongeren, A. R., and Beck, W. (2019). Rigorously Valuing the Role of U.S. Coral Reefs in Coastal Hazard Risk Reduction Prepared in cooperation with the University of California Santa Cruz and The Nature Conservancy. Technical report.

Storlazzi, C. D., Elias, E. P., and Berkowitz, P. (2015). Many Atolls May be Uninhabitable Within Decades Due to Climate Change. *Scientific Reports*, 5(1):14546.

Storlazzi, C. D., Gingerich, S. B., Van Dongeren, A., Cheriton, O. M., Swarzenski, P. W., Quataert, E., Voss, C. I., Field, D. W., Annamalai, H., Piniak, G. A., and McCall, R. (2018). Most atolls will be uninhabitable by the mid-21st century because of sea-level rise exacerbating wave-driven flooding. *Science Advances*, 4(4).

Storlazzi, C. D., Ogston, A. S., Bothner, M. H., Field, M. E., and Presto, M. K. (2004). Wave- and tidally-driven flow and sediment flux across a fringing coral reef: Southern Molokai, Hawaii. *Continental Shelf Research*, 24(12):1397–1419.

Symonds, G., Huntley, D. A., and Bowen, A. J. (1982). Two-dimensional surf beat: long wave generation by a time-varying breakpoint. *Journal of Geophysical Research*, 87(C1).

Torres-Freyermuth, A., Mariño-Tapia, I., Coronado, C., Salles, P., Medellín, G., Pedrozo-Acuña, A., Silva, R., Candela, J., and Iglesias-Prieto, R. (2012). Wave-induced extreme water levels in the Puerto Morelos fringing reef lagoon. *Natural Hazards and Earth System Sciences*, 12(12):3765–3773.

Ursell, F. (1953). The long-wave paradox in the theory of gravity waves. *Mathematical Proceedings of the Cambridge Philosophical Society*, 49(4):685–694.

van Dongeren, A., Battjes, J., Janssen, T., van Noorloos, J., Steenhauer, K., Steenbergen, G., and Reniers, A. (2007). Shoaling and shoreline dissipation of low-frequency waves. *Journal of Geophysical Research*, 112(C2):C02011.

Van Dongeren, A., Lowe, R., Pomeroy, A., Trang, D. M., Roelvink, D., Symonds, G., and Ranasinghe, R. (2013). Numerical modeling of low-frequency wave dynamics over a fringing coral reef. *Coastal Engineering*, 73.

Veldt, T. (2019). *The effect of wave directional spread on coastal hazards at coastlines fronted by a coral reef*. PhD thesis.

Vetter, O., Becker, J. M., Merrifield, M. A., Pequignet, A.-C., Aucan, J., Boc, S. J., and Pollock, C. E. (2010). Wave setup over a Pacific Island fringing reef. *Journal of Geophysical Research*, 115(C12):C12066.

Wilson, B. W. (2000). THE MECHANISM OF SEICHES IN TABLE BAY HARBOR, CAPE TOWN. *Coastal Engineering Proceedings*, 1(4).

Zijlema, M. (2012). MODELLING WAVE TRANSFORMATION ACROSS A FRINGING REEF USING SWASH. *Coastal Engineering Proceedings*, 1(33):26.

Zijlema, M., Stelling, G., and Smit, P. (2011). SWASH: An operational public domain code for simulating wave fields and rapidly varied flows in coastal waters. *Coastal Engineering*, 58(10):992–1012.

Zou, G. L. and Zhang, Q. H. (2013). Improvement of absorbing boundary conditions for non-hydrostatic wave-flow model SWASH. *Applied Mechanics and Materials*, 353-354:2676–2682.